Theses and Dissertations

2015

Engineered 3D Microenvironments to Direct Osteogenic Differentiation and Modulate Inflammation

Katherine Elizabeth Rutledge
University of South Carolina

Follow this and additional works at: https://scholarcommons.sc.edu/etd

Part of the Chemical Engineering Commons

Recommended Citation

ENGINEERED 3D MICROENVIRONMENTS TO DIRECT OSTEOGENIC
DIFFERENTIATION AND MODULATE INFLAMMATION

by

Katherine Elizabeth Rutledge

Bachelor of Science
University of Arkansas, 2011

_____

Submitted in Partial Fulfillment of the Requirements

For the Degree of Doctor of Philosophy in

Chemical Engineering

College of Engineering and Computing

University of South Carolina

2015

Accepted by:

Ehsan Jabbarzadeh, Major Professor

Esmaiel Jabbari, Committee Member

Melissa Moss, Committee Member

Tarek Shazly, Committee Member

John Weidner, Committee Member

Lacy Ford, Senior Vice Provost and Dean of Graduate Studies

DEDICATION

This dissertation is lovingly dedicated to my sister, Jessica Naughton.

ABSTRACT

Current methods of treating critical size bone defects (CSDs) include autografts and allografts, however both present major limitations including donor-site morbidity, risk of disease transmission, and immune-rejection. Tissue engineering provides a promising alternative to circumvent these shortcomings through the use of stem cells, three dimensional (3D) scaffolds, and growth factors. Cells receive signals from their microenvironment that determine cell phenotype, and a combination of physical cues and chemical factors is thought to have the most profound influence on stem cell behavior. A major focus of tissue engineering strategies is scaffold design to recapitulate *in vivo* microenvironmental architecture to direct stem cell lineage commitment. In combination with relevant microenvironment design, the success of bone tissue engineering strategies critically depends on the rapid formation of a mature vascular network in the scaffolds after implantation. However, conventional approaches fail to consider the role of the host response in regulating tissue ingrowth and extent of vascularization. The work presented here focuses on i) designing an osteomimetic 3D substrate to guide human embryonic stem cell (hESC) differentiation towards bone lineage, and ii) investigating the ability of the polyphenol resveratrol to harness the potential of the inflammatory response to enhance angiogenesis and osseointegration in 3D scaffolds for bone repair.

The osteomimetic scaffold with native bone extracellular matrix (ECM) components successfully directed the osteogenic differentiation of hESCs. A microsphere-sintering technique was used to fabricate poly(lactic-*co*-glycolic acid)

(PLGA) scaffolds with optimum mechanical properties, and human osteoblasts (hOBs) were seeded on these scaffolds to deposit bone ECM. This was followed by a decellularization step leaving the mineralized matrix intact. hESCs were seeded on the osteomimetic substrates in the presence of osteogenic growth medium, and osteogenicity was determined according to calcium content, osteocalcin expression, and bone marker gene regulation. The results from this study demonstrate the potential of PLGA scaffolds with native bone ECM components to direct osteogenic differentiation of hESCs and induce bone formation.

Engineered resveratrol nanoparticle-incorporated PLGA scaffolds enabled the concurrent (i) mediation of inflammatory (M1) to wound healing (M2) macrophage differentiation, (ii) natural release of angiogenic factors by M2 macrophages and (iii) enhanced osteogenic differentiation of human mesenchymal stem cells (hMSCs). To this end, we mapped the time-dependent response of macrophage gene expression as well as hMSC osteogenic differentiation to varying doses of resveratrol. Our results delineate the potential to synergistically control angiogenic factor secretion and downstream osteogenic signaling pathways by "dialing" the appropriate degree of resveratrol release from nanoparticle-incorporated PLGA scaffolds.

TABLE OF CONTENTS

LIST OF TABLES

LIST OF FIGURES

LIST OF SYMBOLS

α   ALPHA

β   BETA

°   DEGREES

γ   GAMMA

κ   KAPPA

μ   MICRO

LIST OF ABBREVIATIONS

2D...Two Dimensional

3D...Three Dimensional

AD-hMSCs .... Adipose-derived Human Mesenchymal Stem Cells

ANOVA ....Analysis of Variance

ALP ....Alkaline Phosphatase

BM-hMSCs............................... Bone Marrow-derived Human Mesenchymal Stem Cells

BMP-2..Bone Morphogenetic Protein-2

CAD .... Computer Aided Design

CNT... Carbon Nanotube

CSD.. Critical-size Defect

DAPI ....4'-6'diamidino-2-phenylindole

DI ....Deionized

DMEM ....Dulbecco's Modified Eagle Medium

DMSO ....Dimethyl Sulfoxide

EB .... Embryoid Bodies

EC .... Endothelial Cell

ECGF1 ....Platelet-derived Endothelial Cell Growth Factor

ECM ....Extracellular Matrix

FAK...Focal Adhesion Kinase

FBS ....Fetal Bovine Serum

CHAPTER 1: Bone Tissue Engineering

1.1 Tissue Engineering

In recent years, tissue engineering has emerged as a potential method for treating numerous diseases and regenerating damaged cells. By applying engineering approaches to knowledge of biological systems, a tissue engineered substitute can be generated to restore, replace, or maintain partial if not entire organ function [1]. The key to tissue engineering strategies is coordinating cell behavior with specific growth factors and biomaterials in order to regenerate functional tissues, however this is difficult to experimentally control *in vitro*.

Like many tissues in the body, bone has a natural ability to repair minor injuries resulting from disease or small fractures. Despite this, it is estimated that over 800,000 bone graft procedures are completed yearly in the United States to facilitate repair from large-scale trauma [2-4]. Current treatment methods for critical-sized defects (CSDs) include (i) autografts, where the patient's own bone tissue is removed from one area and placed in the site of deficiency, (ii) allografts, where bone from a cadaver is used to replace the damaged tissue, (iii) and synthetic grafts, where manufactured materials are implanted and used to treat the CSD [5-7]. Autografts are considered the gold standard in clinical applications because of their osteoconductivity, osteoinductivity, and osteogenecity, however a secondary surgery is required for implementation. There is also

a risk of disease transfer, rejection by the host, and large bone defects cannot be treated by autografts [8-13]. Long-term storage of bone tissue for allografts causes bone architecture to dramatically weaken and most of the osteoprogenitor cells are no longer viable. Synthetic grafts cannot fully incorporate with the host tissue and are susceptible to fatigue, fracture, and wear [14]. Therefore, there is a need for better treatment options for patients with CSDs, and tissue engineering offers bone graft alternatives.

1.2 Bone Physiology and Microenvironment

Bone macrostructure generally has two layers, which includes the outer dense compact bone and the inner spongy trabecular bone. The compact, or cortical bone, provides strength and support to the structure. The trabecular bone is porous with cells interwoven between calcified lattices. Simply described, bone architecture can be broken down into this sequential arrangement: (i) the macrostructure which is made up of cortical and cancellous bone, (ii) the microstructure which is composed of osteons, haversian systems, and trabeculae, (iii) the submicrostructure which is comprised of the lamellae, (iv) the nanostructure which is predominately composed of collagen I fibers, and (v) the sub-nanostructure made up of mineralized matrix, smaller collagen subunits, and other organic proteins [15].

The extracellular matrix (ECM) is a dynamic arrangement of molecules such as collagen, con-collagenous glycoproteins, hyaluronan, and proteoglycan that are produced by cells, and in turn, regulate cell phenotype [16]. Native bone ECM is mainly composed

2

of type I collagen, upon which carbonated apatite is laid down to create a crystalline anisotropic fibril [17]. Serum albumin and α2-HS-glycoprotein are noncollagenous proteins that bind to hydroxyapatite due to their acidic properties [18]. Other noncollagenous proteins found in bone ECM include osteocalcin, alkaline phosphatase, osteonectin, osteopontin, and bone sialoprotein [18]. Cells residing in bone ECM secrete growth factors, matrix-degrading enzymes, and inflammatory mediators [16].

Bone is a highly vascularized tissue. The nutrient or diaphyseal artery, periosteal arteries, metaphyseal arteries, and epiphyseal arteries are the four arterial inputs that supply nutrients in adult bones. The nutrient artery is responsible for the bulk of the total blood supply with over 50% of the blood flow due to its arterial output [19, 20]. Periosteal arteries are responsible for the membrane covering the outside of bones called the periosteum. The periosteum is a significant source of stem cells and has been utilized in previous regenerative studies [21, 22]. The diaphyseal nutrient artery enters the shaft through one or two nutrient foramina leading into the nutrient canals. These arteries then enter the medullary cavity where they divide into ascending and descending branches to supply the cortical and marrow microcirculations. The cortical branches of the arteries passing through the endosteal canals feed the capillaries in the Haversian and Volkmann's canals and generally conform to the canal shape [23]. For bone marrow circulation, capillaries drain into vascular channels surrounded by a layer of fenestrated endothelium [24, 25]. The central venous sinus is responsible for the draining of the veins and runs along the paths of the nutrient arteries and leaves the bone through veins

[20, 23]. Blood flow in the bone generally occurs at 5-20 ml/min per 100 grams of wet bone tissue [23].

1.3 Challenges to Bone Tissue Engineering Approaches

Although much progress has been made in the field of tissue engineering, critical barriers such as lack of scaffold vascularization, the host inflammatory response, and the need to use high doses of growth factors to differentiate cells must be overcome in order to effectively create functional tissues. In dealing with vascularization, tissue engineering meets a mass transfer challenge, which limits scaffold construct size *in vivo* regardless of tissue specific goals. The majority of cells are situated within 100-200 microns [26] of capillaries where sufficient oxygen and nutrition is provided and metabolic waste is able to be transported [27]. It is difficult to engineer scaffolds less than a few hundred microns thick, therefore the ability for angiogenesis to occur in large scaffolds becomes a critical consideration.

Another important factor is translating *in vitro* success to *in vivo* applications by accounting for the host immune response to implanted biomaterials that can lead to graft rejection. This reaction protects the body from harmful intruders and is beneficial on small time scales, but chronic inflammation can interfere with tissue engineering approaches to repair damaged tissue. The complicated interplay of cells and cytokines at the interface of an implanted biomaterial that governs success versus failure of an implant is still difficult to understand, but must be deconstructed in order to properly design an approach to harness inflammation and promote wound healing.

After a biomaterial is inserted into the host tissue, a sequence of reactions occur (Figure 1.1). First, injury to the vasculature causes blood to contact the material. Proteins from the serum bind to the implanted biomaterial and form a provisional matrix composed of fibrin, platelet granule components such as thrombospondin, transforming growth factor alpha (TGF-α) transforming growth factor beta (TGF-β), platelet-derived growth factor (PDGF), platelet factor 4 (PF4), and platelet-derived endothelial cell growth factor (ECGF1) [28]. Monocytes exit the capillaries, attach to the matrix that has formed on the biomaterial surface, and differentiate into pro-inflammatory M1 macrophages. M1 macrophages release cytokines such as tumor necrosis factor alpha (TNF-α), interleukin-1 beta (IL-1β), interleukin-6 (IL-6), and monocyte chemotactic protein 1 (MCP-1) that drive the acute inflammation response [29, 30]. The next event in the host response to an implanted biomaterial is chronic inflammation, which is defined by the presence of macrophages, monocytes, lymphocytes, blood vessel proliferation, and connective tissue formation [31-34]. Foreign body giant cells and macrophages will generally exist at the tissue-implant interface for the duration of the biomaterial's lifetime [35-39]. A fibrous capsule usually forms around the foreign body reaction, separating the biomaterial from the host tissue [28]. In some tissue types, acute inflammation stimulates M1 pro-inflammatory macrophages to change phenotype into wound healing M2 macrophages. This polarization from M1 to M2 is a critical component of avoiding graft and biomaterial rejection.

Several approaches have been taken to control host inflammation in response to implanted biomaterials such as casing the scaffold with biocompatible coating,

incorporating anti-inflammatory pharmaceuticals in the substrate, and releasing angiogenic growth factors at the site of graft insertion. Biocompatible material coatings generally rely on creating a hydrophilic boundary between the implant and the host tissue [40, 41] which lessens the immune response, and subsequently maintains functionality of the implant for a slightly longer time period than an unmodified substrate [42-44]. Natural and synthetic polymers are typically used for this process, however, natural polymers can be immunogenic, decompose quickly at elevated temperatures that are necessary in manufacturing processes, and can exhibit much material inconsistency [41]. On the other hand, synthetic polymers offer the ability to tune the material specifically for the application, but generally have low adhesion capabilities for binding to the biomaterial, low mechanical strength, toxic chemicals are usually used to crosslink the polymer, and synthetic polymers present biocompatibility issues [41, 45]. Another well-utilized method of promoting implanted material success is to induce angiogenesis using vascular endothelial growth factor (VEGF) [46-48]. Although somewhat successful, this method can overexpose tissues to growth factors which can cause arthritis or tumor formation [49-51]. Additionally, angiogenic growth factor release is not effective since multiple signals are required in the neovascularization cascade and temporal release of the cytokines is difficult to control. Anti-inflammatory drugs inhibit secretion of inflammatory mediators like leukotrienes and prostaglandins, reduce the amount of inflammatory cells, and lessen fibroblast recruitment at the site of implantation [52]. These drugs are typically administered systemically, therefore a drawback of this method arises with unwanted side effects occurring throughout the body [53]. Furthermore, anti-
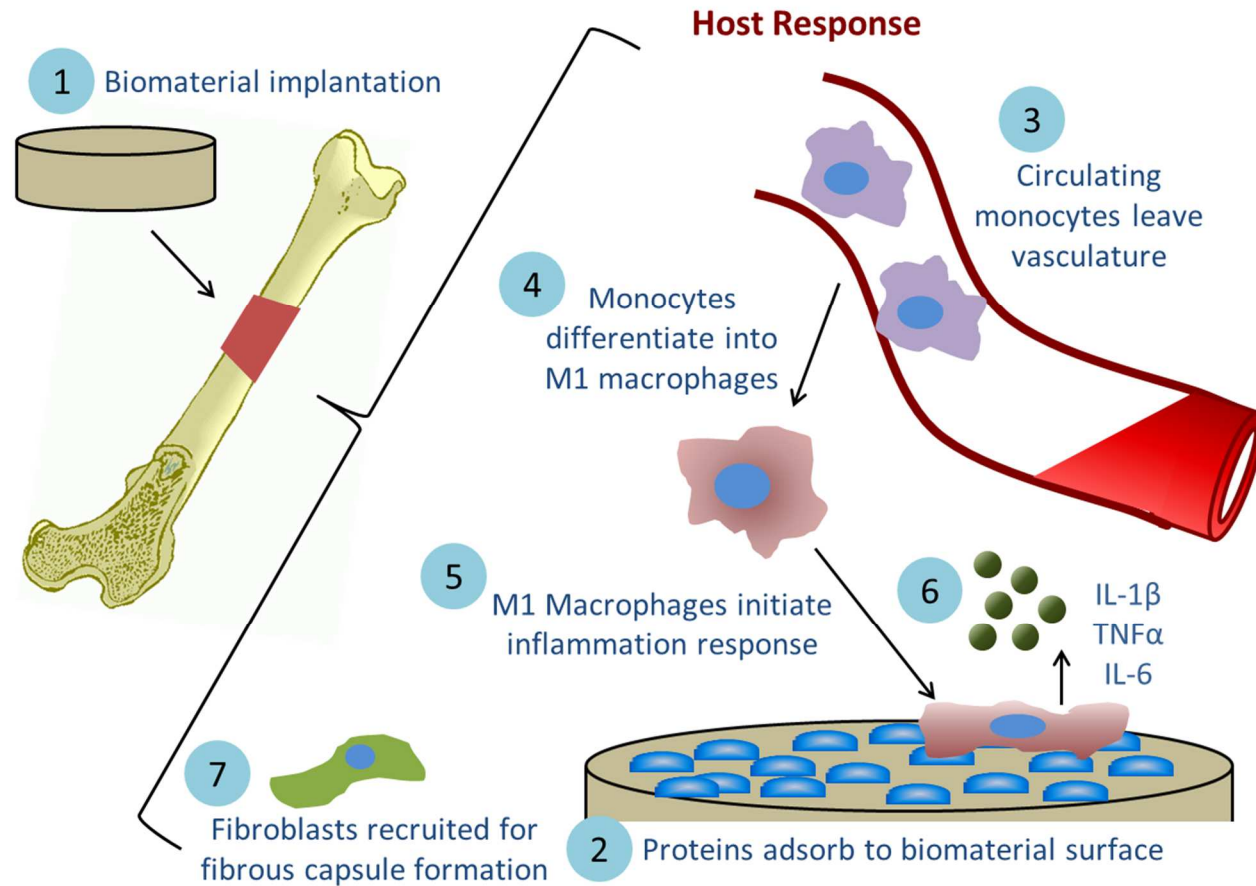
Figure 1.1 Inflammation cascade after implantation of a biomaterial. 1) Biomaterial is implanted, and 2) proteins from the disrupted capillaries adsorb to the biomaterial surface. 3) Monocytes that are circulating in the vasculature migrate to the site of implantation, and 4) differentiate into M1 macrophages. 5) M1 macrophages are pro-inflammatory and initiate the host inflammation response by 6) releasing cytokines to 7) recruit fibroblasts for fibrous capsule formation.

inflammatory drugs such as corticosteroid drugs downregulate VEGF, thus inhibiting

new blood vessel formation necessary for nutrient exchange in the implanted tissue [54,

55].

CHAPTER 2: CELL SOURCES FOR TISSUE ENGINEERING

2.1 Introduction

Choosing the correct cell type as part of a tissue engineering approach to create a functional bone graft substitute is essential for success of the implant. Cell types such as lineage committed progenitor cells, adult stem cells, and pluripotent stem cells all present viable options. Cell type selection is an important factor to consider, as cells seeded on scaffolds may stimulate signaling events that trigger host cells to migrate and integrate with the newly formed tissue, thus accelerating wound healing process following scaffold implantation.

2.2 Progenitor Cells

Progenitor cells are lineage-committed and maintain the tissue in which they reside [56]. These progenitor cells have been discovered in muscle tissue [57], cartilage [58], bone [58, 59], tissue in the central nervous system [60], in the bulge of the hair follicle [61], as well as many other locations. Like human mesenchymal stem cells (hMSCs), progenitor cells have a finite limit to proliferation and follow Hayflick's limit of 50-70 population doublings [56, 62]. Progenitor cells have the advantage of patient specific treatment, however their narrow differentiation capabilities and limited proliferation potential present severe drawbacks.

2.3 Adult Stem Cells

Numerous studies have demonstrated the potential of human mesenchymal stem cells in bone tissue engineering applications [63-68]. While they eliminate the controversy surrounding human embryonic stem cells (hESCs), they also present disadvantages such as the loss of proliferation capabilities with increasing passages and their infrequency in the stroma indicates a limited population of cells that can actually differentiate into osteogenic lineage [69, 70]. Studies conducted in animal models demonstrated that the amount of bone formed from hMSCs was insufficient to bridge a large bone defect [71]. Another shortcoming with using hMSCs for tissue engineering studies is that multipotency limits their differentiation potential to specific cell types [73, 74]. However, when exposed to the correct chemical signals, adipose-derived hMSCs (AD-hMSCs) can differentiate towards osteogenic, chondrogenic, adipogenic, myogenic, and hepatic lineages, as well as become endothelial cells [75-78]. Bone marrow-derived hMSCs (BM-hMSCs) are a type of adult stem cell that can differentiate to bone, cartilage, muscle, ligament, tendon, adipose, and stroma lineages [79-82]. Although hMSCs have disadvantages, their ability of patient-specific treatment and differentiation capabilities into osteogenic lineage offer immense potential for use in bone tissue engineering strategies.

2.4 Embryonic Stem Cells

Both human mesenchymal stem cells and human embryonic stem cells have been investigated as a source of new bone tissue for grafts. hESCs possess the unique ability to self-renew and have the potential to differentiate into any cell type formed from the three

germ layers [83, 84]. hESCs offer a promising tool for biomedical research as they can be used in developmental studies, disease modeling, drug testing, and regenerative medicine [85]. These stem cells are derived from the inner cell mass of a pre-implantation embryo during the blastocyst stage [86-88]. The maintenance and culture of hESCs usually involves growing cells in feeder-dependent or feeder-free conditions, and cells are kept in colonies in order to preserve an undifferentiated state. Embryoid bodies (EBs) are commonly used to mimic the three-dimensionality of development during gastrulation and the formation of the three germ layers *in vivo* [89]. The limitation of employing EBs for differentiation studies arises from the fact that the yield of desired cells is much lower than the initial amount of cells [90]. In order to use hESCs for differentiation experiments, cells must retain pluripotency and self-renewal capabilities, and it is imperative to parse the underlying developmental mechanisms involved in osteogenesis in order to successfully engineer bone tissue.

hESCs are promising candidates for bone tissue engineering applications since they can differentiate into every cell type found in bone [91-96]. Osteoblasts, osteoclasts, nerve cells, and vascular cells all contribute to bone architecture and function, and given the correct signals, hESCs will become these cell types [97]. hESCs are a superior choice for bone tissue regeneration strategies based on their pluripotency and proliferation capabilities, but they offer obstacles to overcome as well.

hESCs are difficult to culture and scaffold surface modification is required for cell attachment; substrates traditionally have been coated with protein cocktails such as Matrigel or Geltrex to promote cell adhesion. Bone-forming osteoblast cells or

osteoprogenitor cells can also be used to deposit natural extracellular matrix proteins onto the substrate for hESC attachment. To date, great strides have been taken in using native bone components to create scaffolds to promote the growth of osteoblast-like cells, however most approaches focus on one element of the ECM as opposed to the entire network [98-107]. Decellularized scaffolds composed of the organic and inorganic elements of bone ECM are osteoinductive as well as osteoconductive. The interactions between cells and the ECM have the ability to define cell development and function [108]. By using osteoblasts to deposit ECM, a natural bone microenvironment is created that will stimulate hESCs to differentiate into osteogenic lineage. Although numerous studies have shown the potential of decellularized scaffolds, there is a lack of characterization of the signals involved in using natural ECM to direct the differentiation of hESCs and there is a need for determining which spatial and temporal cues control the diverse development of bone.

2.5 Induced Pluripotent Stem Cells

Induced pluripotent stem cells (iPSCs) were first created by introducing four pluripotency transcription factors (Oct3/4, Sox2. C-Myc, and Klf4) to a mouse fibroblast cell, after which the fibroblast exhibited properties of undifferentiated hESCs [109]. These stem cells have the ability to differentiate into cells of all three germ layers, can self-renew, and proliferate indefinitely [110, 111]. Unlike hESCs, iPSCs offer the opportunity for patient specific treatment since somatic cells can be taken from the target host, reprogrammed through the addition of transcription factors, cultured to increase cell

number, differentiated towards the desired lineage, and finally implanted back into the patient. Since the genetic material in the implanted cells is the same as in the host's cells, the risk of immunorejection is low.

One obstacle with using iPSCs for tissue engineering approaches is that this cell source uses a viral vector to introduce the pluripotency transcription factors to the stromal cell. This has raised concern regarding unwanted side effects in patients, even though the vector portion is composed of just the viral envelope. Another barrier for using hESCs and iPSCs in regenerative medicine is that teratoma formation in implanted tissue can occur when cells have not fully and uniformly differentiated into the target tissue [112, 113]. Therefore, it is extremely important to develop a direct approach to exclusively generate desired cells in order to avoid spontaneous teratoma formation.

CHAPTER 3: METHODS TO RECAPITULATE *IN VIVO* MICROENVIRONMENT

3.1 Cell-ECM Interactions Determine Cell Phenotype

Although hESCs, iPSCs, and hMSCs are promising cell sources for tissue engineering applications and invaluable tools for studying developmental biology, there are still many fundamental aspects of stem cell biology that are unknown. Specifically, researchers are striving to understand and deconstruct the mechanisms by which the microenvironment effects lineage determination, as well as cell phenotype and function.

The native microenvironment is composed of the ECM, which is a network of proteins that provides physical and chemical cues determining cell behavior [114-117]. Cell biologists have analyzed numerous cytokines and soluble factors responsible for stem cell regulation, however, recent studies indicate that these soluble factors work in conjunction with the insoluble components present in the ECM such as adhesive, mechanical, and topographical cues [118-122]. Specifically, insoluble factors are made up of collagens, non-collagenous glycoproteins (laminin, elastin, fibronectin), and hydrophilic proteoglycans [123]. Stem cells can detect and respond to signals simultaneously presented in the microenvironment; cell mechanotransduction machinery converts these soluble and insoluble cues to signal upregulation of various genes and subsequent lineage commitment [122].

Past biomaterial design has focused on microscale technologies to drive stem cell lineage commitment, but the *in vivo* tissue structure also provides cues to cells at a

nanoscale level. Furthermore, cells tend to respond to some microscale fiber scaffolds the same way that they do when cultured on a 2D polystyrene cell culture plate. Cell morphology becomes flat, which causes a lopsided attachment of focal adhesions [123]. Therefore, for certain tissue engineering approaches to generate softer tissues, providing signals at the microscale level might be physiological inconsistent for directing stem cell differentiation [124]. There is a need to engineer functional nanoscale microenvironments for tissue engineering applications. The field of nanotechnology in relation to tissue engineering involves designing novel materials with at least one dimension between 1-100 nm to use as scaffolds for influencing cell behavior [125]. Section 3.5 will discuss different techniques for creating biomaterials with nanoarchitectural features.

Nano and microscale signals such as shear stress, strain, material elasticity, topographical variation, and cell shape all affect cellular function and lineage specification. Cells experience mechanical cues such as stress and strain in the *in vivo* microenvironment. Muscle contraction and relaxation, bone compression and decompression, cell migration, fluid flow, and tissue regeneration all cause variations of mechanical forces in the body. The ECM also has a range of elastic moduli that generate physical stimuli for attached cells through focal adhesions. These mechanical cues are transduced through focal adhesion kinase (FAK) and Src family signaling [122]. Furthermore, integrins are activated by stress, strain, and differing elastic moduli. This in turn increases focal adhesion strength and upregulates integrin mediated signaling throughout the cell. The biochemical pathways that are activated as a result of physical stimuli are part of a positive-feedback loop which further activates actomyosin cytoskeleton tension and increases focal adhesion strength [122, 126, 127]. As a result,

researchers have explored how varying signals alter hESC behavior *in vitro* with hopes of determining what physical forces, separately or in combination, control lineage commitment.

The effect of mechanical cues on cell function has been reviewed for many cell types, and has established general knowledge regarding cell behavioral responses [121, 128-131]. Recent studies have made great strides in determining the impact physical stimuli have on hESCs. For example, the effect of cyclic strains on hESCs inhibited differentiation and increased self-renewal [132]. This was caused by the upregulation of TGFβ1, Activin A, and nodal which initiates the phosphorylation of Smad 2/3 [133]. Another study showed that cyclic stress through integrin-mediated adhesions induces spreading of mouse ESCs and decreased the expression of pluripotency marker Oct3/4 [134].

Shear flow has also been investigated as a mechanical cue for ESCs since it is a dynamic stress found *in vivo*, most commonly exerted on cells in the circulatory system [135]. Mouse ESCs placed in a microfluidic chamber demonstrated that a higher flow rate of 1.1 μL/min produced larger, round colonies as compared to slower rates of 0.001 μL/min and 0.019 μL/min [136]. This rounded phenotype indicates decreased cytoskeletal tension. When ESCs are subjected to highly controlled shear flow they differentiate into endothelial or specialized cardiovascular cells [137, 138]. Furthermore, ESCs exposed to culture conditions with shear stress express greater levels of endothelial cell proteins CD31 and Runx1, and cells formed hematopoietic colonies [139].
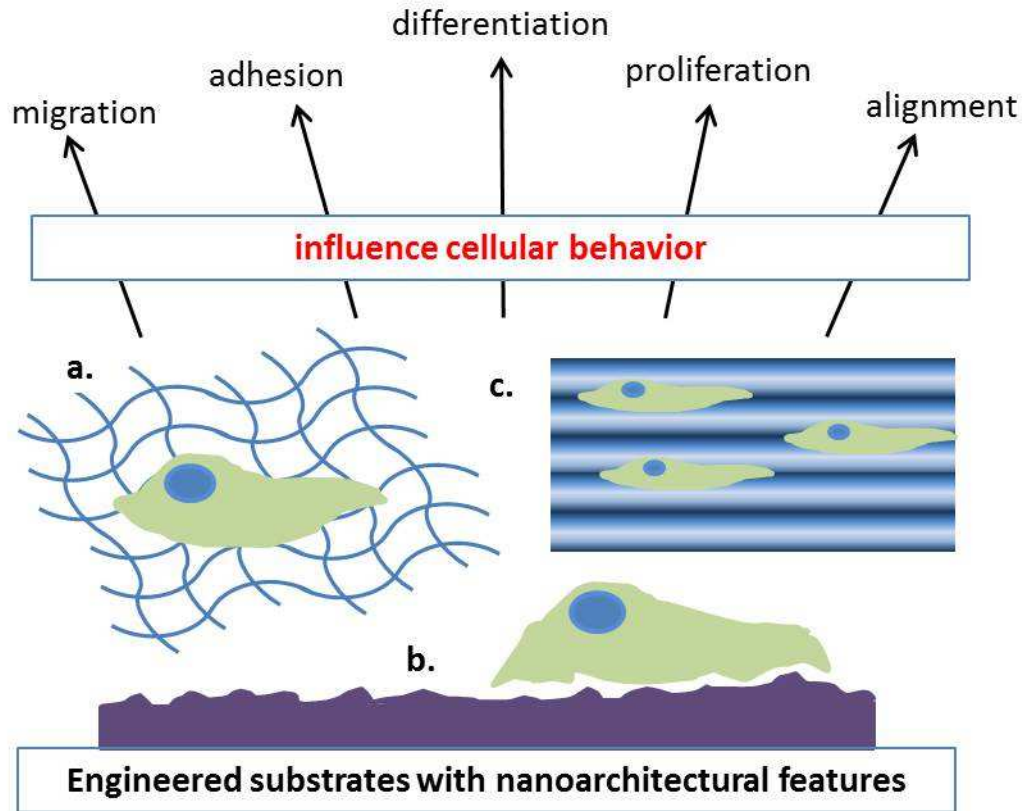
Figure 3.1 Biomaterials with (a) fibrous architecture, (b) surface roughness and varying nanotopographical features, and (c) nano grooves/ridges provide cues to cells. These microenvironmental signals, along with other mechanical cues mentioned in this review, have the ability to cause cell migration, adhesion, differentiation, proliferation, and alignment.

3.2 Material Properties Influence Cell Behavior

A recent study demonstrated that matrix elasticities of 1 kPA, 8 kPa, and 25 kPa lead hMSCs respectively towards neurogenic, myogenic, and osteogenic lineage [131]. This discovery, along with the known fact that matrix mechanics are a definitive factor in tissue morphogenesis and cell function [140-142], influenced researchers to investigate the response of ESCs to material properties.

ESCs are generally cultured on stiff 2D cell culture plates. Studies have shown that cell traction and colony stiffness increase when ESCs are grown on traditional rigid substrates, which also correlates with the downregulation of Oct3/4 in mouse ESCs [134, 143]. Cells grown on soft polyacrylamide gels with a stiffness of 0.6 kPA formed round, compact colonies that had high Oct3/4, Nanog, and Alkaline Phosphatase expression compared to the polystyrene plates with stiffness of approximately 4 MPa [143]. This study demonstrated that soft materials cause cells to exhibit low traction forces and colony stiffness, and as a result, self-renewal and pluripotency of ESCs is maintained.

3.3 Cell Shape Governs Phenotype

Stem cell shape regulates physiology, controls proliferation, and ultimately governs lineage specification [144, 145]. Cells have particular shapes that optimize carrying out specific cellular functions: neurons have long bodies to efficiently deliver signals that can span the entire length of the human figure, where adipocytes are spherical to store lipids [122]. From a developmental point of view, signals from the stem cell

niche induce conformational changes which then influence tissue structure and purpose [146-148].

One of the first experiments demonstrating the impact of cell size on behavior used 20 μm^2 and 75 μm^2 fibronectin islands to show that size directly controls apoptosis and proliferation, respectively [149]. Furthermore, studies have shown that restricting hESC colony size regulates differentiation, with smaller cell groupings favoring endoderm commitment over ectoderm [150]. Patterning adhesive ligands to control hESC colony size determined large colonies with a high cell density microenvironment promote pluripotency, controlled through a BMP-mediated Smad1 gradient. This gradient forms due to the interaction of hESCs and hESC-derived extraembryonic endoderm [151]. These findings are thought to occur due to cell-cell contact, varying mechanical stresses throughout the body of cells, and soluble factor gradients.

3.4 Substrate Topography Provides Important Cell-ECM Signals

Topography plays a key role in cell maintenance and function. Nanoscale architecture has grooves, ridges, pits, and pores *in vivo*; for example proteins in the ECM are generally arranged in a fibrous manner with these topographical properties. These fibrillar networks are approximately 10-100 nanometers but can be several microns [152, 153], and the bone marrow contains numerous nanoscale pores that provide additional cues for stem cells [135]. Nanotopography is important because cells receive signals through specific binding sites that integrins recognize, and integrin signaling is controlled through nanoscale ECM-cell interactions [124]. Surface features as small as 10 nm have

the ability to influence cell adhesion [154]. When cells bind to integrins, tyrosine kinase and phosphatase signaling is activated, and both are important for cell fate and gene expression [122]. Through these biophysical cues, stem cell adhesion and cytoskeleton organization are regulated, thus cell decisions regarding proliferation, migration, elongation, cell alignment, polarization and differentiation are impacted [152, 155-162]. Studies using MSCs determined that the nanoscale topography potentially acts through spatial control of ligands and regulatory factors, and the interplay between physical and biochemical cues determine cell morphology and phenotype [135]. This, among other principles discovered by examining hMSC response to alterations in topography, can be applied to human pluripotent stem cells (hPSCs).

Topography is a powerful tool since, not only is cytoskeleton tension altered like in cell shape experiments, but entire molecular arrangement and dynamic organization of cellular adhesion mechanisms are effected [122]. Polymethylglutarimide (PMGI) nanofibers were used as scaffolds to maintain mouse ESC stemness and it was concluded that fiber density and structure were important factors in retaining pluripotency. This study also found that mouse ESCs had the ability to differentiate into all three germ layers on this substrate [163]. Studies observing the response of hESCs to nanotopography have used fibronectin coated poly(di-methyl siloxane) (PDMS) substrates with 600 nm ridges, 600 nm spacing, and 600 +/- 150 nm height. Single cells were placed on the surface for 24 and 48 hours, and it was determined that the nanotopographic surfaces increased cell alignment and elongation, but decreased projected cell area and proliferation [164]. An experiment utilizing polyamide nanofibrillar surfaces covalently linked to FGF-2 found that this substrate enhanced

hESC proliferation [165]. The use of fibrillar nano architecture in scaffolds has the potential to spatially align and organize cells while retaining pluripotency, however cell proliferation capabilities depends on the ridge size and surface chemistry of the scaffold and must be further optimized to sustain hPSC growth.

Another study used UV-assisted capillary force lithography to create 350 nm ridge/groove pattern arrays, then demonstrated the ability of the surface topography to direct hESCs towards neuronal lineage in the absence of differentiation-inducing soluble factors [166]. Furthermore, neural differentiation of ESCs was demonstrated in an experiment using poly(L-lactic acid) (PLLA) electrospun nanofibers incorporated with single wall carbon nanotubes (SWNTs) and multi wall carbon nanotubes (MWNTs). Scaffolds containing the carbon nanotubes promoted greater differentiation towards neural lineage, shown by an upregulation of Map-2. Differentiated cells aligned on the fibers demonstrating the influence of physical cues on cell morphology and lineage commitment [167]. Another recent study also investigated the effects of topography on human iPSC differentiation towards neuronal lineage [168]. A PDMS substrate was patterned with ridges/grooves of width 350 nm and groove depth of 300 nm, then single cells were placed on the nanostructures and allowed to differentiate for 4 days. Cell alignment on the 350 nm width groove substrate was compared to surfaces with 2 μm and 5 μm widths, and it was found that cells responded with the highest degree of alignment to the nanogrooves. Additionally, human iPSCs placed on the 350 nm substrate expressed the highest levels of neuroectodermal markers NPY and SYT4, demonstrating the importance of topography in guiding pluripotent stem cell phenotype. Collectively, these results indicate that controlling hPSC alignment on nanogroove structures directs cell

differentiation towards neuronal lineage, and ESCs on random electrospun fibers incorporated with carbon nanotubes will purposefully elongate with the direction of the fibers and upregulate neuronal marker gene Map-2.

MWNT films were employed to investigate the response of hESCs to surface roughness. hESC colonies favored rougher surfaces for attachment, exhibited flattened morphology with standard colony size, and retained pluripotency when cultured on MWNT films [169]. A similar study grafted CNTs with poly(acrylic acid) (PAA) to form a thin film, and the results indicated that this substrate, in combination with neural growth factors, stimulates hESC differentiation towards neural lineage at a higher rate than a conventional poly-L-ornithine (PLO) substrate often used in generating neurons from stem cells [170]. Another study utilized an array of CNTs conjugated with ECM proteins to determine the hPSC behavioral response when cultured on this platform. This array was found to support undifferentiated hESC and iPSC growth as well as self-renewal and pluripotency marker expression [171]. Furthermore, it was shown that both types of hPSCs cultured on the CNT arrays were able to differentiate towards ectoderm, mesoderm, and endoderm lineages [171]. The hPSCs grown on the CNT arrays were then directed towards spontaneous differentiation, and in reaction to the CNT topography, preferentially expressed mesodermal markers due to the physical stimuli exerted on the cells [171]. A similar study investigated culturing hESCs on a collagen/CNT matrix. Colonies were placed on tissue culture plates coated with gelatin, collagen, and collagen/CNTs and allowed to spontaneously differentiate. Colony morphology on the gelatin substrates was random and spread out, while hESCs on the collagen as well as the collagen/CNT matrices exhibited an elongated shape that aligned with the fibrils. By day

3, hESCs on the collagen/CNT surface expressed the early neural progenitor marker nestin significantly higher than the cells on the collagen substrate. By day 6, all three groups expressed nestin, with the highest levels detected in the collagen/CNT group followed by the collagen and gelatin groups, respectively [172]. These groundbreaking studies involving CNTs have provided insight on stimuli controlling hPSC lineage specification. CNT films maintain hPSC pluripotency and undifferentiated colony phenotype, substrates containing fibrillar architecture with CNTs promote hESC differentiation towards neural lineage, and CNT arrays exert physical forces on hPSCs that guide them towards mesoderm lineage commitment.

In another study, surface nanoroughness of silica-based glass wafers was altered and hESCs were placed on the various substrates in single cells. hESCs on the control glass surface demonstrated highly branched morphology with many cytoplasmic extensions, while cells on the nanorough glass were compact with few, short filapodia. Cells on a rough surface patterned with square-shaped smooth islands favored attachment to the smooth glass instead of the nanorough areas and expressed pluripotent marker Oct3/4, and hESCs placed on an exclusively rough surface spontaneously differentiated. Proliferation of hESC colonies was determined by placing cells on smooth glass and nanorough substrates, and it was determined that doubling time of hESCs on the control surface was 41 hours compared to a slower 71 hour doubling time of colonies on the rough surface [173]. In opposition, a study showed that silica colloidal crystal with diameters of 120, 400, and 600 nm coated with collagen I maintained the expression of murine ESC markers in comparison to smooth glass. However, colonies exhibited reduced spreading on the surface with altered topography [174]. Another study coated

cell culture plates with poly[2-(methacryloyloxy)ethyl dimethyl-(3-sulfopropyl)ammonium hydroxide], then demonstrated that hESC colonies cultured on this substrate maintained their proliferation, self-renewal, and pluripotency capabilities [175]. A unique study used graphene and graphene oxide to coat glass coverslips and observed mouse iPSC behavior on the different substrates. It was found that iPSCs on the graphene and smooth glass surfaces proliferated at similar rates, but cells on the graphene oxide substrate had greater adhesion and proliferation. The graphene substrate maintained cells at an undifferentiated state, while the graphene oxide surface promoted spontaneous differentiation [176]. Overall, rough surfaces promote PSC adhesion with a more compact morphology, however, studies have found opposing evidence for whether or not nanorough surfaces maintain pluripotency and an undifferentiated state, or promote spontaneous differentiation. There are also conflicting results determining if these surfaces foster or hinder proliferation, therefore more studies are warranted to understand how PSCs respond to rough culture substrates.

3.5 Nanoscale Technologies

The *in vivo* microenvironment is composed of channels, pores, and ridges that provide physical cues to cells at a nanoscale level [124]. Knowledge of how these factors influence stem cell behavior is necessary to effectively design scaffolds that differentiate stem cells to the desired lineage. To analyze the impact of nanofeatures on cell behavior, engineers and scientists have combined principles of chemistry, physics, material science, and biology to create specialized substrates. Fabrication techniques such as soft lithography, deposition of nanostructures, microfluidics, and electrospinning all create

ways for researchers to manipulate topography [177-179]. These platforms have been used to determine specific cues that regulate stem cell function.

Electrospinning is a technique that can form a network of polymer fibers down to the size of 10 nm [180]. To generate electrospun scaffolds, a voltage is applied to a polymer solution, the charged solution is ejected though a needle, and electric forces stretch the polymer jet so that fibers with submicroscale diameters form on the grounded collector surface [181]. Since the fiber diameters are much smaller than cellular surface area, this platform allows cells to organize around the fibers [182] and attach with a spread morphology with numerous focal adhesions [183]. Another advantage of this technique is the ability to create electrospun scaffolds from synthetic as well as natural polymers [181]. However, one challenge with this fabrication method is that cells cannot migrate throughout the scaffold due to pore sizes being smaller than that of a cell [123]. Recent progress has overcome this limitation by using self-assembly of nanofibers around the cells [184]. Knowledge of protein self-assembly and optimization of noncovalent intermolecular interactions produced this revolutionary approach to forming the nanofibrillar architecture around cells without damaging them [185, 186]. This technique allows the scientist to spatially and mechanically organize cells, which is critical to tissue engineering strategies since cells in the body are arranged in specific patterns that form tissues and organs [123]. This fabrication process is able to create substrates that mimic grooves, ridges, and the fibrillar ECM structure, and recent advancements with assembling the scaffold material around target cells has overcome the previous inability of cells to infiltrate the scaffold.

The general method of soft lithography uses elastomeric stamps to print nanoscale polymers on a surface [187-190]. Patterned polymers can range from 30 nm to several microns [191]. This is a useful technique because the engineer has full control over spatial distribution of polymer molecules placed on the substrate, which subsequently determines cell spreading and shape [192-194]. Soft lithography is an invaluable tool because it creates a platform on which researchers can isolate and control mechanical cues exposed to single cells [195] and also pairs or triplets of cells [196]. This technique is very useful in deciphering cellular reactions to individual physical cues since the polymers can be easily manipulated to express specific mechanical characteristics. However, a limitation with this platform is that soft lithography is only able to provide a narrow range of ECM signals for the cell to receive, which is inconsistent with the many microenvironmental cues provided to cells *in vivo*.

Hydrogels are a popular tissue engineering scaffold with proven success in medicine and biological research due to their tunable tissue-like properties [197-201]. The goal of hydrogel design is to mimic natural ECM, which is accomplished by crosslinking polymers. The intricate linking of these hydrophilic molecules forms a network with tissue-like viscoelastic mechanical properties, as well as similar interstitial flow to the *in vivo* microenvironment. Similar diffusive transport also occurs in hydrogel cell culture platforms, and hydrogels can be designed to incorporate cell adhesion ligands and other biologically relevant components [123]. Although hydrogels are an extremely moldable substrate and offer numerous advantages as scaffolds for tissue engineering, they have low mechanical strength, they are difficult to sterilize, and loading drugs and

cells in the matrix before crosslinking the material is difficult [202, 203]. Further optimization studies are warranted to overcome these barriers.

Carbon nanotubes possess ideal qualities for tissue regeneration strategies such as tunable chemical and mechanical properties, electrical conductivity, cytocompatibility, and nanoscale dimensions that serve as topographical cues [204]. Furthermore, CNTs have numerous applications for directing cell behavior such as drug delivery, gene modifications, and incorporation in the *in vitro* 3D cell microenvironment to add roughness [205-207]. When placed in fetal bovine serum (FBS), proteins readily adsorb to the surface of CNTs subsequently promoting cell attachment [208]. Several studies have demonstrated the potential of CNTs for bone tissue engineering applications [209-212], myoblastic cell attachment and growth [208] as well as neuronal cell proliferation [213], but little is known regarding the effect of CNTs on stem cell fate. In order to hypothesize how CNTs could influence pluripotent stem cell behavior, an analysis of studies conducted on the effect of CNTs on other cell types must be done, with further scrutiny on how individual characteristics of CNTs control the cellular response. Towards this goal, a recent study has shown that the mechanical properties of CNTs promote differentiation of MC3T3-E1 osteoblasts towards osteogenic lineage [209]. A study isolating the conductivity attribute of CNTs demonstrated that multiwall carbon nanotube-incorporated hydrogels increased cell proliferation of myocytes as well as fostered the growth of multinucleated cells with higher actin filament interactions as compared to the control groups [214]. CNTs can be functionalized to exhibit varying chemical properties that influence cell phenotype, shown in a study investigating single wall carbon nanotube conjugation with poly(*m*-aminobenzene sulfonic acid) and

poly(ethylene glycol) in which neurons exposed to more positively charged groups exhibited greater neurite length and had additional growth cones [215]. Since CNTs exhibit numerous traits that have the potential to impact cell lineage commitment, there is a need to delineate the effects of each specific CNT characteristic on hPSC behavior.

Microfluidics allows for precise regulation of fluid flow and microenvironmental geometry, usually in the form of channels with similar dimensions to that of the cell type under investigation. Volumes can easily be controlled to levels of 10^{-18} liters [216], and the flow rates are manipulated so that shear stress in the *in vitro* microenvironment is optimized. Microfluidic platforms have been used extensively to study cell biology, specifically cellular adhesion forces [217], the cytoskeleton [218], and the culture of embryos [219-221]. This platform is useful in determining the influence of shear stress on individual cells, as well as mimicking the effects of capillary and interstitial flow, but the scale of this technique is not practical for larger magnitude tissue regeneration studies.

3.6 Microscale Technologies

Cellular scaffolds mimicking tissue generally have large, macroscale features that promote cell adhesion, migration, and proliferation. However, microscale features are needed to allow vascularization of thick tissue requiring higher levels of oxygen diffusion than connective tissues, such as the skin [222, 223], bladder [224], and the cornea [225, 226]. By altering the physical topography of 3D scaffold structures, cell function can be controlled through a variety of means such as cell-cell contact, cell morphology, and cell orientation [227, 228]. Micro-fabrication of vascular networks for scaffolds is generally

achieved using methods such as photolithography, 3D printing, and soft lithography [229-238]. The approach behind these methods is to allow oxygen into deeper portions of the developing tissue to stimulate *in vitro* vascularization and more efficient nutrient exchange.

Photolithography is a highly utilized approach to creating substrates for tissue engineering strategies. This method creates micro-patterned scaffolds through the use of a photomask, which is an opaque plate that allows light to pass through only at specific transparent points that are composed of patterns [239-243]. This approach uses pre-polymers that crosslink when exposed to UV light, a photomask, and a photoinitiator. When the pre-polymer is placed under the photomask, only pre-polymer that is below the transparent regions is crosslinked, polymerized, and therefore patterned through light exposure. The photoinitiator catalyzes the reaction of the pre-polymer with the UV light, and is ideally nontoxic to cells. Micro-patterning hydrogels such as poly(ethylene glycol) [244-247], methacrylated hyaluronic acid [248-251], and gelatin methacrylate [252, 253] has been successful in tissue engineering approaches. In a recent study [244], bio-active poly(ethylene glycol) diacrylate (PEGDA) was micro-patterend with adhesive ligand RGD in various concentrations and geometries. Endothelial cells were cultured on the substrates and cells formed cords resembling capillaries on 50 μm wide strips of RGD. Furthermore, cells formed cords at an RGD concentration of 20 μg/cm^2, but did not arrange in this manner at higher RGD concentrations. Photolithography is a powerful yet simple tool for studying tissue morphogenesis. The fabrication process is straightforward and provides a method to study cellular phenotype in response to microscale structures.

3D printing, or rapid prototyping, is a relatively new method of creating three dimensional objects. Rapid prototyping is an approach to fabricate 3D structures from model data usually using a layer-by-layer approach. These processes generally follow a similar pattern including the initial computer aided design (CAD) model of the part, conversion to an appropriate file format, slicing the file into thin layers for deposition, and the final layer by layer construction phase. CAD programs such as SolidWorks or AutoCad are used in the first step to create the customized part for manufacture, and then CAD files are converted to the standardized STL file format. The initial study that started the rapid prototyping methods was Charles W. Hull in 1986 who patented stereolithography (US Pat. 4,575,330). This method utilizes a layer-by-layer technique to building 3D models with photolabile polymers, or resin, that are cured when exposed to UV light. This happens with a platform that is submerged in a container of uncured resin slightly below the platform. A focused UV laser then traces out the first cross section leaving the remaining tray of resin in liquid form. The platform slowly moves down leaving the laser to trace each cross section of the part until a fully cured part remains. This approach has been used for hard tissue applications [232] as well as soft tissue applications [254-256]. For a soft tissue study [254] a group used poly(ethylene glycol) hydrogels at differing PEGDA concentrations and laser energies for use in determining hydrogel thickness. These hydrogels were used to study encapsulated cell viability in fabricated 3D PEGDA structures, which showed at least 87% viability after 24 hours, thus proving that rapid prototyping is a viable option for soft tissue engineering.

As mentioned in section 3.5, soft lithography is a valuable tool in the in the field of tissue engineering with capabilities for duplicating nanometer to micrometer structures. This is accomplished using stamps, molds, and photomasks. Furthermore, soft lithography can be combined with microfluidic methods for vascular tissue engineering strategies. This approach uses soft lithography to create branched networks mimicking *in vivo* vasculature, seeds cells on the substrates, and connects the system to a microfluidic perfusion bioreactor to replicate shear stress [257]. Furthermore, 3D vascularized scaffolds have been created by using a layer by layer microfluidic approach [237, 258, 259]. Microfluidic channels have been generated using polymers such as PDMS, PLGA, and PGS, and endothelial cells are cultured on these substrates for vascular engineering approaches [229, 260, 261]. This is a precise technique to stimulate the formation of capillaries in a way that replicates *in vivo* structures. A recent study used soft lithography techniques to pattern non-adherent agarose templates in order to recapitulate early actions of angiogenesis [262]. Human mesenchymal stem cells and human umbilical vein endothelial cells were placed on these substrates, and VEGF expression was monitored as a means of determining mechanical impacts of the microenvironment on angiogenesis.

3.7 Scaffold Design for Bone Tissue Engineering

Tissue engineering presents a new avenue for developing bone grafts by combining the use of cells, specific signaling molecules, and three-dimensional (3D) substrates [263-266]. Recent efforts towards developing bone graft substitutes focus on 3D scaffold design. The 3D matrix should mimic the structure of bone, in which porosity

and mechanical strength are important characteristics. A scaffold should also guide the integration of host cells, the differentiation of transplanted cells, and promote bone ECM formation on the surface of the substrate [267]. In this spirit, biodegradable scaffolds provide a temporary matrix for cells to attach, proliferate, and deposit ECM [268-272]. Polymers such as poly(lactic acid) (PLA), poly(glycolic acid) (PGA) and their copolymers poly(lactic-*co*-glycolic acid) (PLGA) have demonstrated success in bone tissue engineering applications due to their biocompatibility, osteoconductivity, and mechanical properties [273-277]. Various scaffold fabrication methods used in tissue engineering studies include phase separation [278], freeze drying [279], solute leaching [280] and gas foaming [281]. Newer methods such as electrospinning [282] provide a porous structure, and this technique as well as 2D patterning are becoming increasingly popular in scaffold design. The phase separation technique utilized in this presented work is depicted in Figure 3.2.

Towards this effort of directing cell behavior, various biomaterials as well as different cell types and signaling molecules have been investigated. Recent studies have examined the ability of mechanical signals to influence stem cell lineage commitment since cells in the body reside in different tissue niches with variable mechanical properties that effect cellular function. From this information, biomaterials have been designed to harness tissue-specific mechanical properties to guide stem cells to the targeted cell type. Specifically, 3D platforms with nano and microscale features are utilized since they offer a unique ability to mimic the physical cues that cells receive from their microenvironment. Researchers have developed materials with tunable matrix
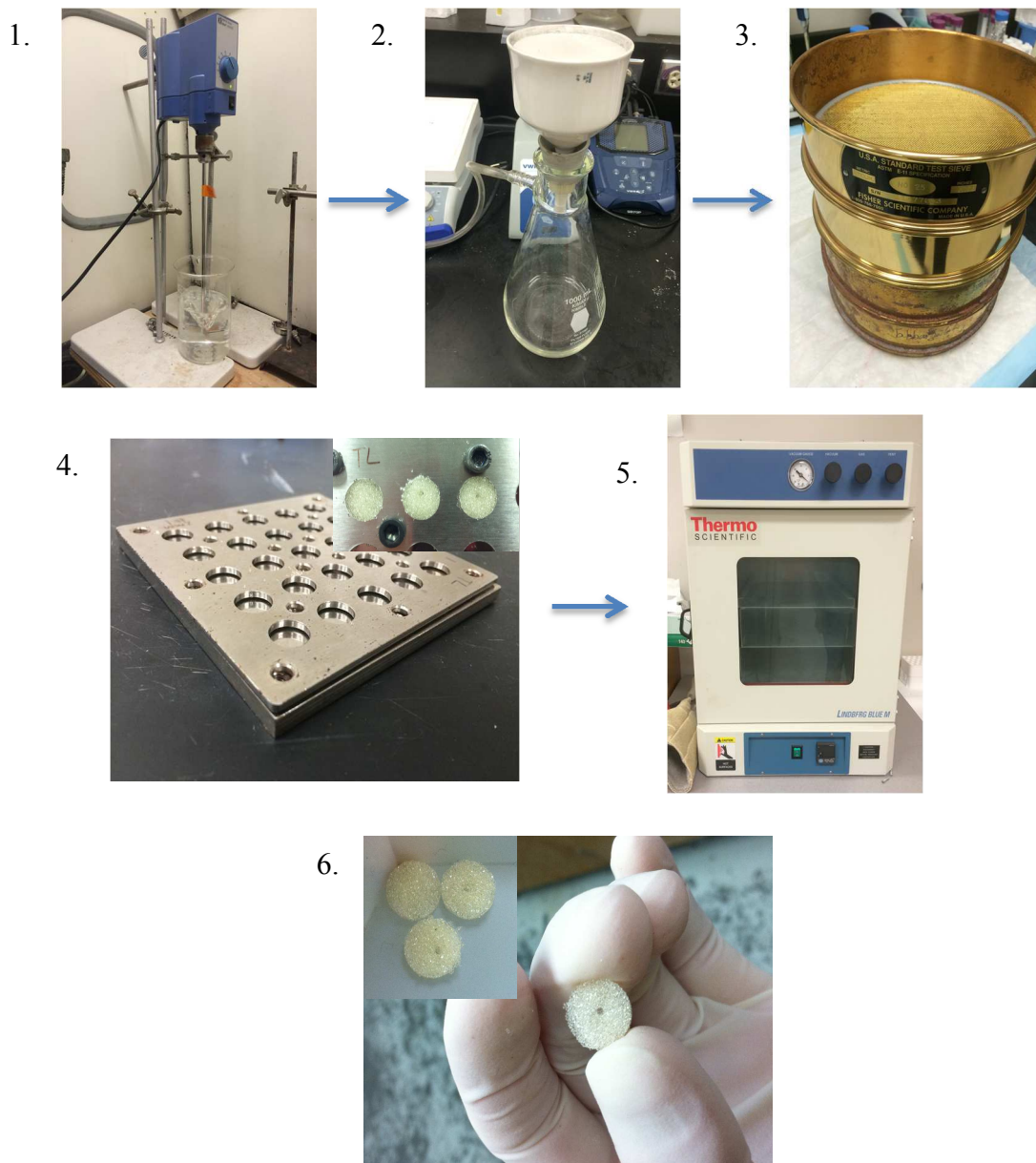
Figure 3.2 Fabrication of PLGA microsphere-sintered scaffolds. A mixture of 1:4 PLGA dissolved in dichloromethane is slowly poured into a 1% Poly(vinyl alcohol) solution stirred at 330 RPM (1). Microspheres are stirred for 24 hours, then collected via vacuum filtration (2). After a lyophilization step, microspheres are sorted according to size by using a micron sieve (3). Microspheres are placed in stainless steel molds to form scaffolds (4), and heated for 4 hours at 85 °C to sinter (5). Final scaffolds are 10 mm in diameter and 2 mm in height (6).

elasticities, nanotopographies, and nanoscale patterns that have the ability to manipulate

cell phenotype.

CHAPTER 4: DESIGN OF AN OSTEOMIMETIC SCAFFOLD FOR
ENHANCED hESC DIFFERENTIATION

4.1 Introduction

Scaffold design is a crucial component in bone tissue engineering strategies. The ideal scaffold should provide a substrate for cells to attach and proliferate, as well as direct stem cell phenotype into the desired tissue type. In this study, we developed an osteomimetic PLGA scaffold that allows for hESC attachment, proliferation, and differentiation into osteogenic lineage. As previously mentioned, hESCs require surface modification in order to be able to attach to 3D substrates. The ECM placed on the scaffold can provide signals through proteins interacting with integrins, which in turn influences cell phenotype. We hypothesized that native bone ECM deposited by human osteoblasts (hOBs) will cover the surface of microsphere-sintered PLGA scaffolds, and will direct the differentiation of hESCs into bone lineage by providing a natural bone tissue microenvironment. This hypothesis is based on studies demonstrating the use of native bone ECM components in stimulating hESCs and hMSCs to differentiate into osteoblasts [98, 99]. To this end, the properties of the osteomimetic scaffolds such as ECM composition and morphology as well as the *in vitro* differentiation of hESCs into bone tissue were investigated.

4.2 Synthesis of PLGA Microsphere-sintered Scaffolds

Scaffolds with diameters of 10 mm and heights of 2 mm were fabricated and used in this study. Briefly, PLGA (75:25 lactide to glycolide ratio) (Lactel Absorbable Polymers) was dissolved in dichloromethane (Sigma) to form a 1:4 w/v polymer solution. This solution was added to a 1% poly(vinyl alcohol) solution (Sigma) while being stirred at 330 rotations per minute (RPM) for 24 hours to allow for adequate evaporation of the solvent. After harvesting the microspheres by vacuum filtration, the samples were washed with deionized (DI) water and stored at -20°C for 24 hours. The microspheres were lyophilized to completely remove all moisture. Commercially available micron sieves were used to isolate microspheres of diameter 500-700 μm and they were placed into stainless steel molds, heated at 85°C for 12 hours, and sintered into cylindrical disks.

4.3 Human Osteoblast (hOB) Cell Culture and PLGA Scaffold Seeding

P3 human osteoblasts hFOB 1.19 (ATCC) were cultured in osteogenic differentiation medium consisting of DMEM/F12 (Gibco), 10% FBS (Atlas), 10 mM β-glycerophosphate (Sigma), 50 μg/mL ascorbic acid (Sigma), 1 μM dexamethasone (Sigma), and 1% penicillin/streptomycin (Invitrogen). Medium was changed every other day and cells were passaged once 80% confluency was reached. After two passages, hOBs were trypsinized and seeded on the scaffolds.

Before seeding hOBs on the PLGA substrates, scaffolds were sterilized by immersion in 70% ethanol for 10 minutes, washed 3x with phosphate buffered saline (PBS), and exposed to UV light for 30 minutes on each side. hOBs were detached from

the culture flask using trypsin and 20 μL (containing 5 x 10^5 cells) of cell suspension were seeded per scaffold. Cells were cultured in osteogenic medium for 14 days and culture medium was changed every other day.

Cell attachment and proliferation was analyzed during the 14 day culture period using [3-(4,5-dimethylthiazol-2-yl)-5-(3-carboxymethoxyphenyl)-2-(4-sulfophenyl)-2H-tetrazolium (MTS) (Promega) colorimetric assay. 300 μL of fresh media was added to each scaffold, and incubated for 2 hours with 60 μL of MTS solution. The resulting solution was diluted 1:5 and the absorbance was read at 492 nm using a UV Vis Spectrophotometer.

4.4 Decellularization and Analysis

PLGA scaffolds were decellularized by adding a sterile solution of 0.25% Triton X-100 (Sigma) and 0.25% deoxycholate (Alfa Aesar) dissolved in PBS for 30 minutes at 4°C, followed by incubation at 37°C for several hours. The decellularization solution was removed and scaffolds were washed 3x with PBS.

Decellularized scaffolds were characterized by Alizarin Red S staining, calcium quantification, alkaline phosphatase (ALP) staining, collagen II staining, and scanning electron microscopy (SEM). To visualize the mineralized ECM, samples were first fixed in 10% formalin for 30 minutes and washed 3x with DI water. Alizarin Red S staining solution (pH 4.2-4.5) (Alfa Aesar) was added to the samples at a concentration of 0.02 mg/mL and incubated for 5 minutes. Samples were washed for 5 hours in 100% ethanol

and ethanol was changed every 30 minutes. Mineralized ECM was visualized with a Zeiss light microscope. To quantify the mineralized calcium, the O cresolphthalein complexone (Sigma) method was used. DI water was used to wash the scaffolds 3x, and 0.6 mol/L hydrochloric acid was employed to homogenize the samples followed by 4 hours of shaking at 4 °C for calcium extraction. The amount of calcium was determined by reading the absorbance at 570 nm with a UV Vis spectrophotometer. Alkaline phosphatase was detected by using alkaline phosphatase kit #85 (Sigma) in which scaffolds were fixed with 10% formalin for 30 minutes and washed 3x with PBS. The Fast Blue capsule was dissolved in napthanol to prepare the staining solution, added to the scaffold, and incubated for 30 minutes. The scaffolds were washed 3x with PBS followed by incubation in the Mayer's Hematoxylin solution for 10 minutes. ALP was observed and photographed using a Nikon E600 light microscope. To determine collagen II expression, scaffolds were fixed in 10% formalin for 30 minutes and washed 3x with PBS. After washing, scaffolds were permeabilized using 0.1% Triton X-100 solution for 15 minutes. Cells were washed 3x with PBS and blocked using 1% bovine serum albumin (BSA) (Sigma) in PBS for 30 minutes. FITC-conjugated anti-collagen II antibody (1:100) (Thermo) was added to the scaffolds for 1 hour followed by washing 3x with PBS. Cell nuclei were stained by adding 4'-6-diamidino-2-phenylindole (1:25) (DAPI) (Sigma) antifade to the decellularized constructs. The samples were visualized using a Zeiss 510 LSM confocal microscope and a water immersion lens. For SEM analysis, cells on the scaffolds were fixed in 1% glutaraldehyde for 1 hour followed by fixation in 3% glutaraldehyde at 4°C overnight. The scaffolds were dehydrated sequentially by a series of increasing ethanol concentrations (10, 30, 50, 70, 90, 95, 95,

100, 100%) for 15 minutes each. PGLA scaffolds were dried overnight and coated with gold/palladium. Scaffolds were observed under Zeiss Ultra Plus FESEM after coating.

4.5 hESC Seeding

hESCs from cell line h9 (Wicell) p38 were grown on a feeder layer of mitomycin C inactivated mouse embryonic fibroblasts (cell line PMEF-CFL) (Millipore) in medium consisting of DMEM/F12 (Gibco), 20% Knock-out serum replacement (Gibco), 3.5 mM L-Glutamine (Invitrogen), 100 μM β-mercaptoethanol (Sigma), 1% non-essential amino acids (Invitrogen), and 10 ng/mL bFGF (Peprotech). The PMEF cell line was used as a feeder layer and cultured in high glucose with L-glutamine DMEM (Gibco) supplemented with 10% FBS and 1% penicillin/streptomycin (Invitrogen). Mitomycin C (10 mg/mL) (Sigma) was used to inactivate PMEF cells for 2.5 hours, after which cells were seeded at a density of 2.1 x 10^4 cells/cm^2 on tissue culture plastic coated with 1% gelatin (Sigma). Cells were cultured for 1 day in PMEF media prior to hESC seeding. hESCs were detached from the tissue culture plate by a combination of the enzyme collagenase IV (Sigma) and by manually scraping. Approximately 50,000 hESCs were seeded per scaffold, and conditioned medium was used to ensure cell attachment overnight. The following day, culture medium was changed from conditioned medium to osteogenic differentiation medium. Osteogenic differentiation medium was changed the following day to remove cell debris, then every 3 days for the remainder of the experiment.

For the control groups, two dimensional (2D) tissue culture polystyrene (TCPS) and Geltrex-coated PLGA scaffolds were used. To coat the PLGA scaffolds and 2D culture plates, 2.5 µL of Geltrex (Invitrogen) was mixed with 1 mL of cold DMEM/F12, added to the scaffolds and plates, and incubated at 37°C for 1 hour, then incubated at room temperature for 1 hour. Approximately 50,000 hESCs were seeded per well of a 24-well plate, and per Geltrex-coated PLGA scaffold.

4.6 Cell Attachment, Growth, and Morphology

At predetermined time points, cell morphology was assessed using SEM. Cells on the scaffolds were prepared as previously described and observed under a Zeiss Ultra Plus FESEM after coating.

Cell proliferation on scaffolds was assessed using [3-(4,5-dimethylthiazol-2-yl)-5-(3-carboxymethoxyphenyl)-2-(4-sulfophenyl)-2H-tetrazolium (MTS) (Promega) colorimetric assay. 300 µL of fresh media was added to each scaffold, and incubated for 2 hours with 60 µL of MTS solution. The resulting solution was diluted 1:5 and the absorbance was read at 492 nm using a UV Vis Spectrophotometer.

Cytoskeleton formation was observed by F-actin staining. Cells on the scaffolds were fixed at room temperature in 10% formalin for 30 minutes. After washing scaffolds 3x with PBS, cells were permeabilized using a 0.1% Triton X-100 solution for 15 minutes. Cells were then washed 3x with PBS and blocked using 4% Goat Serum in PBS for 30 minutes. TRITC-conjugated phalloidin (1:40) (Invitrogen) was added to the scaffolds for 1 hour, samples were washed 3x with PBS, and cell nuclei were stained with

4'-6-diamidino-2-phenylindole (1:25) (DAPI) (Sigma). Stained cells were visualized using a Zeiss 510 LSM confocal microscope under a water immersion lens.

4.7 Assessment of Osteogenic Differentiation

Osteogenic differentiation was assessed by monitoring the calcium deposition, osteocalcin expression, and qRT-PCR analysis of RUNX2 and BGLAP genes.

Calcium was quantified using the O cresolphthalein complexone (Sigma) method. At predetermined time points, cell culture medium was removed from the scaffolds and cells were washed 3x with DI water. 0.6 mol/L hydrochloric acid was used to homogenize the samples followed by 4 hours of shaking at 4 °C for calcium extraction. Samples were compared against $CaCl_2$ standards and the amount of calcium was determined by reading the absorbance at 570 nm with a UV Vis spectrophotometer.

ECM mineralization was assessed using Alizarin Red S staining. Samples were fixed in 10% formalin for 30 minutes and washed 3x with DI water. Alizarin Red S staining solution
(pH 4.2-4.5) (Alfa Aesar) was added to the samples at a concentration of 0.02 mg/mL and incubated for 5 minutes. Samples were washed for 5 hours in 100% ethanol, and ethanol was changed every 30 minutes. Mineralized ECM was visualized with a Nikon E600 light microscope.

Osteocalcin was qualitatively observed by immunofluorescence staining. In brief, cells were fixed in 10% formalin for 30 minutes, followed by washing 2x with a rinse

41

buffer (20 mM Tris-HCL and 0.05% Tween- 20 in PBS) (Sigma). The sample was then permeabilized with 0.1% Triton X-100 (Sigma) in PBS for 15 minutes, and washed 2x with the rinse buffer. Cells were blocked with 4% goat serum in PBS for 30 minutes. The primary antibody, osteocalcin (1:50) (R&D Systems), was added to the scaffolds and incubated for 60 minutes. Following the primary antibody incubation, the samples were washed 3x with the rinse buffer for 5 minutes each time. Then Alexafluor 594 (1:1000) (Invitrogen) was added to the samples and incubated for 1 hour, followed by 4'-6-diamidino-2-phenylindole (1:25) (DAPI) (Sigma) nuclear stain. Stained cells were visualized using a Zeiss 510 LSM confocal microscope under a water immersion lens.

Total RNA was extracted from the samples using the GeneJET RNA Purification Kit (Thermo Scientific). One μg of RNA was used as a template for single-strand cDNA synthesis with the RevertAid First Strand cDNA Synthesis Kit (Thermo Scientific). In brief, RNA was prepared by first removing genomic DNA from the sample. The reaction buffer with $MgCl_2$, DNase I, and nuclease-free water was added to 1 μg of RNA to a total volume of 10 μL. The sample was incubated at 37 °C for 30 minutes, then 1 μL 50 mM EDTA was added and incubated at 65 °C for 10 minutes. The template RNA was mixed with 1 μL oligo $(dT)_{18}$ primer and nuclease-free water to a volume of 12 μL, followed by the addition of 4 μL of 5x Reaction Buffer, 1 μL Ribolock RNase Inhibitor, 2 μL 10 mM dNTP Mix, and 1 μL RevertAid M-MuLV Reverse Transcriptase. This mixture was then incubated at 42 °C for 1 hour. The SensiFAST SYBR No-ROX Kit (Bioline) was used for qPCR. 100 ng of cDNA was mixed with 10 μL 2x SensiFAST SYBR No-ROX Mix, 10 μM forward primer, 10 μM reverse primer, (see Table 1 for sequences) and nuclease-

free water to 20 μL. A 3-step cycling was used on a Bio-Rad CFX96 instrument: 1 cycle of 95 °C for 2 minutes to activate the polymerase, followed by 40 cycles of 95 °C for 5s to denature, 65 °C for 10s for annealing, then 10s at 72 °C for extension. Gene expression of RUNX2 and BGLAP were normalized to GAPDH and presented as relative values.

4.8 Statistical Analysis

Three samples (n=3) were analyzed per condition unless otherwise stated. Error bars in graphs represent mean ± standard deviation (SD). One-way analysis of variance (one-way ANOVA) was used to determine statistical significance. Comparison between the two means was determined by the Tukey test and statistical significance was defined as $p \leq$ 0.05.

4.9 Results

Figure 4.1 demonstrates the growth of hOBs on PLGA scaffolds during the 14 day culture period. The number of cells was determined for days 1, 4, 7, and 14. Cells attached to the scaffolds and cell number steadily increased at each sequential time point. From this assay it was confirmed that cells were proliferating, therefore depositing ECM on the substrate.

Table 4.1 Primer sequences used in qRT-PCR to analyze osteogenic differentiation of hESCs on osteomimetic PLGA.

Primer Name	Sequence
RUNX2 Forward	5'-CTC ACT ACC ACA CCT ACC TG-3'
RUNX2 Reverse	5'-TCA ATA TGG TCG CCA AAC AGA TTC-3'
BGLAP Forward	5'-GGC GCT ACC TGT ATC AAT GG-3'
BGLAP Reverse	5'-TCA GCC AAC TCG TCA CAG TC-3'

Figure 4.2 shows characterization of the microsphere-sintered PLGA scaffolds. The scaffolds were all highly porous with interconnected structures, and demonstrated similar architecture to that of trabecular bone. SEM images of decellularized scaffolds (Figure 4.2A) showed ECM deposition covering the surface of the microspheres, with collagen fibrils clearly defined. Alizarin Red S staining indicated the presence of calcium in the mineralized ECM (Figure 4.2B), while collagen II staining demonstrated the presence of collagen II in the ECM (Figure 4.2C). The enzyme ALP was also found on the surface of the decellularized PLGA scaffolds, as shown by the purple/blue stain indicative of ALP (Figure 4.2D). The quantification of the mineralized calcium on the decellularized scaffolds indicated that an average of 1.17 µg of calcium was present per construct.

Figure 4.3 demonstrates cell attachment and morphology of hESCs (Figure 4.3A), and proliferation and morphology of hESC-derived osteogenic progenitors (Figure 4.3B). The hESC colonies were able to attach to the decellularized matrix, initially in large, compact colonies (Figure 4.3A). They continued to grow and spread, and after 7 days the cells no longer exhibited an undifferentiated hESC phenotype (Figure 4.3B). The cells formed bridges between microspheres and fully covered the scaffold surface at day 35 (Figures 4.3C and 4.3D). Cell proliferation was monitored by the MTS assay, and in all conditions, cells increased in number (Figure 4.4). Interestingly, the decellularized scaffold group had the highest cell numbers compared to the Geltrex-coated PLGA group, with the exception of day 7. Cytoskeleton organization and morphology was observed by SEM and immunofluorescence staining of F-actin and DAPI (Figure 4.5A
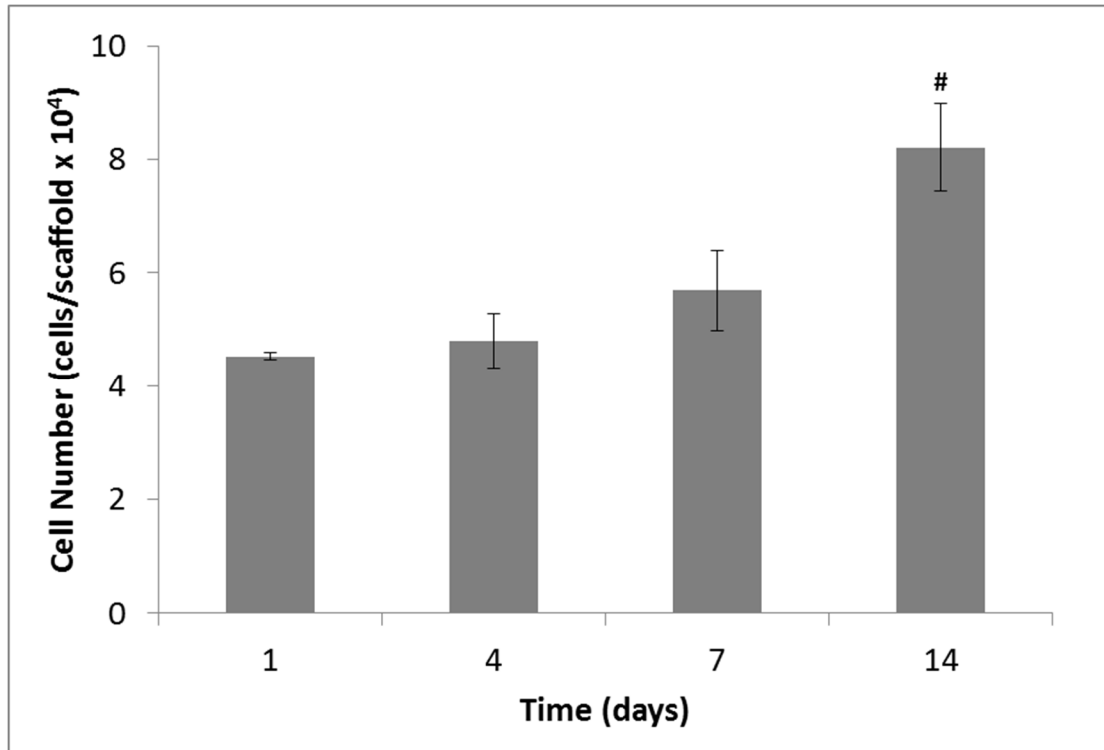
Figure 4.1 Proliferation of hOBs on PLGA scaffolds at time points of day 1, day 4, day 7, and day 14. Cell number steadily increased during the 14 day culture period. # represents a significant difference in cell number between day 14 and day 1 at a significance level of p<0.2.
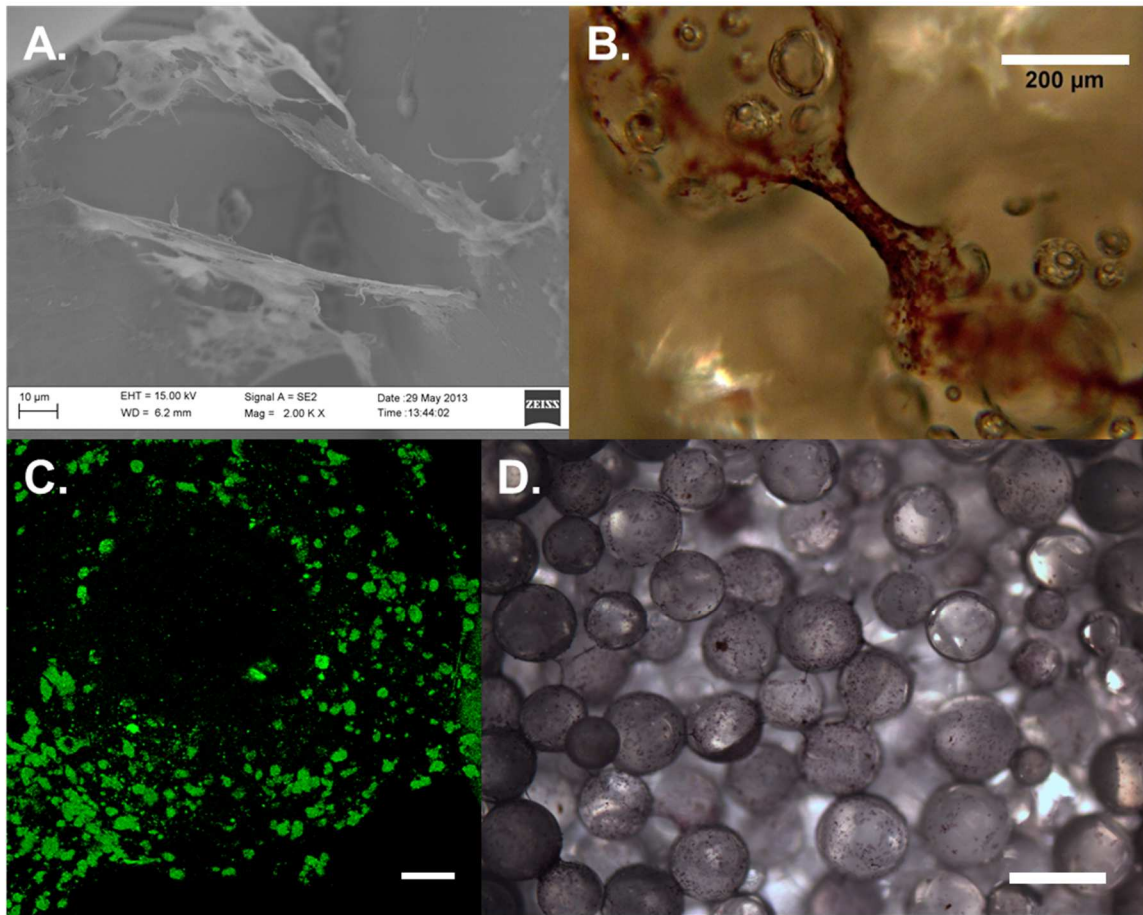
Figure 4.2 Analysis of osteomimetic scaffolds. (**A**) SEM image of ECM covering surface of PLGA scaffold, scale bar 10 μm and magnification 2000x; (**B**) Alizarin Red S staining of calcium depostited by hOBs on scaffold surface, scale bar 200 μm and magnification 10x; (**C**) Collagen II staining of ECM confirms ECM composition, scale bar 50 μm and magnification 20x; (**D**) ALP staining of ECM covering surface of PLGA scaffold, scale bar 500 μm and magnification 4x.

and 4.5B, respectively). We observed that the cells proliferated on the surface of the scaffolds and within the pores, and there was no noticeable variation in cytoskeleton structure and morphology among the groups.

Osteogenic differentiation was assessed by observing calcium content, osteocalcin expression, and qRT-PCR to quantify osteogenic marker genes. The highest level of calcium content was expressed by the hESCs on the decellularized scaffolds, followed by the Geltrex-coated PLGA group, with the 2D TCPS group demonstrating the least amount of mineralized matrix (Figure 4.6A). The immunofluorescence staining of the differentiated cells on the scaffolds showed that osteocalcin was present in the differentiated hESCs on the decellularized scaffolds, Geltrex-coated PLGA scaffolds, and 2D TCPS. The highest level of osteocalcin was detected in the decellularized scaffold, as shown in figure 4.5C. In order to quantitatively evaluate the marker genes indicative of osteogenic differentiation, qRT-PCR was employed. It was found that the decellularized scaffolds as well as the PLGA scaffolds exhibited the highest expression of RUNX2 as compared to the 2D culture plate (Figure 4.6B). BGLAP levels were the highest in decellularized scaffolds, followed by the PLGA scaffolds and 2D TCPS (Figure 4.6C).
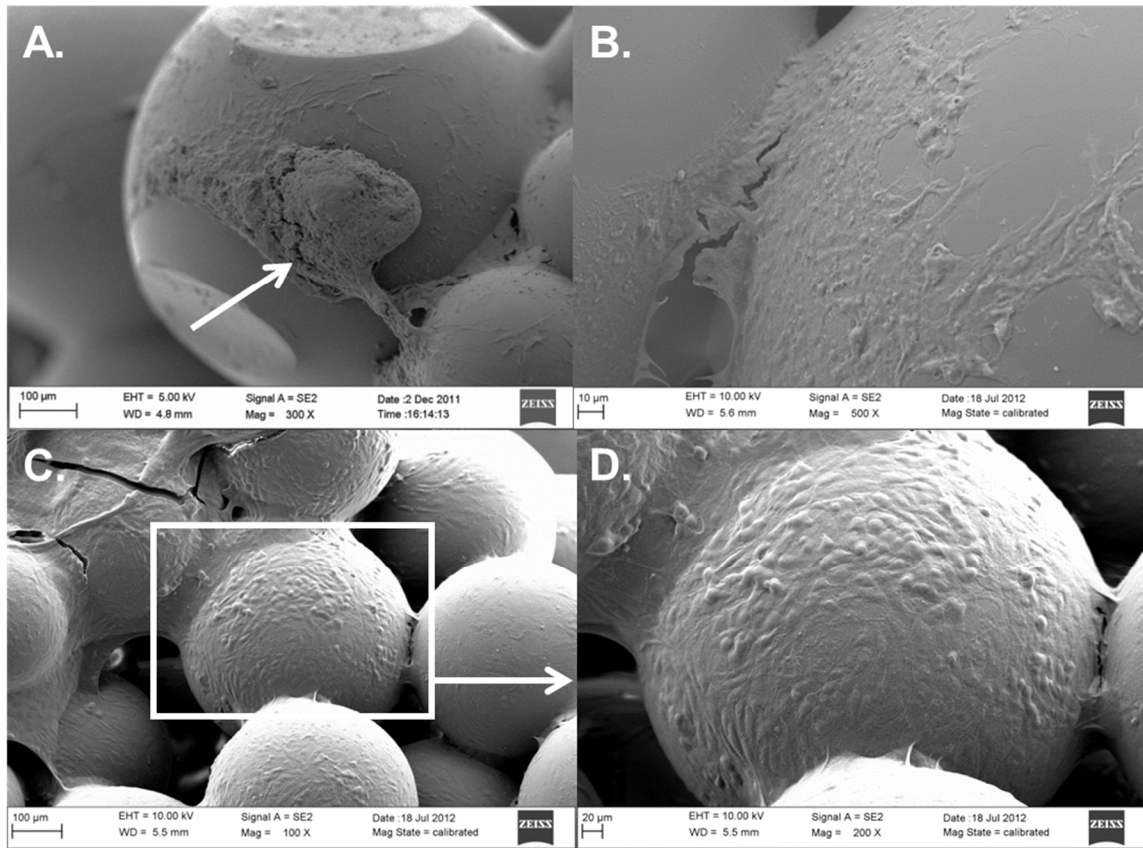
Figure 4.3 SEM images of hESCs and hESC-derived osteogenic progenitors on osteomimetic scaffolds. (**A**) Day 0 shows colony attachment, indicated by white arrow, scale bar 100 μm and magnification 300x; (**B**) Day 7 demonstrates the onset of differentiation, scale bar 10 μm and magnification 500x; (**C**) Day 35 shows differentiated cells with osteoblast-like morphology, scale bar 100 μm and magnification 100x; (**D**) Day 35 differentiated hESCs, scale bar 20 μm and magnification 200x.
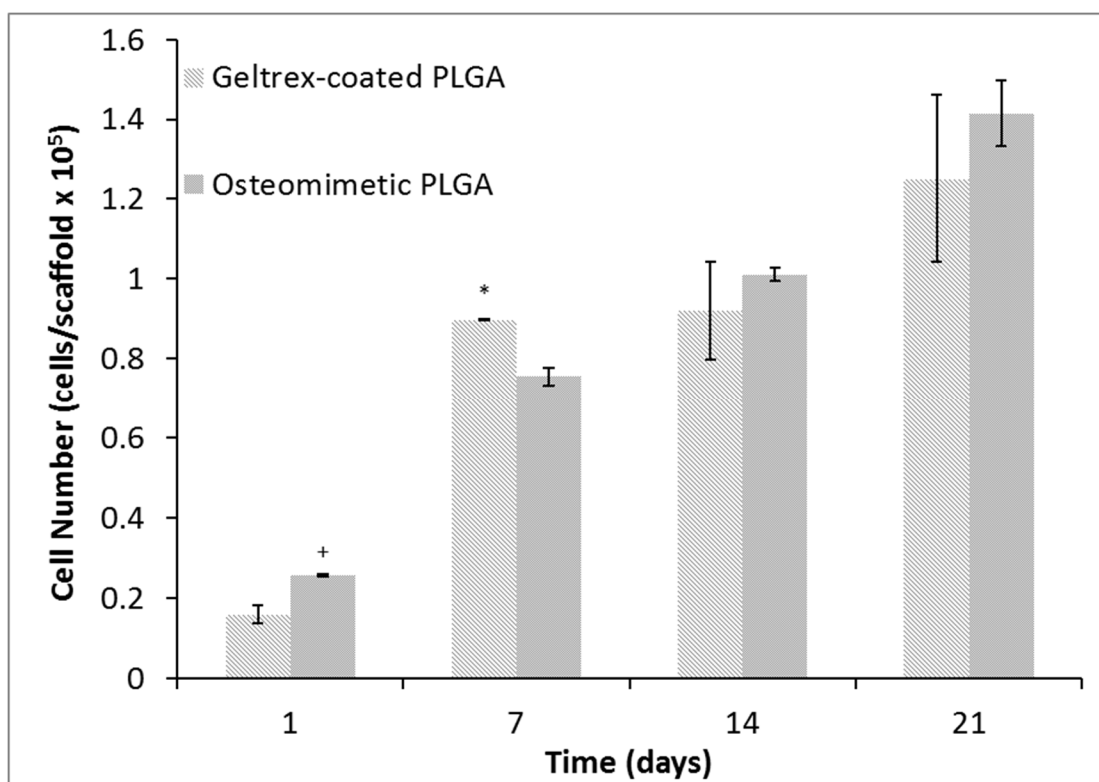
Figure 4.4 Proliferation of hESCs on Geltrex-coated PLGA and osteomimetic scaffolds, shown as cell number/scaffold. * and + represent significant difference in cell number between the Geltrex-coated PLGA and the osteomimetic scaffolds at significance levels of $p<0.05$ and 0.1, respectively.
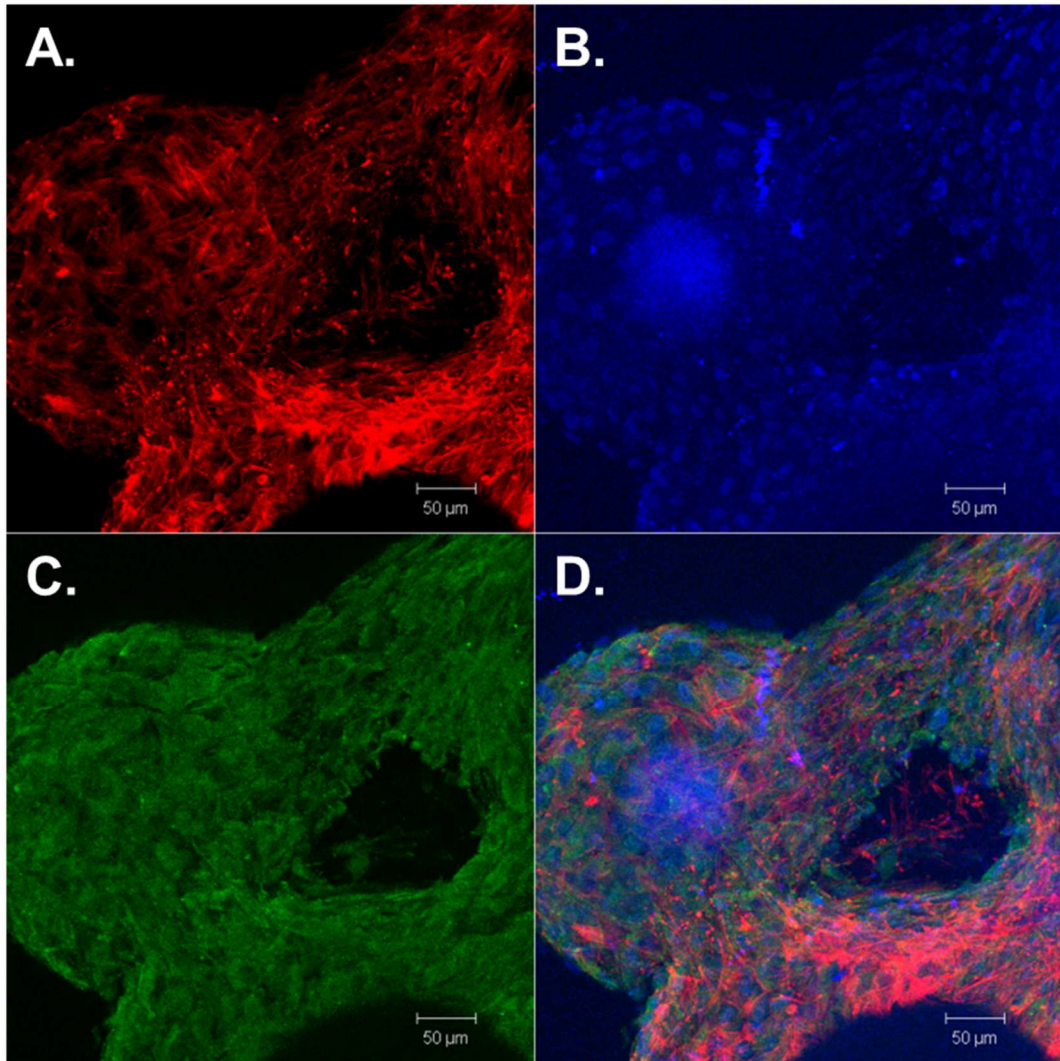
Figure 4.5 Confocal images of day 35 differentiated hESCs on osteomimetic PLGA, scale bars 50 μm and magnification 20x. (**A**) Actin demonstrates cytoskeleton formation; (**B**) DAPI shows nuclear staining; (**C**) Osteocalcin expression; and (**D**) a merged image of actin, DAPI, and osteocalcin.
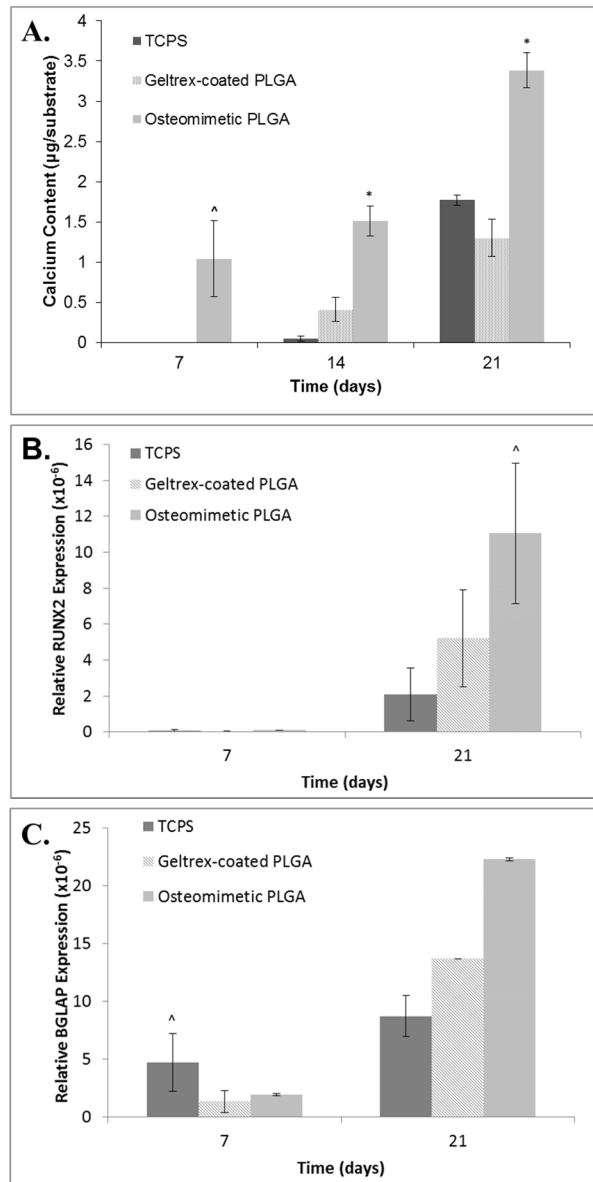
Figure 4.6 Calcium deposition and gene expression of differentiated hESCs on 2D culture plates, Geltrex-coated PLGA, and osteomimetic PLGA. *, +, and ^ represents significant difference in calcium content and gene expression by cells on osteomimetic scaffolds compared to Geltrex-coated PLGA and 2D tissue culture plates at significance levels of $p < 0.05$, 0.1, and 0.5, respectively. (**A**) Calcium quantification for each group represented as μg/substrate where the substrate is the scaffold for the osteomimetic PLGA and geltrex-coated PLGA groups, and the 2D well surface for the TCPS group; (**B**) Relative RUNX2 gene expression (n=2); (**C**) Relative BGLAP gene expression (n=2). All values were normalized to GAPDH.

4.10 Discussion

The ability to develop a 3D porous scaffold with comparable mechanical and structural properties to that of natural bone governs the success of many bone tissue engineering endeavors. Bone is a complex tissue composed of an architectural hierarchy: (i) the macrostructure which is made up of cortical and cancellous bone, (ii) the microstructure which is composed of osteons, haversian systems, and trabeculae, (iii) the submicrostructure which is comprised of the lamellae, (iv) the nanostructure which is predominately composed of collagen I fibers, and (v) the sub-nanostructure made up of mineralized matrix, smaller collagen subunits, and other organic proteins [15]. Due to this intricate tissue configuration, recreating bone structure is a major hurdle in generating scaffolds. Another obstacle in bone tissue engineering studies is deciphering specific roles of scaffold design parameters governing *in vitro* osteogenic differentiation and *in vivo* osteointegration.

The research work described in this study centers in on designing an osteomimetic scaffold composed of microsphere-sintered PLGA scaffolds and native bone ECM components secreted by osteoblast cells. These scaffolds were then applied to an *in vitro* study that analyzed the osteogenic differentiation of hESCs seeded on these decellularized scaffolds as compared to the control Geltrex-coated PLGA scaffolds and 2D tissue culture polystyrene group. It was hypothesized that hESCs seeded on the native bone ECM scaffolds would exhibit faster osteogenic differentiation as well as greater expression of mineralized matrix, higher levels of osteocalcin expression, and greater

levels of bone marker genes such as RUNX2 and osteocalcin. A rationale for this work was based off of recent studies that demonstrated the potential of decellularized bone matrices in directing the differentiation of hESCs and hMSCs into osteogenic lineage [98, 99].

In this study, we used microsphere-sintering to develop scaffolds. This fabrication technique produces scaffolds of tunable porosity and mechanical strength within the range of trabecular bone [276, 283]. Osteoblasts readily attach to PLGA substrates through proteins in the FBS adsorbing to the surface of scaffolds allowing for integrin-ligand interactions, however hESCs need surface modifications in order to adhere to the scaffolds. To alter the surface of the substrate for promoting the attachment of hESCs, a native bone microenvironment was generated by seeding hOBs on the PLGA scaffolds, then removing the cells while leaving the ECM intact. During the 14 day culture period, hOBs proliferated on the scaffolds and deposited ECM on the surface of the substrate. The ECM secreted by the osteoblasts contained calcium, alkaline phosphatase, collagen II, and other proteins found in bone structure. Since bone is formed via endochondral ossification in the embryo, the collagen II structure laid down by the hOBs is thought to stimulate the natural signaling pathways for hESCs to differentiate into osteogenic lineage [284].

Cell attachment and morphology was assessed by using SEM. Cell shape is indicative of adhesion since cells that have a spread-out morphology have more focal adhesions and greater cell-substrate contact than cells exhibiting a round morphology. Differentiated hESCs on the Geltrex-coated PLGA scaffold and decellularized PLGA scaffold demonstrated a spread phenotype, and the cells were able to migrate throughout the

54

scaffold by forming extensions between adjacent microspheres. This result is consistent with previous studies demonstrating the proliferation of primary fibroblasts and osteoblasts on PLGA microsphere-sintered scaffolds [276, 283, 285].

In line with other studies, our *in vitro* evaluation of the decellularized scaffolds demonstrated a higher level of osteogenic differentiation as compared to the control groups. hESCs underwent differentiation over a 35 day period as a result of physical cues from the native ECM scaffolds and chemical growth factors in the differentiation media. The extent of differentiation was measured by quantifying calcium expression, as well as immunofluorescence staining of osteocalcin and by analyzing gene expression of osteocalcin and RUNX2 by qRT-PCR. Common methods of analyzing osteogenic differentiation include quantifying alkaline phosphatase, collagen I, non-collagenous proteins such as osteocalcin, and the existence of bone apatite [286]; however these qualities are not unique to bone-forming osteoblasts. The most stand-alone method of determining osteoblast differentiation besides analyzing mRNA is the observation of a cell-mediated calcified extracellular matrix [287]. We determined calcium content of each experimental group, and the osteomimetic scaffolds expressed the highest amount as compared to the 2D control and Geltrex-coated PLGA scaffolds. Our study showed that 3D microenvironments produced from microsphere-sintered PLGA scaffolds generates a higher level of hESC differentiation into osteogenic lineage as compared to cells grown on 2D tissue culture plates. Furthermore, our results from these tests demonstrate that the presence of native bone ECM on 3D PLGA scaffolds leads to an elevated expression of osteogenic markers. RUNX2 is the main transcription factor for the osteoblast, and it is exclusively required for osteoblast differentiation [97]. RUNX2 expression determines

osteogenic lineage commitment, therefore the upregulation of RUNX2 mRNA quantified by qRT-PCR demonstrates the differentiation of hESCs into osteoblasts.

The advantage of our synthetic scaffolds coated with bone ECM is that we can design the polymer to mimic the structure of trabecular bone while exhibiting similar mechanical properties. This eliminates the risk of immunogenicity associated with using bone from humans or animals that has been decellularized. Decellularized scaffolds offer a native bone microenvironment in which stem cells can receive signals from the proteins and embedded growth factors. These signals govern cell type and function.

The enthusiasm for using hESCs as a source for bone tissue is hindered by ethical concerns as well as the need to establish protocols to obtain a homogenous population of differentiated cells [83, 288]. Also, the risk of teratoma formation is a major issue in using hESCs *in vivo* [289, 290]. Future directions of this study include delineating the mechanisms by which native bone ECM components and architecture modulates the osteogenic differentiation of hESCs. This will enable us to design a scaffold that induces cells to exclusively form components of bone and it will ensure that teratoma formation will not occur.

4.11 Conclusions

In this study, osteomimetic PLGA scaffolds were fabricated by microsphere-sintering and by utilizing hOBs to deposit bone ECM on the surface of the polymer. The native bone ECM substrates resembled bone tissue in composition. The potential of these scaffolds as bone graft substitutes was evaluated by the *in vitro* differentiation of hESCs on the osteomimetic substrates as well as Geltrex-coated PLGA and 2D tissue culture

plates. Our results demonstrated that the decellularized scaffolds promoted cell adhesion, proliferation, and osteogenic differentiation. Incorporating native components of bone-ECM with PLGA scaffolds has proven to be a successful approach to tissue engineering bone. A more detailed study is warranted to parse the *in vivo* mechanisms by which ECM proteins regulate osteogenesis.

CHAPTER 5: RESVERATROL AS A STIMULATOR OF OSTEOGENESIS AND
MODULATOR OF INFLAMMATION

5.1: Introduction

Tissue engineering offers a revolutionary approach to restore bone tissue and heal critical-size defects resulting from trauma, infection, tumor resection or other musculoskeletal diseases [1]. This is traditionally accomplished by utilizing a combination of biomaterials, cells, and signaling factors. Biomaterials provide a three-dimensional substrate with specific engineered characteristics for cells to attach and proliferate. Growth factors supply essential signaling cues for cells to migrate and differentiate into the desired tissue type. Cells seeded on 3D biomaterials contribute to the healing process through signaling events that guide newly formed tissue integration with the host tissue.

The success of tissue engineering strategies is contingent on the ability of blood vessels to form within the scaffolds and supply nutrients to the transplanted cells [291]. This process is controlled through a cascade of events that are mediated by chemotaxis and the host inflammatory response. Inflammation is the process by which the body protects itself from intruders, and if left uncontrolled, potentially interferes with the integration of implanted biomaterials. The complicated interplay of immune cells and signaling molecules at the interface of an implanted engineered graft must be parsed in

order to effectively design a method to harness host inflammation to promote wound healing.

As mentioned in Chapter 1, Section 3, the body responds to an implanted biomaterial with a critical sequence of the host immune reactions. The host inflammatory response is commonly initiated when native vasculature is disrupted, and the release of serum proteins from the vasculature adsorb to the implanted biomaterial surface. This forms the provisional matrix composed of fibrin, platelet granule components such as thrombospondin, TGF-α, TGF-β, PDGF, PF4, and ECGF1 [28]. Monocytes exit the capillaries, differentiate into pro-inflammatory M1 macrophages, and attach to the provisional matrix. The secretion of cytokines such as TNF-α, IL-1β, IL-6, and MCP-1 drives the acute inflammation response [29, 30]. Following the acute inflammatory response, chronic inflammation manifests at the biomaterial-host interface. This is defined by the presence of macrophages, monocytes, lymphocytes, blood vessel proliferation, and connective tissue formation [31-34]. Foreign body giant cells and macrophages will exist at tissue-implant interface for the duration of the biomaterial's lifetime [35-39]. A fibrous capsule forms as a result, separating the biomaterial from the host tissue [28]. In some tissue types, acute inflammation stimulates M1 pro-inflammatory macrophages to change phenotype into wound healing M2 macrophages. The polarization of M1 to M2 is a critical component of attenuating graft and biomaterial rejection.

Several strategies have been designed to mediate the host inflammation in response to biomaterials. In one approach, a hydrophilic boundary between implant and

host tissue [40, 41] was created to enhance the biocompatibility of implants [42-44]. In another approach, anti-inflammatory biomolecules were utilized to inhibit the secretion of mediators such as leukotrienes and prostaglandins, and delay fibroblast capsule formation [52]. A major drawback of this method is the numerous undesired systemic side effects [53]. For example, anti-inflammatory corticosteroid based drugs inhibit new blood vessel formation necessary for nutrient exchange in the implanted tissue [54, 55]. Another commonly used method is the induction of angiogenesis based on the use of growth factors [46-48]. Despite its limited success, this method can overexpose tissues to growth factors leading to arthritis and tumor formation [49-51].

Efforts to identify compounds with anti-inflammation properties have led to discovery of resveratrol, a polyphenol found in the skin of grapes [292, 293]. Strikingly, this molecule has been shown to exhibit therapeutic effects in a number of diseases including cancer, cardiovascular failure, viral infections, neurodegeneration, and ischemic injuries [294-304]. The exact mechanisms by which resveratrol impacts inflammation is under intense investigation. Suppression of transcription factor nuclear factor kappa B (NF-κB), TNF-α and interleukin-1 (IL-1), prostaglandin E2 (PGE2), and nitric oxide (NO) synthesis have demonstrated to be potential means by which resveratrol attenuates inflammation [305-307]. Further studies are warranted to explore the signaling cascades governing the anti-inflammatory potential of resveratrol in the context of wound healing and implant integration.

In addition to its anti-inflammatory characteristic, resveratrol has been found to possess pro-osteogenic properties. Augmentation of the canonical Wnt signaling

pathway, activation of sirtuin 1 (SIRT-1), and acetylation of runt-related transcription factor 2 (RUNX2) have been shown to be the underlying mechanism behind the induction of osteogenesis in stem cells by resveratrol [308-311]. Additionally, reports of the bone inductive effects of resveratrol through the activation of estrogen receptor have highlighted this natural compound as a viable candidate factor for bone tissue engineering applications.

The main objective of this study is to determine the potential of resveratrol to lessen inflammation and stimulate hMSCs towards bone lineage in 2D culture systems. The hypothesis behind our effort is that resveratrol can be utilized to (i) induce the osteogenic differentiation of hMSCs, and (ii) switch macrophage polarization from a pro-inflammatory M1 to a wound healing M2 phenotype. We tried this hypothesis by assessing the time-dependent effect of varying resveratrol doses on macrophage gene expression as well as hMSCs osteogenic differentiation in 2D culture systems. The approach developed in this study has the potential to be applied to 3D scaffold design for harnessing inflammation and promoting bone tissue formation.

5.2: Human Monocyte Cell Culture

Human THP-1 monocytes (sigma) were cultured in basal medium consisting of RPMI 1640 (Sigma), 2 mM L-Glutamine (Gibco), 10% FBS (Atlas), and 1% penicillin/streptomycin (Invitrogen). Medium was changed every other day, and cells were kept at a density of 3-8 x 10^6 cells/mL in order to maintain growth. THP-1 monocytes were seeded in each well of a 24 well plate at a number of 500,000 cells per

well. Depending on the experimental conditions, cells were kept at an undifferentiated state, were differentiated to M0 macrophages, or were differentiated to M1 macrophages.

5.3: Differentiation of Monocytes to Macrophages

THP-1 monocytes were differentiated to M0 macrophages by adding 200 nM phorbol 12-myristate 13-acetate (PMA) to the basal medium for 24 hours after which cells adhered to the tissue culture plate. To differentiate M0 macrophages to M1 macrophages, basal medium supplemented with 1 μg/mL LPS (Sigma) and 20 ng/mL recombinant interferon gamma (IFNγ) (Peprotech) was added to the wells for 24 hours. Differentiation of M0 macrophages to M2 macrophages was accomplished by adding 20 ng/mL recombinant interleukin 4 (IL-4) (Peprotech) as well as 20 ng/mL recombinant interleukin-13 (IL-13) (Peprotech) to the basal medium, and then culturing M0 macrophages in the differentiation medium for 18 hours.

5.4: Effect of Resveratrol on M1 Macrophages

Resveratrol was added to basal THP-1 monocytes culture medium at concentrations of 1 μM, 10 μM, and 25 μM, and gene expression of cytokines VEGF, TNF-α, IL-6, macrophage mannose receptor 1 (MRC-1), and interleukin 10 (IL-10) were analyzed using qRT-PCR after resveratrol exposure durations of 2 and 5 days.

The total RNA was extracted and purified from the samples using the GeneJET RNA Purification Kit (Thermo Scientific). Briefly, RNA (0.5 μg) was prepared as a template for single-strand cDNA synthesis using the RevertAid First Strand cDNA Synthesis Kit

(Thermo Scientific). First, genomic DNA was removed from the RNA sample by applying a mixture of the supplied reaction buffer with $MgCl_2$, DNase I, and nuclease-free water to a total volume of 10 μL. The samples were then incubated at 37 °C for 30 minutes, after which 1 μL 50 mM EDTA was added. The samples were placed in a 65 °C water bath for 10 minutes. The template RNA was mixed with 1 μL oligo $(dT)_{18}$ primer and nuclease-free water to a volume of 12 μL, followed by the addition of 4 μL of 5x Reaction Buffer, 1 μL Ribolock RNase Inhibitor, 2 μL 10 mM dNTP Mix, and 1 μL RevertAid M-MuLV Reverse Transcriptase. This mixture was incubated at 42 °C for 1 hour in a Bio-Rad CFX96 thermocycler instrument. To detect gene expression, the SensiFAST SYBR No-ROX Kit (Bioline) was used for qPCR. Briefly, 100 ng of cDNA was mixed with 10 μL 2x SensiFAST SYBR No-ROX Mix, 10 μM forward primer, 10 μM reverse primer, (see Table 5.1 for primer sequences, Integrated DNA Technologies) and nuclease-free water to 20 μL. A 3-step cycling was used on a Bio-Rad CFX96 instrument: 1 cycle of 95 °C for 2 minutes to activate the polymerase, followed by 40 cycles of 95 °C for 5s to denature, 65 °C for 10s for annealing, and 10s at 72 °C for extension. Gene expression of VEGF, TNF-α, IL-6 MRC-1, and IL-10 were normalized to GAPDH and presented as relative values.

5.5: Human Mesenchymal Stem Cell Culture and Osteogenic Differentiation with Resveratrol

Human mesenchymal stem cells were cultured in a basal medium consisting of DMEM/F12 (Gibco), 10% FBS (Atlas), and 1% penicillin/streptomycin (Invitrogen).

Table 5.1. Primers used for quantitative real-time polymerase chain reaction to demonstrate macrophage phenotype and hMSC differentiation.

Gene	5'-3' primer sequences: (F: forward R: reverse)
VEGF-A	F: ATC TGC ATG GTG ATG TTG GA R: GGG CAG AAT CAT CAC GAA GT
IL-10	F: GTG ATG CCC CAA GCT GAG A R: CAC GGC CTT GCT CTT GTT TT
TNF-α	F: CTG CTG CAC TTT GGA GTG AT R: AGA TGA TCT GAC TGC CTG GG
MRC-1	F: CAG CGC TTG TGA TCT TCA TT R: TAC CCC TGC TCC TGG TTT TT
IL-6	F:AGC CAC TCA CCT CTT CAG AAC R: GCC TCT TTG CTG CTT TCA CAC
BGLAP	F: GGC GCT ACC TGT ATC AAT GG R: TCA GCC AAC TCG TCA CAG TC
RUNX2	F: CTC ACT ACC ACA CCT ACC TG R: TCA ATA TGG TCG CCA AAC AGA TTC
GAPDH	F: GTG GAC CTG ACC TGC CGT CT R: GGA GGA GTG GGT GTC GCT GT

Medium was changed every 5 days and cells were passaged once 80% confluency was reached.

To study the impact of resveratrol on osteogenic differentiation, hMSCs were seeded in a 24 well plate (50,000 cells/well) for 24 h after which the culture medium was changed. Four conditions were considered in this study: basal medium (negative control), basal medium supplemented with 12.5 μM resveratrol (Sigma), osteogenic medium, or osteogenic medium supplemented with 12.5 μM resveratrol. Growth media was exchanged 3 times per week for all groups.

5.6: Analysis of hMSC Proliferation and Osteogenic Differentiation

Samples were characterized by MTS proliferation assay, osteocalcin immunofluorescence staining, Alizarin Red S staining, calcium quantification, alkaline phosphatase (ALP) staining, and ALP quantification.

Cell proliferation was monitored using [3-(4,5-dimethylthiazol-2-yl)-5-(3-carboxymethoxyphenyl)-2-(4-sulfophenyl)-2H-tetrazolium (MTS) (Promega) colorimetric assay. Fresh media was added to each well at a volume of 100 μL, and incubated for 4 hours with 20 μL of MTS solution. The resulting solution was diluted 1:5 and the absorbance was read at 492 nm using a Biotek Synergy 2 plate reader.

Osteocalcin was qualitatively assessed using immunofluorescence staining. Cells were fixed in 10% formalin for 30 minutes, followed by washing with a rinse buffer (2x) (20 mM Tris-HCL and 0.05% Tween- 20 in PBS) (Sigma). The samples were

permeabilized with 0.1% Triton X-100 (Sigma) in PBS for 15 minutes. Cells were washed 2x with the rinse buffer, and blocked with 4% goat serum in PBS for 30 minutes. The primary antibody, osteocalcin (1:50) (R&D Systems), was added to the samples and incubated overnight at 4°C. Following the primary antibody incubation, the cells were washed 3x with the rinse buffer for 5 minutes each time. Then Alexafluor 594 (1:1000) (Invitrogen) was added to the samples and incubated for 1 hour at room temperature, followed by 4'-6-diamidino-2-phenylindole (1:25) (DAPI) (Sigma) nuclear stain. Images of stained cells were obtained using a Nikon Eclipse 80i with NIS-Elements imaging software.

To visualize the mineralized calcium, samples were fixed in 10% formalin for 30 minutes and washed 3x with DI water. Alizarin Red S staining solution (pH 4.2-4.5) (Alfa Aesar) was added to the samples at a concentration of 0.02 mg/mL and incubated for 5 minutes. Samples were washed for 6 hours in 100% ethanol as ethanol wash solution was changed every 30 minutes. Mineralized ECM was imaged with a Nikon E600 light microscope. To quantify the mineralized calcium, the O cresolphthalein complexone (Sigma kit #MAK022) method was employed. The scaffolds were washed with deionized (DI) water 3x followed by the use of 0.6 mol/L hydrochloric acid to homogenize the samples and 4 hours of shaking at 4°C for total calcium extraction. Each sample was added to individual wells of a 96 well plate at a volume of 50 μL, and 90 μL of the supplied chromogenic reagent was placed in each well containing the samples. After mixing gently, a total of 60 μL of calcium assay buffer was added to each well and carefully merged with the other components. The reaction was incubated for 10 minutes

in the dark, and the amount of calcium was determined by reading the absorbance at 575 nm with a Biotek Synergy 2 plate reader.

ALP expression was quantified using a Bio-Rad Alkaline Phosphatase Substrate Kit (#172-1063). Briefly, cells were washed 3x with PBS, then lysed using 0.1% Triton X-100 (Sigma) in PBS for 15 minutes at 4 °C. The substrate solution was reconstituted by mixing 1 mL of 5x diethanolamine buffer with 4 mL DI water, then dissolving 1 tablet of 5 mg p-nitrophenylphosphate in the buffer mixture. Each sample was placed in individual wells of a 12 well plate at a volume of 400 μL. A total of 100 μL substrate solution was added to the samples and incubated at 37 °C for 30 minutes in the dark after which 100 μL 0.4 M NaOH to stop the reaction. The absorbance was read at 405 nm using a Biotek Synergy 2 plate reader. ALP was quantitatively detected by using alkaline phosphatase kit #85 (Sigma) in which scaffolds were fixed with 10% formalin for 30 minutes and washed 3x with PBS. The Fast Blue capsule was dissolved in napthanol to prepare the staining solution, added to the scaffold, and incubated for 30 minutes. The scaffolds were washed 3x with PBS followed by incubation in the Mayer's Hematoxylin solution for 10 minutes. ALP was observed and imaged using a Nikon E600 light microscope.

5.7: Resveratrol Modulates Inflammation by Inducing Macrophage Phenotypic Switch

Figure 5.1 shows the dose dependent effects of resveratrol on M1 macrophages. Analysis of inflammatory gene (IL-6, TNF-α) and anti-inflammatory gene (VEGF, MRC-1 and IL-10) expression by qRT-PCR demonstrated that resveratrol modulates

inflammation and promotes anti-inflammatory cytokine expression. Inflammatory marker IL-6 was significantly lowered with the addition of 10 μM and 25 μM resveratrol at day 2, and reduced equally by all concentrations of resveratrol by day 5 (Figure 5.1A). Consistently, TNF-α was greatly reduced at the 2 day time point by 25 μM of resveratrol. Day 5 showed a dose dependent trend of lowered TNF-α expression, with a statistically significant reduced inflammatory cytokine level expressed in the 25 μM resveratrol containing group (Figure 5.1B). The expression of anti-inflammatory marker IL-10 significantly increased at the 2 day and 5 day time points with the addition of 25 μM resveratrol (Figure 5.1C). Similarly, VEGF expression increased with the addition of resveratrol, and day 2 expression showed statistically significant levels in the 1 μM group as compared to the control (Figure 5.1D). By day 5, VEGF levels were the greatest with M1 macrophages cultured with 25 μM, followed by 10 μM and 1 μM. In line with these results, MRC-1 levels were statistically significant for the M1 macrophages cultured with 25 μM resveratrol at both time points, as compared to the control group (Figure 5.1E).

5.8: Resveratrol Drives the Osteogenic Differentiation of hMSCs

Figure 5.2 demonstrates the effect of resveratrol on the osteogenic stimulation of hMSCs. Cells were cultured in basal hMSC medium, basal medium supplemented with resveratrol, osteogenic differentiation medium, and osteogenic differentiation medium supplemented with resveratrol. Differentiation was analyzed over a period of 21 days. It is important to note that in all of the 2D study, hMSCs exhibited a normal proliferation curve with no significant difference in cell growth between the study groups.

Osteogenesis was assessed based on calcium, ALP, and OCN expression. Calcium expression was analyzed at days 7, 14, and 21 (Figure 5.2A). At each time point, cells cultured in osteogenic medium supplemented with resveratrol produced significantly higher amounts of calcium as compared to all other groups. Cells in basal medium with resveratrol as well as hMSCs cultured in osteogenic medium demonstrated a statistically higher level of calcium at days 14, and 21, as compared to the control. Calcium expression for hMSCs cultured in osteogenic medium with resveratrol is further demonstrated by Alizarin Red S Staining (Figure 5.2B) which shows a bright red color indicating mineralized matrix.

Alkaline Phosphatase expression was determined at time points of 7, 14, and 21 days. Cells cultured in osteogenic medium supplemented with resveratrol exhibited a statistically higher amount of ALP at every time point as compared to all other groups (Figure 5.2C). Cells cultured in basal medium with resveratrol as well as osteogenic medium showed significant ALP expression at day 21. ALP staining confirmed the expression at day 21 of culture in osteogenic medium with resveratrol, as shown by the bright purple-blue color of the cells (Figure 5.2D).

Gene expression analysis of OCN demonstrated a significant higher level of gene expression in the basal medium supplemented with resveratrol at day 7 (Figure 5.2E). At days 14 and 21, cells cultured with resveratrol in osteogenic medium expressed statistically higher OCN, as compared to the control. Osteocalcin immunofluroescent staining further confirmed OCN level at day 21 expressed by hMSCs cultured in 12.5 μM resveratrol (Figure 5.2F).
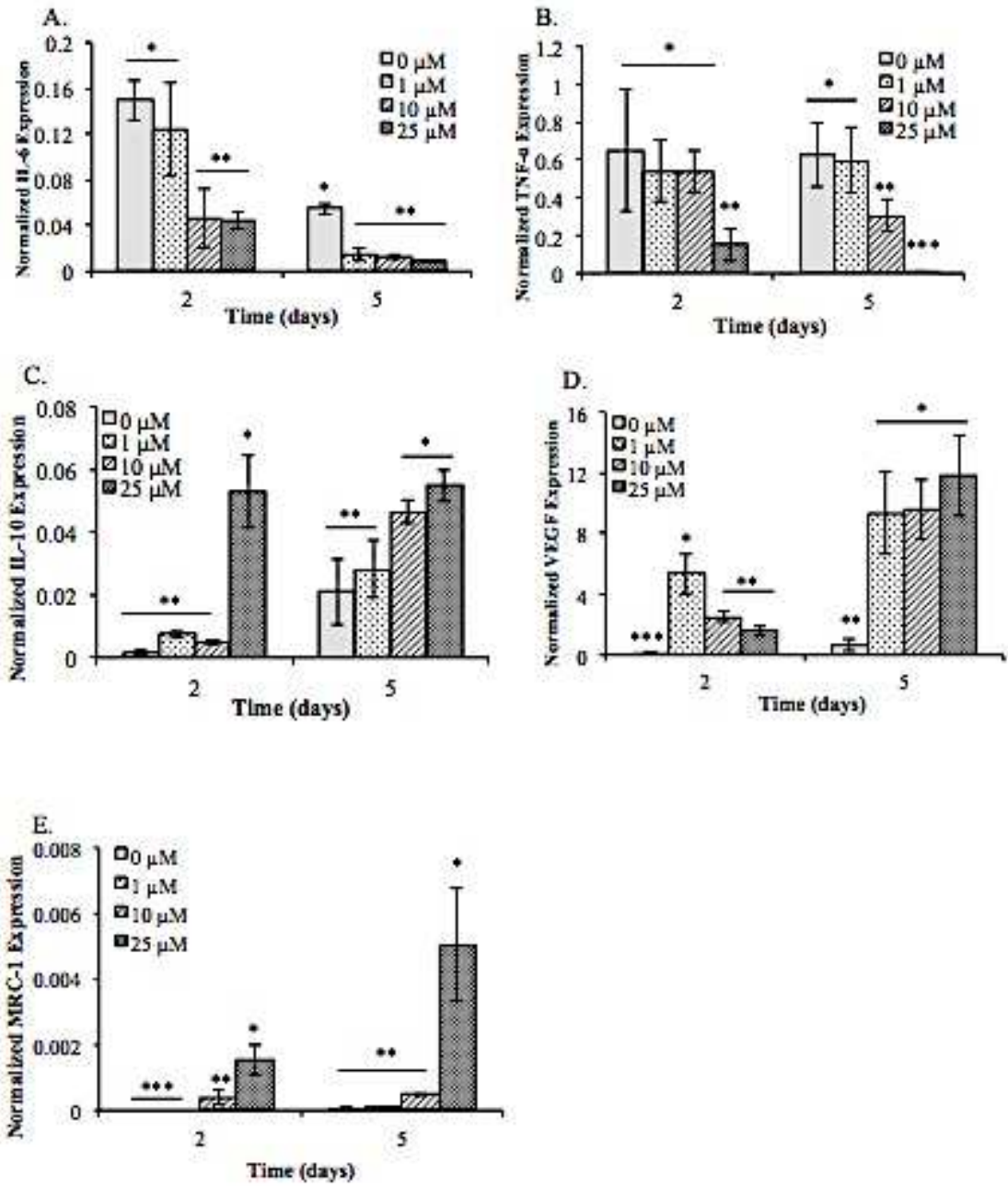
Figure 5.1 Gene expression by M1 macrophages cultured under different resveratrol concentration was analyzed by measuring the levels of (**A**) IL-6, (**B**) TNF-α, (**C**) IL-10, (**D**) VEGF, and (**E**) MRC-1using qRT-PCR. A single asterisk denotes significantly higher as compared to groups denoted by two asterisks. Two single asterisk denotes significantly higher as compared to groups denoted by three asterisks. Results demonstrated the highest level M2 signatory genes in the presence of resveratrol demonstrating the potential to drive the pro-angiogenic and anti-inflammatory response.
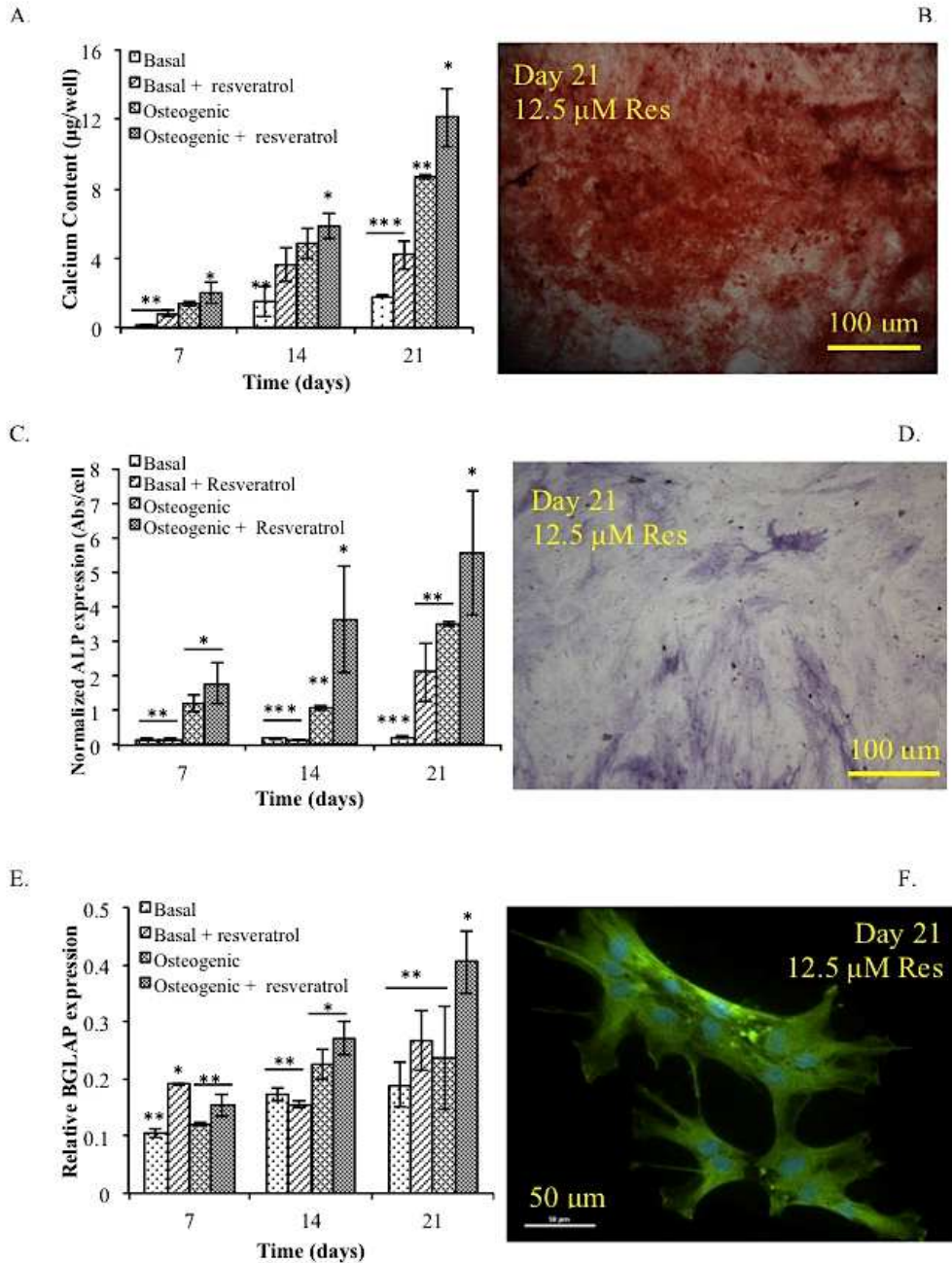
Figure 5.2 **(A)** Calcium expression was the greatest for hMSCs cultured in osteogenic medium + resveratrol. **(B)** Alizarin Red S staining confirmed calcium deposition by hMSCs cultured in osteogenic medium + resveratrol at day 21, scale bar is100 μm. **(C)** ALP expression was the highest for hMSCs in osteogenic medium + resveratrol for each time point. **(D)** ALP staining of hMSCs at day 21 cultured in osteogenic medium + resveratrol, scale bar is 100 μm. **(E)** qRT-PCR showed the highest level of BGLAP in hMSCs in osteogenic medium + resveratrol for days 14 and 21. **(F)** OCN staining of day 21 hMSCs cultured in osteogenic medium + resveratrol, scale bar is 50 μm. * denotes significantly higher as compared to groups denoted by **. ** denotes significantly higher as compared to groups denoted by ***.

5.9: Statistical Analysis

Three samples (n=3) were analyzed per condition unless otherwise stated. Studies investigating the dose dependent effect of resveratrol on M1 macrophages and the effect of resveratrol on hMSCs were done in duplicate trials. Error bars in graphs represent mean ± standard deviation (SD). Two-way analysis of variance (two-way ANOVA) was calculated using GraphPad Prism software and used to determine statistical significance between experimental groups. One-way analysis of variance (one-way ANOVA) with a Tukey post-test was used to calculate significance between individual groups at different time points. Statistical significance was defined as $p \leq 0.05$.

5.10: Conclusions

This study determined the effectiveness of resveratrol as a potent immunomodulator and promoter of osteogenesis. We set out to determine the dose dependent effect of resveratrol on M1 macrophage phenotype as well as the regulation of hMSC differentiation towards bone lineage.

Our experiments investigating the dose dependent regulation of inflammatory cytokines by resveratrol indicated that M1 macrophages produce less IL-6 and TNF-α when cultured with the anti-inflammatory polyphenol. This is coupled with higher expression of anti-inflammatory markers VEGF, IL-10, and MRC-1 after 48 hours of exposure to resveratrol. Cells cultured with 25 μM resveratrol demonstrated the greatest expression of wound healing markers VEGF, MRC-1 and IL-10. Consistently, M1 macrophages cultured with 25 μM resveratrol exhibited the lowest amount of

inflammatory cytokine TNF-α. Inflammatory marker IL-6 reduction by resveratrol was not statistically different between the 10 μM and 25 μM groups.

To analyze osteogenic differentiation of hMSCs, we cultured cells in basal medium, basal medium with 12.5 μM resveratrol, osteogenic medium, and osteogenic medium with 12.5 μM resveratrol. Cells exposed to osteogenic medium supplemented with resveratrol produced significantly higher levels of calcium, alkaline phosphatase, and osteocalcin. These results altogether show the exciting potential for resveratrol to be used in tissue engineering approaches for attenuating host inflammation and stimulating osteogenic differentiation, and can be applied to a 3D scaffold design to incorporate resveratrol.

CHAPTER 6: ENGINEERED RESVERATROL NANOPARTICLE-INCORPORATED SCAFFOLDS TO DIRECT OSTEOGENIC DIFFERENTIATION OF hMSCS AND MODULATE INFLAMMATION OF M1 MACROPHAGES

6.1: Introduction

Biomaterial design is an essential component of successful bone tissue engineering strategies. The ideal scaffold should be osteoinductive, osteoconductive, and osteogenic. Osteoinductivity refers to the ability of a biomaterial to stimulate undifferentiated stem cells to develop into bone-forming cell lineage [312]. Osteoconductive scaffolds foster bone growth on the material surface by promoting cell attachment, proliferation, and allowing cell infiltration and matrix deposition [312, 313]. Osteogenicity signifies the scaffold contains cells that are able to differentiate into osteoblasts [314].

PLGA microsphere-sintered scaffolds are osteoconductive, and when combined with the appropriate cell source and signaling cues, become osteogenic as well as osteoinductive. However, a significant challenge to bone tissue engineering strategies is biomaterial rejection due to the host immune response, as well as scaffold integration with the native tissue. In the previous chapter, we determined the ability of the natural compound resveratrol to synergistically modulate inflammation and stimulate osteogenesis of hMSCs in 2D.

74

The main objective of this study is to delineate the potential of resveratrol to accelerate the formation of bone and vasculature in tissue engineered scaffolds. The major hypothesis underlying our effort is that resveratrol can be used to simultaneously (1) induce the osteogenic differentiation of hMSCs seeded onto 3D porous scaffolds, and (2) switch the invading macrophages from a pro-inflammatory M1 to a pro-angiogenic M2 phenotype. We tested this hypothesis by assessing the time-dependent effect of a controlled release of resveratrol on macrophage gene expression as well as hMSCs osteogenic differentiation in 3D culture systems. Insufficient vascularization and lack of control on host inflammatory response to implantable scaffolds are profound barriers in regenerative medicine. The system developed in this study has the potential to be applied to bioengineering of other musculoskeletal tissues in addition to bone.

6.2: Fabrication of PLGA Resveratrol Nanoparticles and Determination of Resveratrol Release Profile

Nanoparticles with diameters of 150-350 nm were synthesized. Two different molecular weights of poly(lactic-co-glycolic acid) (PLGA) (Lactel Absorbable Polymers) were used to fabricate the resveratrol nanoparticles in order to test individual release profiles and optimize the resveratrol dosage in the 3D scaffolds (Table 6.1). A steric solution of 2.5% poly(vinyl alcohol) (Sigma) and 0.95 g of 2-morpholinoethanesulfonic acid monohydrate buffer (MES) (Sigma) pH of 5.0 in 100 mL of deionized water was created. The polymer-resveratrol conjugation solution was made by dissolving 100 mg of PLGA and 2.5 mg of resveratrol (Sigma) in 5 mL of acetone (Macron). The polymer-

resveratrol solution was added drop-wise at a rate of 1 mL/minute to the steric solution while being stirred at 300 rpm. This colloidal suspension was stirred for 24 hours to ensure complete evaporation of acetone. Nanoparticles were harvested through a centrifugation step followed by lyophilization.

Transmission Electron Microscopy (TEM) was used to analyze nanoparticle size. Briefly, nanoparticles were suspended in DI water and a drop of the solution was placed on a thin carbon film. The film was placed in a vacuum to allow for water evaporation and the sample was placed on a TEM grid. Images were taken using a JEOL 200CX transmission electron microscope.

Using a UV-Vis Spectrophotometer, a calibration curve was generated to correlate the absorption at 327 nm (peak absorbance of resveratrol) for various concentrations. Nanoparticles with different molecular weights were incubated in PBS at 37°C, and the supernatant was collected every 24 hours to read the absorbance with the UV-Vis Spectrophotometer. As it will be shown in the results, the 75:25 PLGA demonstrated the optimum release profile and was selected for use in the remainder of experiments.

6.3: Synthesis of PLGA Microsphere-sintered and Resveratrol Nanoparticle-incorporated Scaffolds

Scaffolds with diameters of 10 mm and heights of 2 mm were fabricated according to established laboratory procedures [315-317]. Briefly, PLGA (85:15 lactide to glycolide ratio) (Lactel Absorbable Polymers) was dissolved in dichloromethane

Table 6.1. The chemical characteristics of PLGA used to design nanoparticles for resveratrol encapsulation and release in scaffolds.

Lactide to Glycolide Ratio	Molecular Weight (kDa)	Functional Group
75:25	75-100	Ester Terminated
50:50	16-29	Ester Terminated

(Sigma) to form a 1:4 w/v polymer solution. The solution was slowly poured into a 1% poly(vinyl alcohol) solution (Sigma) while being stirred at 330 rpm for 24 hours to allow for adequate evaporation of the solvent. Vacuum filtration was used to collect the microspheres, and the samples were washed with DI water and stored at -20°C for 24 hours. The microspheres were lyophilized to completely remove all moisture. Micron sieves were used to isolate microspheres of diameter 500-700 μm. Microspheres of the size range 500-700 μm were placed into stainless steel molds, heated at 80ºC for 4 hours, and sintered into cylindrical disks. Scaffolds that were to be incorporated with nanoparticles were sintered for 3.5 hours to account for the additional sintering time needed to attach nanoparticles to the microspheres.

The target resveratrol release from the nanoparticles is based on 2D studies demonstrating the optimum resveratrol dose for hMSC differentiation [310, 318], and the desire to i) use acute inflammation to drive early osteogenesis and ii) switch macrophage phenotype to M2 after one week to promote wound healing and angiogenesis. To this end, initial resveratrol release is designed to attain 1-3 μM resveratrol for days 1-7, and 5-12.5 μM for days 7-21 to optimize inflammation modulation and osteogenesis of hMSCs. To accomplish this, nanoparticles were suspended in DI water at a desired concentration of 180 μg resveratrol nanoparticles/μL based on the ratio of resveratrol to PLGA in the loaded nanoparticles (1:80). Next, 10 μL of the nanoparticle solution was placed on each scaffold and allowed to disperse throughout the substrate. Scaffolds with nanoparticles were sintered for an additional 30 minutes at 85ºC.

Nanoparticle incorporation onto the PLGA scaffolds was determined using Scanning Electron Microscopy (SEM). Briefly, scaffolds were dehydrated using an ethanol sequence (10, 30, 50, 70, 90, 95, 95, 100, 100%) for 15 minutes each. Scaffolds were dried overnight in a fume hood to allow for ethanol evaporation, and coated with gold/palladium. Scaffolds were observed under Zeiss Ultra Plus FESEM after coating.

6.4: hMSC and Macrophage Seeding on Resveratrol-incorporated PLGA Scaffolds

To confirm the effect of resveratrol on osteogenic differentiation, we analyzed the growth and lineage specification of hMSCs as cultured on resveratrol-incorporated 3D PLGA scaffolds. PLGA scaffolds were first sterilized by immersion in 70% ethanol for 10 minutes. Scaffolds were washed 3x with PBS, and exposed to UV light for 1 hour per side to further sterilize the substrates. To seed cells on scaffolds, hMSCs were trypsinized, counted, centrifuged, and resuspended in basal medium at a concentration of 2,500 cells/μL. Cell suspension was added to each scaffold at the amount of 20 μL/scaffold. Samples were incubated for 20 minutes to ensure optimum cell attachment. Next, the remaining culture medium was placed in each well containing scaffolds. Culture medium was changed to osteogenic medium after 24 hour of incubation with basal media. Cell proliferation was assessed using MTS colorimetric assay. Osteogenic differentiation was analyzed based on the quantification of ALP and calcium expression.

THP-1 monocytes were differentiated to M1 macrophages at a seeding density of 50,000 cells/well of a 24 well plate. This was accomplished according to the protocol mentioned in the Chapter 5 Section 4. Resveratrol nanoparticle-incorporated scaffolds

were prepared using the method described in the Chapter 6 Section 3. Scaffolds were sterilized by immersion in 70% ethanol for 10 minutes followed by rinsing 3x with PBS. Scaffolds were placed under UV light for 1 hour per side. Scaffolds were placed in the wells with M1 macrophages and timepoints were taken at days 3, 7, 14, and 21. Gene expression of IL-6, TNF-α, IL-10, and VEGF was determined using qRT-PCR methods previously described in Chapter 5 Section 4.

6.5: Statistical Analysis

Three samples (n=3) were analyzed per condition unless otherwise stated. Studies investigating the osteogenic differentiation of hMSCs on resveratrol nanoparticle-incorporated PLGA was done in duplicate trials. Error bars in graphs represent mean ± standard deviation (SD). Two-way analysis of variance (two-way ANOVA) was calculated using GraphPad Prism software and used to determine statistical significance between experimental groups. One-way analysis of variance (one-way ANOVA) with a Tukey post-test was used to calculate significance between individual groups at different time points. Statistical significance was defined as $p \leq 0.05$.

6.6: Results

Resveratrol release from the nanoparticles and incorporation into PLGA scaffolds was assessed. Figure 6.1 includes the characterizations of PLGA scaffold with resveratrol encapsulated nanoparticle. We observed that scaffolds possessed an interconnected porous structure consisting of microspheres sintered together. We confirmed the

distribution of resveratrol nanoparticles throughout the scaffolds using SEM (Figure 6.1A) and TEM (Figure 6.1B). The images demonstrated a homogenous spreading of nanoparticles (average diameter size of 250 nm) on the surface of microspheres. As expected, the nanoparticles were sintered into the PLGA scaffolds following the heating step, as manifested in high magnification images. To tune the release of resveratrol throughout the scaffolds, we varied the molecular weight of PLGA nanoparticles. Our goal was to design a sustained release of resveratrol over several days to give enough time for hMSC osteogenic differentiation and stimulate M1 to M2 differentiation. Figure 6.1D demonstrates the release profile of resveratrol from nanoparticles embedded in scaffolds. As expected, the higher molecular weight of 75-100 kDa allowed for a prolonged controlled release of resveratrol within 3D PLGA sintered microsphere scaffolds.

Resveratrol nanoparticle-incorporated scaffolds control macrophage polarization and enhance osteogenic differentiation of hMSCs. M1 macrophages were cultured on resveratrol incorporated PLGA scaffolds for 21 days, and inflammatory gene expression was analyzed at different time points (Figure 6.2). We observed the expression of IL-6 expression to sustain in day 3 to day 7 time points, and significantly drop by day 14 (Figure 6.2A). Consistently, the gene expression of inflammatory marker TNF-α was significantly lower on later time points (Figure 6.2B). On the other hand, IL-10 and VEGF expression were upregulated at day 7 and 14 time points (Figure 6.2C-D). These results were consistent with our 2D experiments in that resveratrol downregulates the inflammatory markers while stimulating the expression of angiogenic genes. A difference
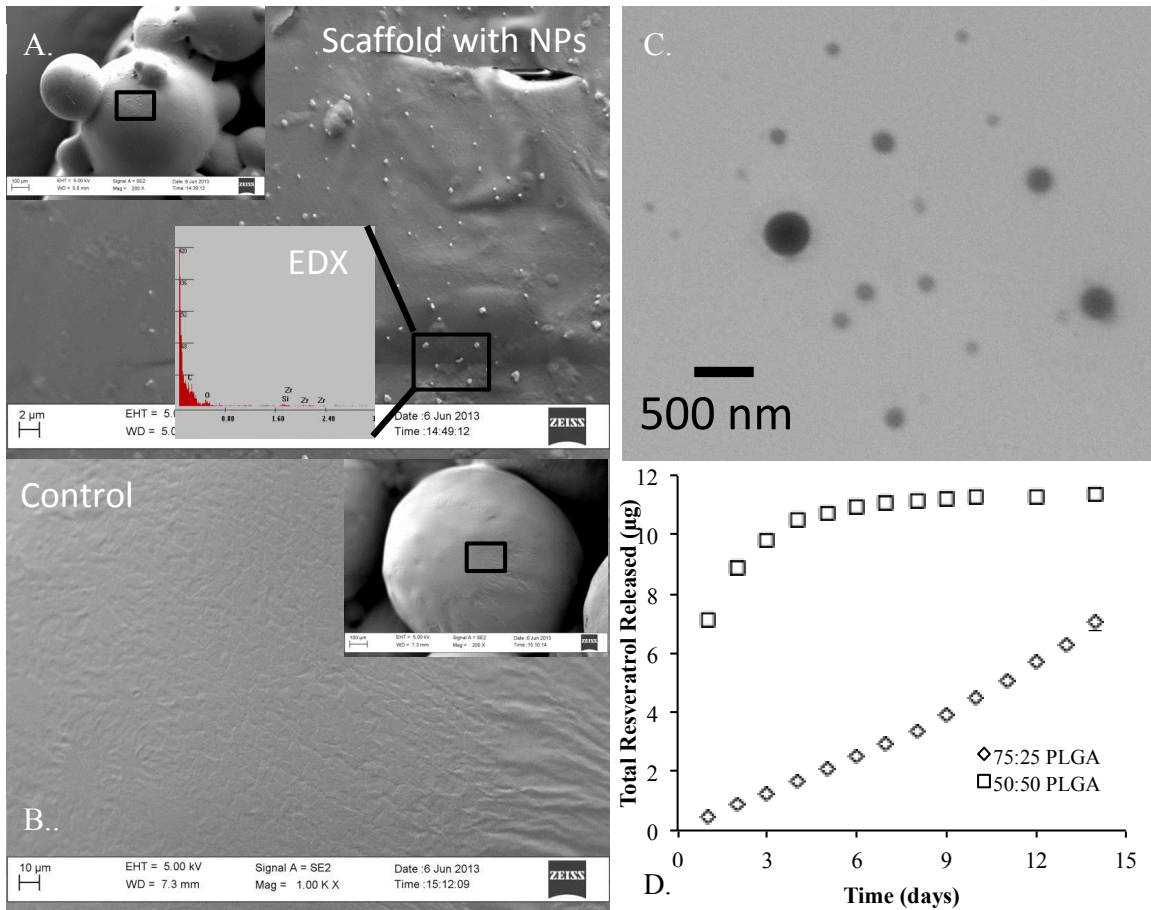
Figure 6.1 (**A**) SEM image of a resveratrol nanoparticle-incorporated scaffold showing the nanoparticles on the surface of the sintered microsphere scaffolds PLGA. (**B**) SEM image of a blank PLGA scaffold (control) demonstrating a smooth surface without nanoparticles. (**C**) TEM image of individual resveratrol encapsulated nanoparticles. The approximate diameter of nanoparticles was 250 nm. (**D**) Resveratrol release profile from the scaffolds demonstrated a slower and more linear release when conjugated with a higher molecular weight of PLGA.

however is manifested in the amounts of these genes due to the 3D nature of scaffolds and the release profile of resveratrol on scaffolds versus 2D condition.

Figure 6.3 demonstrates the results of hMSCs cultured on tissue culture polystyrene (TCPS), 3D PLGA scaffolds, and 3D resveratrol nanoparticle-incorporated PLGA scaffolds. We observed that the cells grow in all conditions; however, hMSCs cultured on TCPS medium had significantly higher cell numbers than both the PLGA and PLGA with resveratrol groups (Figure 6.3A). Furthermore, the cells cultured on blank PLGA reached a significantly higher number compared to hMSCs grown on PLGA with resveratrol nanoparticles.

hMSCs cultured on resveratrol incorporated scaffolds demonstrated significantly greater of ALP expression compared to all other experimental groups at days 3, 7, 14, and 21, while hMSCs on PLGA scaffolds produced the second highest amount of ALP at each time point as compared to TCPS (Figure 6.3B). Consistently, hMSCs cultured on resveratrol nanoparticle scaffolds expressed a significantly higher amount of calcium at days 14 and 21. hMSCs on blank PLGA scaffolds produce the second highest amount of calcium a compared to the control TCPS (Figure 6.3C). These results were consistent with the 2D experiments demonstrating the potential of resveratrol to promote osteogenic differentiation of stem cells.
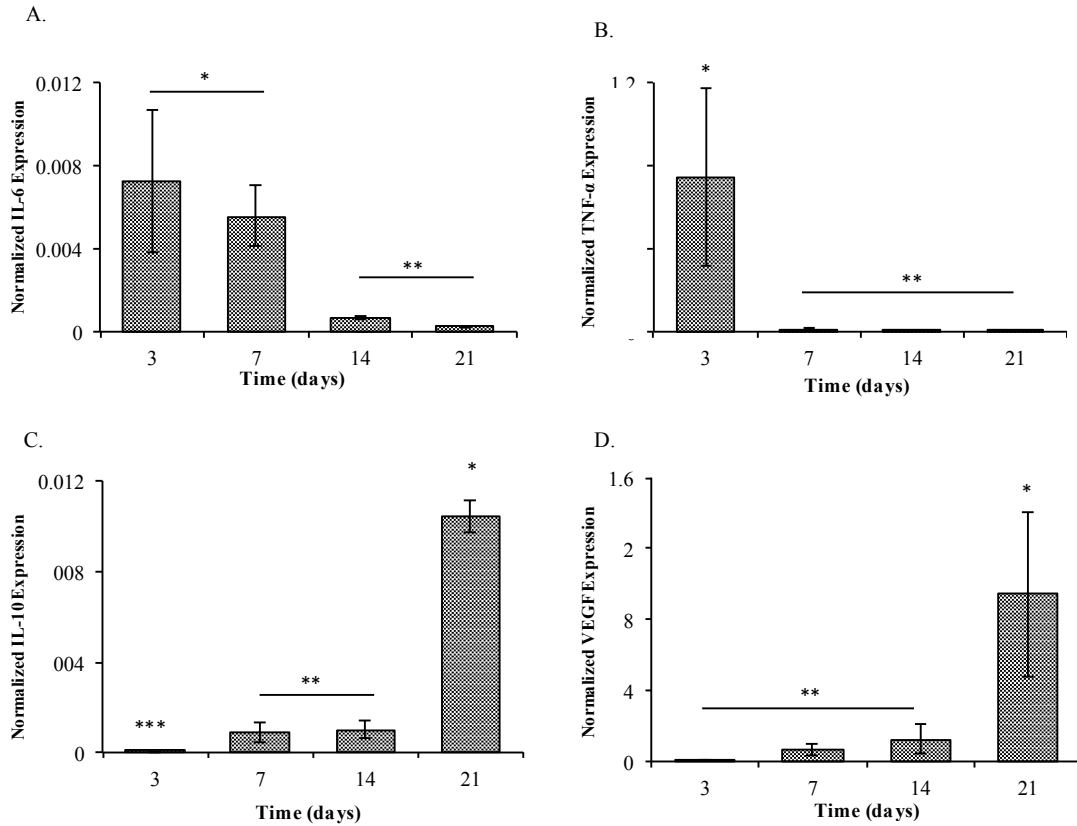
Figure 6.2 Gene expression analysis of M1 macrophages on the resveratrol incorporated scaffolds demonstrated (**A**) IL-6 expression at days 3 to 7, 14 and 21 post-culture. (**B**) TNF-α expression at days 3 to 7, 14 and 21 post-culture. A single asterisk denotes a significantly higher expression of TNF-α at day 3 compared to the previous time point. (**C**) IL-10 expression at days 3 to 7, 14 and 21 post-culture. (**D**) VEGF expression at days 3 to 7, 14 and 21 post-culture. A single asterisk denotes a significantly higher expression of VEGF at day 21. * denotes significantly higher as compared to groups denoted by **. ** denotes significantly higher as compared to groups denoted by ***. Results demonstrated the highest level M2 signatory genes in the presence of resveratrol demonstrating the potential to drive the pro-angiogenic anti-inflammatory response.
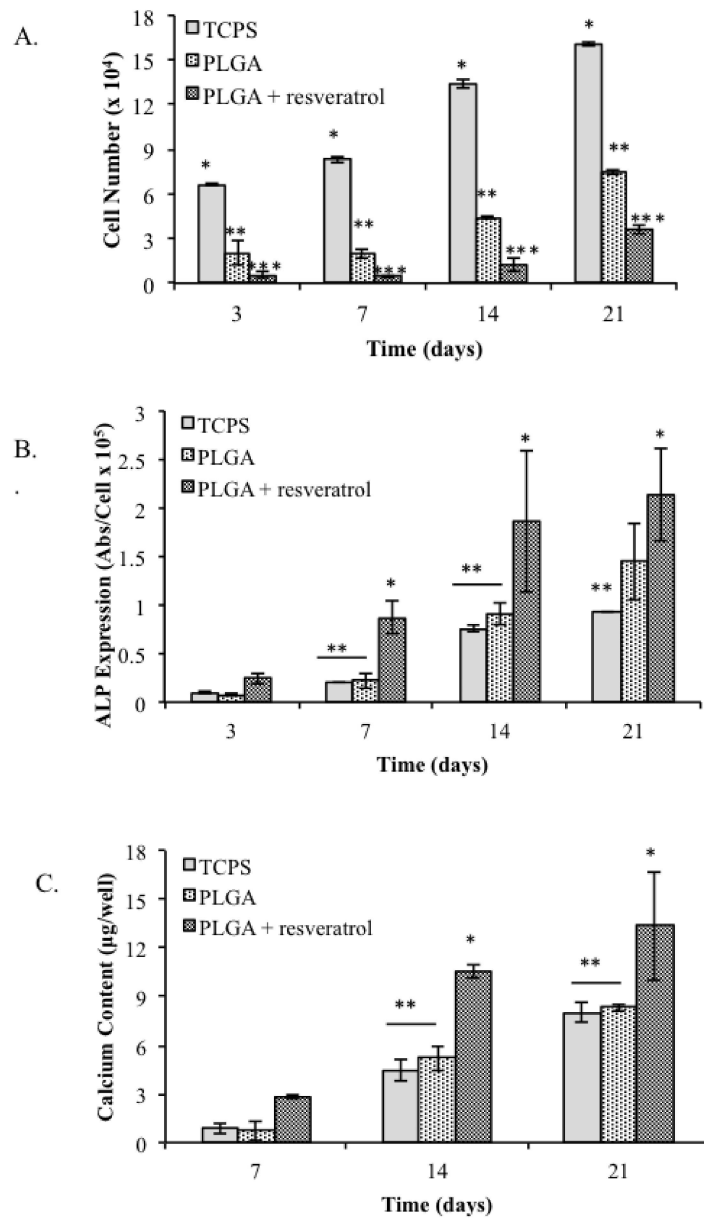
Figure 6.3 (**A**) hMSC proliferation on scaffolds showed a normal cell growth curve. (**B**) ALP expression by hMSCs on TCPS, PLGA scaffolds and PLGA scaffolds with resveratrol nanoparticles. (**C**) ALP expression by hMSCs on TCPS, PLGA scaffolds and PLGA scaffolds with resveratrol nanoparticles. * denotes significantly higher as compared to groups denoted by **. ** denotes significantly higher as compared to groups denoted by ***.

6.7: Discussion

Our study addresses fundamental issues facing osseointegration of biomaterial grafts in an inflammatory microenvironment. We set out to engineer an immunomodulatory and osteoinductive scaffold that can harness the osteogenic and wound healing potential of immune cells, as well as program hMSCs towards bone tissue formation. To accomplish this goal, we demonstrated the ability of resveratrol to control macrophage phenotype from inflammatory to wound healing as well as stimulate osteogenic differentiation of hMSCs. Building on these 2D and 3D proof-of-concept experiments, we designed a specific resveratrol nanoparticle release profile within PLGA scaffolds that would i) control macrophage phenotype and subsequent cytokine secretion and ii) drive the osteogenic differentiation of hMSCs. This resveratrol nanoparticle incorporated scaffold is a novel approach to enhance graft integration and assimilation with native tissue.

Researchers have explored many options to modulate the immune response to prevent biomaterial rejection, such as using polymeric coatings, steroidal anti-inflammatory drugs, and angiogenic factors. These methods have faced many limitations due to immunogenicity, decomposition during the manufacturing process, and poor adhesion characteristics. Anti-inflammation pharmaceutical drugs only temporary suppress inflammation and have been known to reduce angiogenic factors which in turn delays wound healing. Finally, despite their important role in inflammatory cascade of events, the use of angiogenic growth factors is only partially effective due to its physiologic side effects.

Instead of trying to counteract inflammation, our approach aims to utilize a natural polyphenol to regulate immune cell behavior and use their expressed signaling molecules to drive the osteogenic differentiation of hMSCs. Our methods build on the central concepts of the anti-inflammatory and osteogenic properties of resveratrol as well as the known angiogenic signaling molecules produced by macrophages. To this end, we fabricated resveratrol nanoparticle-incorporated scaffolds with a controlled release profile that have the potential to revolutionize biomaterial assimilation with native bone tissue.

Our 2D proof of concept experiments described in Chapter 5 signify that M1 macrophages secrete less IL-6 and TNF-α when exposed to resveratrol. Furthermore, we found that M1 macrophages produce higher levels of anti-inflammatory markers VEGF, IL-10, and MRC-1 after 48 hours of culture with the anti-inflammatory polyphenol. From our results, we determined that 25 μM resveratrol tempers inflammation to the greatest extent as compared to the other concentrations. However, the optimized time scale and amount of resveratrol released from the nanoparticles should account for the target temporal concentration for both osteogenesis and macrophage phenotype polarization.

The use of resveratrol as a stimulator of osteogenesis has been previously demonstrated for hMSCs, human adipose derived stem cells (hADSCs), and pre-osteoblastic MC3T3-E1 cells [308-311, 318-323]. Furthermore, studies have shown resveratrol to affect proliferation and osteogenesis in a dose-dependent manner. hADSCs cultured with 12.5 μM, 25 μM, and 50 μM resveratrol showed the highest proliferation rate when exposed to 12.5 μM resveratrol, and the highest levels of ALP when cultured with 25 μM resveratrol. Doses of 50 μM resulted in extremely low cell numbers and ALP

production. ADSCs cultured with resveratrol exhibited the highest levels of osteocalcin and osteoprotegerin at a concentration of 12.5 μM [318]. Another study concluded that doses of 25 μM resveratrol are potentially cytotoxic, and that 12.5 μM resveratrol results in the greatest mineralized matrix after 4 weeks *in vivo* [310]. Additionally, hMSCs cultured with varying doses of resveratrol produced the highest calcium deposition and greatest proliferative capabilities when exposed to a concentration of 10 μM [323]. Based on these studies, and the fact that M1 macrophages switch phenotype to M2 when exposed to doses as low as 1 μM resveratrol, we selected a target resveratrol concentration of 12.5 μM to stimulate osteogenesis of hMSCs in 2D. Consistent with these, we observed the greatest calcium deposition and ALP expression from cells cultured in osteogenic medium + 12.5 μM. Furthermore, OCN levels were the highest for hMSCs cultured in osteogenic medium + 12.5 μM. To optimize macrophage control and osteogenic differentiation of hMSCs, we targeted a nanoparticle release profile of approximately 1-3 μM resveratrol per day for days 1-7, then approximately 5-12.5 μM resveratrol per day for days 7-21.

To design a biomaterial that allows for modulation of immune response, one must first determine how specific aspects of inflammation, such as macrophage phenotype, influence wound healing and osteogenesis. Preliminary investigations on total joint replacement materials and the surrounding tissue histology from either i) joints that had become loose due to osteolysis, and ii) joints implanted in osteoarthritic patients, have found that the former tissue produced many pro-inflammatory M1 macrophages while the latter demonstrated wound healing M2 macrophages [324, 325]. In another recent study,

porosity was found to drive a higher ratio of M2/M1 macrophages when compared to the non-porous control [326]. Furthermore, scaffolds composed of natural ECM can switch macrophage phenotype to predominantly wound healing by 7-14 days after implantation [327-329]. The common thread that relates all these findings is that they all rely on altering the cytokine release profile by monocyte and macrophages to attenuate the inflammatory response to the biomaterial [330, 331].

Although chronic inflammation is detrimental to wound healing and assimilation of graft with native tissue, recent studies have demonstrated the benefits of monocytes and macrophages in stimulating osteogenic differentiation of stem cells. In a recent published work, hMSCs were cultured in conditioned medium (CM) from M1 macrophages, M2 macrophages, and monocytes, and analyzed for hallmark osteogenic markers such as RUNX2, ALP, and bone morphogenetic protein-2 (BMP-2). hMSCs cultured with M1 CM expressed the highest levels of RUNX2, ALP, and BMP-2 [332]. Another study demonstrated that a member of the IL-6 pro-inflammatory cytokine family, Oncostatin M (OSM), produced by M1 macrophages promoted osteogenic differentiation of hMSCs and inhibited adipogenesis [333]. Macrophages secrete several osteogenic signaling molecules such as bone morphogenic protein-2 (BMP-2), 1, 25-dihydroxyvitamin D3, interleukin-1 beta (IL-1β), and IL-6 [334-336]. During fracture healing, cytokine members of the TGF- β superfamily, such as BMP, promote different stages of wound repair. BMP-2 peaks in expression levels early in the healing process, mediates a cascade of other BMPs associated with intramembranous and endochondral ossification [337]. TNF-α is another cytokine secreted by macrophages during the initial

inflammatory response that is responsible for recruiting hMSCs, and promoting cell survival [338]. Additionally, macrophages secrete angiogenic growth factors such as VEGF and PDGF, and these cytokines are important mediators in bone remodeling. Specifically, the VEGF family recruits endothelial cells, osteoblasts, and osteoclasts, and can promote microvascular endothelial cells to secrete BMPs in a hypoxic microenvironment found in fractured bone tissue [339-341].

In our proof of concept 3D experiments, we were able to successfully engineer a scaffold with a specific resveratrol release profile. M1 macrophages and hMSCs were individually placed on the scaffolds and cultured for 21 days. The gene expression profile of the macrophages showed moderately high expression of IL-6 for day 3 and day 7, and was significantly reduced by day 14. VEGF expression levels were relatively low until day 14, but significantly increased by day 21. This in itself overcomes a critical factor in tissue engineering approaches since lack of vascularization generally leads to failure of the graft. Our method of inducing endogenous VEGF secretion from native macrophages keeps levels physiologically relevant, therefore the risk of overexposing surrounding tissue to high levels of this angiogenic growth factor is almost nonexistent.

Stem cells cultured on the resveratrol-incorporated scaffolds expressed the highest levels of calcium and ALP, demonstrating the effectiveness of the controlled resveratrol release. The mechanism by which resveratrol induces osteogenesis is under deep investigation. Preliminary work by scientists has shown resveratrol to trigger Wnt signaling pathway leading to the upregulation of RUNX2 expression, the transcription factor essential for cell differentiation into osteoblasts [308, 342]. Resveratrol also

promotes osteogenesis through SIRT-1, and it has been shown that FOXO3A protein expression and SIRT-1 activation operate synergistically to mediate RUNX2 gene transcription [309, 322]. When embryonic stem cell-derived mesenchymal progenitors are cultured in adipogenic medium containing resveratrol, RUNX2 and OCN are upregulated while adipogenic genes PPARγ2 and LEPTIN are suppressed [322]. This is extremely important because PPARγ2 can prevent RUNX2 transcription and inhibit osteogenesis [343, 344]. Further studies are warranted to illucidate the temporal effect of resveratrol of osteogenic signaling pathways using appropriate *in vitro* and *in vivo* models.

6.8: Conclustions

For the first time, we demonstrated a novel approach based on the use of resveratrol to concurrently modulate inflammation, stimulate angiogenic growth factor release, and promote osteogenesis. Our results demonstrated the polarization of M1 macrophages from pro-inflammatory to wound healing M2 macrophages releasing pro-angiogenic growth factor VEGF. Resveratrol also accelerated the osteogenic differentiation of hMSCs in both 2D and 3D tissue engineering culture systems. Strikingly, the temporal release profile and amount of resveratrol can be tuned at the same time to concurrently promote osteogenesis and M2 polarization. Together, this study introduces a ground breaking synergistic method to overcome prolonged inflammation in response to implanted biomaterials in bone tissue engineering strategies,

and to harness the inflammatory response towards effective osseointegration and graft success.

CHAPTER 7: SUMMARY OF FINDINGS

The results of the research presented in this dissertation show methods of directing stem cell differentiation towards bone tissue using 3D engineered substrates. Additionally, these findings demonstrate a novel approach for harnessing inflammation to accelerate wound healing and promote osseointegration of implanted scaffolds with native host tissue. This was accomplished by three main studies.

The first investigated the use of decellularized scaffolds containing native bone extracellular matrix to direct hESC differentiation towards osteogenic lineage. Osteomimetic PLGA scaffolds were fabricated by utilizing a microsphere-sintering technique, followed by seeding hOBs on the substrates for 14 days in order to deposit bone ECM on the surface of the polymer. Analysis of the scaffold following hOB decellularization indicated that the deposited ECM had a similar composition to that of bone ECM found *in vivo*. The potential of these scaffolds as bone graft substitutes was evaluated by the *in vitro* differentiation of hESCs on the osteomimetic substrates. The decellularized scaffolds promoted cell adhesion, proliferation, and osteogenic differentiation. Incorporating native components of bone ECM with PLGA scaffolds has proven to be a successful approach to tissue engineering bone, however a more meticulous study is warranted to parse the *in vivo* mechanisms by which ECM proteins regulate osteogenesis.

The next study determined the effectiveness of resveratrol as a modulator of inflammation and promoter of osteogenesis in 2D. Our experiments investigating the dose dependent regulation of inflammatory cytokines by resveratrol demonstrated that M1 macrophages produce less IL-6 and TNF-α when cultured with resveratrol. This is paired with greater expression levels of anti-inflammatory markers VEGF, IL-10, and MRC-1 after 48 hours of exposure to the anti-inflammatory polyphenol. M1 macrophages cultured with 25 μM resveratrol demonstrated the greatest expression of wound healing markers VEGF, MRC-1 and IL-10. Consistently, M1 macrophages cultured with 25 μM resveratrol exhibited the lowest amount of inflammatory cytokine TNF-α. Inflammatory marker IL-6 reduction by resveratrol was not statistically different between the 10 μM and 25 μM groups. After investigating the immunomodulatory effects of resveratrol, we examined how resveratrol influences hMSC lineage commitment. To analyze osteogenic differentiation of hMSCs, we cultured cells in basal medium, basal medium with 12.5 μM resveratrol, osteogenic medium, and osteogenic medium with 12.5 μM resveratrol. Cells exposed to osteogenic medium supplemented with resveratrol expressed significantly higher levels of calcium, alkaline phosphatase, and osteocalcin as compared to the controls. These results altogether show the exciting potential for resveratrol to be used in tissue engineering approaches for attenuating host inflammation and stimulating osteogenic differentiation, and can be applied to a 3D scaffold design to integrate resveratrol.

The last study investigated the incorporation of resveratrol in 3D scaffolds, and observed the efficacy of these scaffolds for immunomodulation and osteogenesis. For the

first time, we demonstrated a novel approach based on the use of resveratrol to concurrently modulate inflammation, stimulate angiogenic growth factor release, and promote osteogenesis. Our results indicated the phenotypic switch of M1 macrophages from pro-inflammatory to wound healing M2 macrophages on the resveratrol-incorporated scaffolds. Along with secreting anti-inflammatory cytokines, the M2 macrophages released pro-angiogenic growth factor VEGF. Furthermore, resveratrol integrated scaffolds accelerated the osteogenic differentiation of hMSCs as compared to cells on control PLGA and TCPS. The temporal release profile and amount of resveratrol leaving the nanoparticles can be tuned to concurrently promote osteogenesis and macrophage polarization. This study introduces a ground breaking synergistic method to overcome inflammation in response to implanted biomaterials in bone tissue engineering strategies, and to harness the inflammatory response towards successful osseointegration of the graft with host tissue.

CHAPTER 8: FUTURE WORK

- Parse the *in vivo* mechanisms by which ECM proteins regulate osteogenesis
- Determine which ECM components have the greatest effect on osteogenic differentiation of hESCs cultured on osteomimetic PLGA
- Implant osteomimetic scaffold in animal model to study *in vivo* capabilities of the graft to repair a critical size defect in bone
- Investigate the interplay between hMSCs and macrophages (M0, M1 and M2) in 2D
- Determine how macrophages regulate the osteogenic differentiation of hMSCs on 3D resveratrol-incorporated scaffolds
- Implant resveratrol PLGA scaffolds in animal model to investigate how the scaffold modulates the *in vivo* inflammation response as well as promotes osteogenesis and osseointegration

References

1. Langer, R. and J.P. Vacanti, *Tissue engineering*. Science, 1993. **260**(5110): p. 920-6.
2. Giannoudis, P.V., H. Dinopoulos, and E. Tsiridis, *Bone substitutes: an update*. Injury, 2005. **36 Suppl 3**: p. S20-7.
3. Parikh, S.N., *Bone graft substitutes in modern orthopedics*. Orthopedics, 2002. **25**(11): p. 1301-9; quiz 1310-1.
4. Laurencin, C.T., et al., *Tissue engineering: orthopedic applications*. Annu Rev Biomed Eng, 1999. **1**: p. 19-46.
5. Biermann, J.S., et al., *Metastatic bone disease: diagnosis, evaluation, and treatment*. J Bone Joint Surg Am, 2009. **91**(6): p. 1518-30.
6. Muscolo, D.L., et al., *Use of distal femoral osteoarticular allografts in limb salvage surgery. Surgical technique*. J Bone Joint Surg Am, 2006. **88 Suppl 1 Pt 2**: p. 305-21.
7. Johari, A., et al., *The use of irradiated allograft in a paediatric population: an Indian experience*. Cell Tissue Bank, 2007. **8**(1): p. 13-22.
8. Laurencin, C.T., et al., *Tissue engineering: Orthopedic applications*. Annual Review of Biomedical Engineering, 1999. **1**: p. 19-46.
9. Buck, B.E., T.I. Malinin, and M.D. Brown, *Bone transplantation and human immunodeficiency virus. An estimate of risk of acquired immunodeficiency syndrome (AIDS)*. Clin Orthop Relat Res, 1989(240): p. 129-36.
10. Lewandrowski, K.U., et al., *Immune response to perforated and partially demineralized bone allografts*. J Orthop Sci, 2001. **6**(6): p. 545-55.
11. Moreau, M.F., et al., *Gamma irradiation of human bone allografts alters medullary lipids and releases toxic compounds for osteoblast-like cells*. Biomaterials, 2000. **21**(4): p. 369-76.
12. Mankin, H.J., F.J. Hornicek, and K.A. Raskin, *Infection in massive bone allografts*. Clin Orthop Relat Res, 2005(432): p. 210-6.
13. Kessler, P., et al., *Harvesting of bone from the iliac crest--comparison of the anterior and posterior sites*. Br J Oral Maxillofac Surg, 2005. **43**(1): p. 51-6.
14. Salgado, A.J., O.P. Coutinho, and R.L. Reis, *Bone tissue engineering: State of the art and future trends*. Macromolecular Bioscience, 2004. **4**(8): p. 743-765.
15. Rho, J.Y., L. Kuhn-Spearing, and P. Zioupos, *Mechanical properties and the hierarchical structure of bone*. Medical Engineering & Physics, 1998. **20**(2): p. 92-102.
16. Gentili, C. and R. Cancedda, *Cartilage and bone extracellular matrix*. Curr Pharm Des, 2009. **15**(12): p. 1334-48.
17. Weiner, S. and L. Addadi, *Design strategies in mineralized biological materials*. J. Mater. Chem., 1997. **7**(5): p. 689-702.
18. Clarke, B., *Normal bone anatomy and physiology*. Clin J Am Soc Nephrol, 2008. **3 Suppl 3**: p. S131-9.
19. Trueta, J., *The Role of the Vessels in Osteogenesis*. Journal of Bone and Joint Surgery-British Volume, 1963. **45**(2): p. 402-418.
20. Johnson, E.O., K. Soultanis, and P.N. Soucacos, *Vascular anatomy and microcirculation of skeletal zones vulnerable to osteonecrosis: vascularization of the femoral head*. Orthopedic Clinics of North America, 2004. **35**(3): p. 285-+.

21.   McCarthy, I., *The physiology of bone blood flow: A review.* Journal of Bone and Joint Surgery-American Volume, 2006. **88A**: p. 4-9.

22.   Hutmacher, D.W. and M. Sittinger, *Periosteal cells in bone tissue engineering.* Tissue Engineering, 2003. **9**: p. S45-S64.

23.   Laroche, M., *Intraosseous circulation from physiology to disease.* Joint Bone Spine, 2002. **69**(3): p. 262-269.

24.   Wilson, A. and A. Trumpp, *Bone-marrow haematopoietic-stem-cell niches.* Nature Reviews Immunology, 2006. **6**(2): p. 93-106.

25.   Draenert, K. and Y. Draenert, *The vascular system of bone marrow.* Scan Electron Microsc, 1980(4): p. 113-22.

26.   Lovett, M., et al., *Vascularization Strategies for Tissue Engineering.* Tissue Engineering Part B-Reviews, 2009. **15**(3): p. 353-370.

27.   Kannan, R.Y., et al., *The roles of tissue engineering and vascularisation in the development of micro-vascular networks: a review.* Biomaterials, 2005. **26**(14): p. 1857-1875.

28.   Anderson, J.M., *Biological responses to materials.* Annual Review of Materials Research, 2001. **31**: p. 81-110.

29.   Wynn, T.A. and L. Barron, *Macrophages: master regulators of inflammation and fibrosis.* Semin Liver Dis, 2010. **30**(3): p. 245-57.

30.   Sindrilaru, A., et al., *An unrestrained proinflammatory M1 macrophage population induced by iron impairs wound healing in humans and mice.* J Clin Invest, 2011. **121**(3): p. 985-97.

31.   Williams, G.T. and W.J. Williams, *Granulomatous inflammation--a review.* J Clin Pathol, 1983. **36**(7): p. 723-33.

32.   Johnston, R.B., *Current Concepts - Immunology - Monocytes and Macrophages.* New England Journal of Medicine, 1988. **318**(12): p. 747-752.

33.   Cotran RZ, K.V., Robbins SL, *Pathologic Basis of Disease.* 1999, Saunders: Philadelphia. p. 50-112.

34.   Gallin JI, S.R., *Inflammation: Basic Principles and Clinical Correlates.* Vol. 2nd edition. 1999, New York: Raven.

35.   Chambers, T.J. and W.G. Spector, *Inflammatory giant cells.* Immunobiology, 1982. **161**(3-4): p. 283-9.

36.   Rae, T., *The Macrophage Response to Implant Materials - with Special Reference to Those Used in Orthopedics.* Crc Critical Reviews in Biocompatibility, 1986. **2**(2): p. 97-126.

37.   Anderson, J.M., *Inflammatory response to implants.* ASAIO Trans, 1988. **34**(2): p. 101-7.

38.   Greisler, H., *Macrophage-biomaterial interactions with bioresorbable vascular prostheses.* ASAIO Trans, 1988. **34**(4): p. 1051-9.

39.   Anderson, J.M., *Mechanisms of Inflammation and Infection with Implanted Devices.* Cardiovascular Pathology, 1993. **2**(3): p. S33-S41.

40.   Gopferich, A., *Mechanisms of polymer degradation and erosion.* Biomaterials, 1996. **17**(2): p. 103-14.

41.   Morais, J.M., F. Papadimitrakopoulos, and D.J. Burgess, *Biomaterials/tissue interactions: possible solutions to overcome foreign body response.* AAPS J, 2010. **12**(2): p. 188-96.

42.   Shastri, V.P., *Non-degradable biocompatible polymers in medicine: past, present and future.* Curr Pharm Biotechnol, 2003. **4**(5): p. 331-7.

43. Shen, M. and T.A. Horbett, *The effects of surface chemistry and adsorbed proteins on monocyte/macrophage adhesion to chemically modified polystyrene surfaces.* J Biomed Mater Res, 2001. **57**(3): p. 336-45.

44. Dalsin, J.L., et al., *Mussel adhesive protein mimetic polymers for the preparation of nonfouling surfaces.* J Am Chem Soc, 2003. **125**(14): p. 4253-8.

45. Williams, D.F., *Tissue - Biomaterial Interactions.* Journal of Materials Science, 1987. **22**(10): p. 3421-3445.

46. Ward, W.K., et al., *Vascularizing the tissue surrounding a model biosensor: how localized is the effect of a subcutaneous infusion of vascular endothelial growth factor (VEGF)?* Biosens Bioelectron, 2003. **19**(3): p. 155-163.

47. Kedem, A., et al., *Vascular endothelial growth factor-releasing scaffolds enhance vascularization and engraftment of hepatocytes transplanted on liver lobes.* Tissue Engineering, 2005. **11**(5-6): p. 715-722.

48. Patil, S.D., F. Papadmitrakopoulos, and D.J. Burgess, *Concurrent delivery of dexamethasone and VEGF for localized inflammation control and angiogenesis.* Journal of Controlled Release, 2007. **117**(1): p. 68-79.

49. Henry, T.D., *Science, medicine, and the future - Therapeutic angiogenesis.* British Medical Journal, 1999. **318**(7197): p. 1536-1539.

50. Epstein, S.E., et al., *Therapeutic interventions for enhancing collateral development by administration of growth factors: basic principles, early results and potential hazards.* Cardiovasc Res, 2001. **49**(3): p. 532-42.

51. Emanueli, C. and P. Madeddu, *Angiogenesis gene therapy to rescue ischaemic tissues: achievements and future directions.* Br J Pharmacol, 2001. **133**(7): p. 951-958.

52. Perretti, M. and A. Ahluwalia, *The microcirculation and inflammation: Site of action for glucocorticoids.* Microcirculation, 2000. **7**(3): p. 147-161.

53. Morais, J.M., F. Papadimitrakopoulos, and D.J. Burgess, *Biomaterials/Tissue Interactions: Possible Solutions to Overcome Foreign Body Response.* Aaps Journal, 2010. **12**(2): p. 188-196.

54. Halaby, I.A., et al., *Glucocorticoid-regulated VEGF expression in ischemic skeletal muscle.* Molecular Therapy, 2002. **5**(3): p. 300-306.

55. Gaytan, F., et al., *Selective apoptosis of luteal endothelial cells in dexamethasone-treated rats leads to ischemic necrosis of luteal tissue.* Biology of Reproduction, 2002. **66**(1): p. 232-240.

56. Young, H.E. and A.C. Black, Jr., *Adult stem cells.* Anat Rec A Discov Mol Cell Evol Biol, 2004. **276**(1): p. 75-102.

57. Mauro, A., *Satellite cell of skeletal muscle fibers.* J Biophys Biochem Cytol, 1961. **9**: p. 493-5.

58. Cruess, R.L., *The Musculoskeletal system : embryology, biochemistry, and physiology.* 1982, New York: Churchill Livingstone. viii, 410 p.

59. Owen, M. and A.J. Friedenstein, *Stromal stem cells: marrow-derived osteogenic precursors.* Ciba Found Symp, 1988. **136**: p. 42-60.

60. Gage, F.H., et al., *Survival and differentiation of adult neuronal progenitor cells transplanted to the adult brain.* Proc Natl Acad Sci U S A, 1995. **92**(25): p. 11879-83.

61. Janes, S.M., S. Lowell, and C. Hutter, *Epidermal stem cells.* Journal of Pathology, 2002. **197**(4): p. 479-91.

62. Hayflick, L., *The Limited in Vitro Lifetime of Human Diploid Cell Strains.* Exp Cell Res, 1965. **37**: p. 614-36.

63. Petite, H., et al., *Tissue-engineered bone regeneration.* Nat Biotechnol, 2000. **18**(9): p. 959-63.

64. Li, C., et al., *Electrospun silk-BMP-2 scaffolds for bone tissue engineering.* Biomaterials, 2006. **27**(16): p. 3115-24.

65. Bruder, S.P., N. Jaiswal, and S.E. Haynesworth, *Growth kinetics, self-renewal, and the osteogenic potential of purified human mesenchymal stem cells during extensive subcultivation and following cryopreservation.* Journal of Cellular Biochemistry, 1997. **64**(2): p. 278-94.

66. Meinel, L., et al., *Bone tissue engineering using human mesenchymal stem cells: effects of scaffold material and medium flow.* Ann Biomed Eng, 2004. **32**(1): p. 112-22.

67. Haynesworth, S.E., et al., *Characterization of Cells with Osteogenic Potential from Human Marrow.* Bone, 1992. **13**(1): p. 81-88.

68. Jaiswal, N., et al., *Osteogenic differentiation of purified, culture-expanded human mesenchymal stem cells in vitro.* Journal of Cellular Biochemistry, 1997. **64**(2): p. 295-312.

69. Verfaillie, C.M., *Adult stem cells: assessing the case for pluripotency.* Trends in Cell Biology, 2002. **12**(11): p. 502-508.

70. Quarto, R., D. Thomas, and C.T. Liang, *Bone Progenitor-Cell Deficits and the Age-Associated Decline in Bone Repair Capacity.* Calcified Tissue International, 1995. **56**(2): p. 123-129.

71. Meijer, G.J., et al., *Cell-based bone tissue engineering.* PLoS Med, 2007. **4**(2): p. e9.

72. Cuomo, A.V., et al., *Mesenchymal stem cell concentration and bone repair: potential pitfalls from bench to bedside.* J Bone Joint Surg Am, 2009. **91**(5): p. 1073-83.

73. Gage, F.H., *Mammalian neural stem cells.* Science, 2000. **287**(5457): p. 1433-8.

74. Lee, R.H., et al., *Characterization and expression analysis of mesenchymal stem cells from human bone marrow and adipose tissue.* Cell Physiol Biochem, 2004. **14**(4-6): p. 311-24.

75. Zuk, P.A., et al., *Multilineage cells from human adipose tissue: implications for cell-based therapies.* Tissue Engineering, 2001. **7**(2): p. 211-28.

76. Zuk, P.A., et al., *Human adipose tissue is a source of multipotent stem cells.* Mol Biol Cell, 2002. **13**(12): p. 4279-95.

77. Seo, M.J., et al., *Differentiation of human adipose stromal cells into hepatic lineage in vitro and in vivo.* Biochem Biophys Res Commun, 2005. **328**(1): p. 258-64.

78. Cao, Y., et al., *Human adipose tissue-derived stem cells differentiate into endothelial cells in vitro and improve postnatal neovascularization in vivo.* Biochem Biophys Res Commun, 2005. **332**(2): p. 370-9.

79. Kuznetsov, S.A., et al., *Single-colony derived strains of human marrow stromal fibroblasts form bone after transplantation in vivo.* Journal of Bone and Mineral Research, 1997. **12**(9): p. 1335-47.

80. Friedenstein, A.J., R.K. Chailakhyan, and U.V. Gerasimov, *Bone marrow osteogenic stem cells: in vitro cultivation and transplantation in diffusion chambers.* Cell Tissue Kinet, 1987. **20**(3): p. 263-72.

81. Haynesworth, S.E., et al., *Characterization of cells with osteogenic potential from human marrow.* Bone, 1992. **13**(1): p. 81-8.

82. Pittenger, M.F., et al., *Multilineage potential of adult human mesenchymal stem cells.* Science, 1999. **284**(5411): p. 143-7.

83. Heng, B.C., et al., *Strategies for directing the differentiation of stem cells into the osteogenic lineage in vitro.* Journal of Bone and Mineral Research, 2004. **19**(9): p. 1379-94.

84. Kwan, M.D., et al., *Cell-based therapies for skeletal regenerative medicine.* Hum Mol Genet, 2008. **17**(R1): p. R93-8.

85.	Menendez, P., C. Bueno, and L. Wang, *Human embryonic stem cells: A journey beyond cell replacement therapies.* Cytotherapy, 2006. **8**(6): p. 530-41.

86.	Evans, M.J. and M.H. Kaufman, *Establishment in culture of pluripotential cells from mouse embryos.* Nature, 1981. **292**(5819): p. 154-6.

87.	Martin, G.R., *Isolation of a pluripotent cell line from early mouse embryos cultured in medium conditioned by teratocarcinoma stem cells.* Proc Natl Acad Sci U S A, 1981. **78**(12): p. 7634-8.

88.	Thomson, J.A., et al., *Embryonic stem cell lines derived from human blastocysts.* Science, 1998. **282**(5391): p. 1145-7.

89.	Itskovitz-Eldor, J., et al., *Differentiation of human embryonic stem cells into embryoid bodies compromising the three embryonic germ layers.* Mol Med, 2000. **6**(2): p. 88-95.

90.	Dang, S.M., et al., *Efficiency of embryoid body formation and hematopoietic development from embryonic stem cells in different culture systems.* Biotechnol Bioeng, 2002. **78**(4): p. 442-53.

91.	Karp, J.M., et al., *Cultivation of human embryonic stem cells without the embryoid body step enhances osteogenesis in vitro.* Stem Cells, 2006. **24**(4): p. 835-43.

92.	Ahn, S.E., et al., *Primary bone-derived cells induce osteogenic differentiation without exogenous factors in human embryonic stem cells.* Biochem Biophys Res Commun, 2006. **340**(2): p. 403-8.

93.	Kuznetsov, S.A., N. Cherman, and P.G. Robey, *In vivo bone formation by progeny of human embryonic stem cells.* Stem Cells Dev, 2011. **20**(2): p. 269-87.

94.	Mateizel, I., et al., *Efficient differentiation of human embryonic stem cells into a homogeneous population of osteoprogenitor-like cells.* Reprod Biomed Online, 2008. **16**(5): p. 741-53.

95.	James, D., et al., *Expansion and maintenance of human embryonic stem cell-derived endothelial cells by TGFbeta inhibition is Id1 dependent.* Nat Biotechnol, 2010. **28**(2): p. 161-6.

96.	Lee, H., et al., *Directed differentiation and transplantation of human embryonic stem cell-derived motoneurons.* Stem Cells, 2007. **25**(8): p. 1931-9.

97.	Zaidi, M., *Skeletal remodeling in health and disease.* Nat Med, 2007. **13**(7): p. 791-801.

98.	Datta, N., et al., *Effect of bone extracellular matrix synthesized in vitro on the osteoblastic differentiation of marrow stromal cells.* Biomaterials, 2005. **26**(9): p. 971-7.

99.	Marcos-Campos, I., et al., *Bone scaffold architecture modulates the development of mineralized bone matrix by human embryonic stem cells.* Biomaterials, 2012. **33**(33): p. 8329-42.

100.	Peel, S.A., Z.M. Hu, and C.M. Clokie, *In search of the ideal bone morphogenetic protein delivery system: in vitro studies on demineralized bone matrix, purified, and recombinant bone morphogenetic protein.* J Craniofac Surg, 2003. **14**(3): p. 284-91.

101.	Zambonin, G. and M. Grano, *Biomaterials in orthopaedic surgery: effects of different hydroxyapatites and demineralized bone matrix on proliferation rate and bone matrix synthesis by human osteoblasts.* Biomaterials, 1995. **16**(5): p. 397-402.

102.	Hott, M., et al., *Proliferation and differentiation of human trabecular osteoblastic cells on hydroxyapatite.* J Biomed Mater Res, 1997. **37**(4): p. 508-16.

103.	Ong, J.L., D.L. Carnes, and A. Sogal, *Effect of transforming growth factor-beta on osteoblast cells cultured on 3 different hydroxyapatite surfaces.* Int J Oral Maxillofac Implants, 1999. **14**(2): p. 217-25.

104.	Toquet, J., et al., *Osteogenic potential in vitro of human bone marrow cells cultured on macroporous biphasic calcium phosphate ceramic.* J Biomed Mater Res, 1999. **44**(1): p. 98-108.

105.   Acil, Y., et al., *Three-dimensional cultivation of human osteoblast-like cells on highly porous natural bone mineral.* J Biomed Mater Res, 2000. **51**(4): p. 703-10.

106.   Knabe, C., et al., *Evaluation of calcium phosphates and experimental calcium phosphate bone cements using osteogenic cultures.* J Biomed Mater Res, 2000. **52**(3): p. 498-508.

107.   Ohgushi, H., J. Miyake, and T. Tateishi, *Mesenchymal stem cells and bioceramics: strategies to regenerate the skeleton.* Novartis Found Symp, 2003. **249**: p. 118-27; discussion 127-32, 170-4, 239-41.

108.   Pham, Q.P., et al., *The influence of an in vitro generated bone-like extracellular matrix on osteoblastic gene expression of marrow stromal cells.* Biomaterials, 2008. **29**(18): p. 2729-39.

109.   Takahashi, K. and S. Yamanaka, *Induction of pluripotent stem cells from mouse embryonic and adult fibroblast cultures by defined factors.* Cell, 2006. **126**(4): p. 663-676.

110.   Takahashi, K., et al., *Induction of pluripotent stem cells from adult human fibroblasts by defined factors.* Cell, 2007. **131**(5): p. 861-872.

111.   Yu, J.Y., et al., *Induced pluripotent stem cell lines derived from human somatic cells.* Science, 2007. **318**(5858): p. 1917-1920.

112.   Tang, C., I.L. Weissman, and M. Drukker, *The safety of embryonic stem cell therapy relies on teratoma removal.* Oncotarget, 2012. **3**(1): p. 7-8.

113.   Chang, Y.L., et al., *Docosahexaenoic acid promotes dopaminergic differentiation in induced pluripotent stem cells and inhibits teratoma formation in rats with Parkinson-like pathology.* Cell Transplant, 2012. **21**(1): p. 313-32.

114.   Hashimoto, J., Y. Kariya, and K. Miyazaki, *Regulation of proliferation and chondrogenic differentiation of human mesenchymal stem cells by laminin-5 (laminin-332).* Stem Cells, 2006. **24**(11): p. 2346-54.

115.   Mizuno, M. and Y. Kuboki, *Osteoblast-related gene expression of bone marrow cells during the osteoblastic differentiation induced by type I collagen.* J Biochem, 2001. **129**(1): p. 133-8.

116.   Salasznyk, R.M., et al., *Adhesion to Vitronectin and Collagen I Promotes Osteogenic Differentiation of Human Mesenchymal Stem Cells.* J Biomed Biotechnol, 2004. **2004**(1): p. 24-34.

117.   Moursi, A.M., R.K. Globus, and C.H. Damsky, *Interactions between integrin receptors and fibronectin are required for calvarial osteoblast differentiation in vitro.* J Cell Sci, 1997. **110 (Pt 18)**: p. 2187-96.

118.   Discher, D.E., D.J. Mooney, and P.W. Zandstra, *Growth factors, matrices, and forces combine and control stem cells.* Science, 2009. **324**(5935): p. 1673-7.

119.   Cohen, D.M. and C.S. Chen, *Mechanical control of stem cell differentiation*, in *StemBook*. 2008: Cambridge (MA).

120.   Guilak, F., et al., *Control of stem cell fate by physical interactions with the extracellular matrix.* Cell Stem Cell, 2009. **5**(1): p. 17-26.

121.   Wang, J.H. and B.P. Thampatty, *Mechanobiology of adult and stem cells.* Int Rev Cell Mol Biol, 2008. **271**: p. 301-46.

122.   Sun, Y., C.S. Chen, and J. Fu, *Forcing stem cells to behave: a biophysical perspective of the cellular microenvironment.* Annu Rev Biophys, 2012. **41**: p. 519-42.

123.   Lutolf, M.P. and J.A. Hubbell, *Synthetic biomaterials as instructive extracellular microenvironments for morphogenesis in tissue engineering.* Nat Biotechnol, 2005. **23**(1): p. 47-55.

124.   Wu, K.C., et al., *Nanotechnology in the regulation of stem cell behavior.* Science and Technology of Advanced Materials, 2013. **14**(5).

125. Stout, D.A. and T.J. Webster, *Carbon nanotubes for stem cell control.* Materials Today, 2012. **15**(7-8): p. 312-318.

126. Chen, C.S., *Mechanotransduction - a field pulling together?* J Cell Sci, 2008. **121**(Pt 20): p. 3285-92.

127. Geiger, B., J.P. Spatz, and A.D. Bershadsky, *Environmental sensing through focal adhesions.* Nature Reviews Molecular Cell Biology, 2009. **10**(1): p. 21-33.

128. Osol, G., *Mechanotransduction by vascular smooth muscle.* J Vasc Res, 1995. **32**(5): p. 275-92.

129. Davies, P.F., *Flow-mediated endothelial mechanotransduction.* Physiol Rev, 1995. **75**(3): p. 519-60.

130. Chien, S., *Mechanotransduction and endothelial cell homeostasis: the wisdom of the cell.* Am J Physiol Heart Circ Physiol, 2007. **292**(3): p. H1209-24.

131. Engler, A.J., et al., *Matrix elasticity directs stem cell lineage specification.* Cell, 2006. **126**(4): p. 677-689.

132. Saha, S., et al., *Inhibition of human embryonic stem cell differentiation by mechanical strain.* J Cell Physiol, 2006. **206**(1): p. 126-37.

133. Saha, S., et al., *TGFbeta/Activin/Nodal pathway in inhibition of human embryonic stem cell differentiation by mechanical strain.* Biophysical Journal, 2008. **94**(10): p. 4123-33.

134. Chowdhury, F., et al., *Material properties of the cell dictate stress-induced spreading and differentiation in embryonic stem cells.* Nat Mater, 2010. **9**(1): p. 82-8.

135. Keung, A.J., S. Kumar, and D.V. Schaffer, *Presentation counts: microenvironmental regulation of stem cells by biophysical and material cues.* Annu Rev Cell Dev Biol, 2010. **26**: p. 533-56.

136. Kim, L., et al., *Microfluidic arrays for logarithmically perfused embryonic stem cell culture.* Lab Chip, 2006. **6**(3): p. 394-406.

137. Illi, B., et al., *Epigenetic histone modification and cardiovascular lineage programming in mouse embryonic stem cells exposed to laminar shear stress.* Circ Res, 2005. **96**(5): p. 501-8.

138. Yamamoto, K., et al., *Fluid shear stress induces differentiation of Flk-1-positive embryonic stem cells into vascular endothelial cells in vitro.* Am J Physiol Heart Circ Physiol, 2005. **288**(4): p. H1915-24.

139. Adamo, L., et al., *Biomechanical forces promote embryonic haematopoiesis.* Nature, 2009. **459**(7250): p. 1131-5.

140. Chun, T.H., et al., *A pericellular collagenase directs the 3-dimensional development of white adipose tissue.* Cell, 2006. **125**(3): p. 577-91.

141. Young, J.L. and A.J. Engler, *Hydrogels with time-dependent material properties enhance cardiomyocyte differentiation in vitro.* Biomaterials, 2011. **32**(4): p. 1002-9.

142. Moore, K.A., et al., *Control of basement membrane remodeling and epithelial branching morphogenesis in embryonic lung by Rho and cytoskeletal tension.* Dev Dyn, 2005. **232**(2): p. 268-81.

143. Chowdhury, F., et al., *Soft substrates promote homogeneous self-renewal of embryonic stem cells via downregulating cell-matrix tractions.* PLoS One, 2010. **5**(12): p. e15655.

144. Folkman, J. and A. Moscona, *Role of cell shape in growth control.* Nature, 1978. **273**(5661): p. 345-9.

145. McBeath, R., et al., *Cell shape, cytoskeletal tension, and RhoA regulate stem cell lineage commitment.* Dev Cell, 2004. **6**(4): p. 483-95.

146. Yang, Y., et al., *Embryonic mesenchymal cells share the potential for smooth muscle differentiation: myogenesis is controlled by the cell's shape.* Development, 1999. **126**(13): p. 3027-33.

147. Manasek, F.J., M.B. Burnside, and R.E. Waterman, *Myocardial cell shape change as a mechanism of embryonic heart looping.* Dev Biol, 1972. **29**(4): p. 349-71.

148. Ingber, D., *Extracellular matrix and cell shape: potential control points for inhibition of angiogenesis.* Journal of Cellular Biochemistry, 1991. **47**(3): p. 236-41.

149. Chen, C.S., et al., *Geometric control of cell life and death.* Science, 1997. **276**(5317): p. 1425-8.

150. Bauwens, C.L., et al., *Control of human embryonic stem cell colony and aggregate size heterogeneity influences differentiation trajectories.* Stem Cells, 2008. **26**(9): p. 2300-10.

151. Peerani, R., et al., *Niche-mediated control of human embryonic stem cell self-renewal and differentiation.* EMBO J, 2007. **26**(22): p. 4744-55.

152. Stevens, M.M. and J.H. George, *Exploring and engineering the cell surface interface.* Science, 2005. **310**(5751): p. 1135-1138.

153. Berkovitz, B.K. and J. Pacy, *Ultrastructure of the human intra-articular disc of the temporomandibular joint.* Eur J Orthod, 2002. **24**(2): p. 151-8.

154. Dalby, M.J., et al., *Investigating the limits of filopodial sensing: a brief report using SEM to image the interaction between 10 nm high nano-topography and fibroblast filopodia.* Cell Biol Int, 2004. **28**(3): p. 229-236.

155. Wong, J.Y., J.B. Leach, and X.Q. Brown, *Balance of chemistry, topography, and mechanics at the cell-biomaterial interface: Issues and challenges for assessing the role of substrate mechanics on cell response.* Surface Science, 2004. **570**(1-2): p. 119-133.

156. Griffith, L.G. and M.A. Swartz, *Capturing complex 3D tissue physiology in vitro.* Nature Reviews Molecular Cell Biology, 2006. **7**(3): p. 211-224.

157. Curtis, A.S.G. and C.D. Wilkinson, *Reactions of cells to topography.* Journal of Biomaterials Science-Polymer Edition, 1998. **9**(12): p. 1313-1329.

158. Flemming, R.G., et al., *Effects of synthetic micro- and nano-structured surfaces on cell behavior.* Biomaterials, 1999. **20**(6): p. 573-88.

159. Lim, J.Y. and H.J. Donahue, *Cell sensing and response to micro- and nanostructured surfaces produced by chemical and topographic patterning.* Tissue Engineering, 2007. **13**(8): p. 1879-91.

160. Kong, H.J. and D.J. Mooney, *Microenvironmental regulation of biomacromolecular therapies.* Nat Rev Drug Discov, 2007. **6**(6): p. 455-63.

161. Reilly, G.C. and A.J. Engler, *Intrinsic extracellular matrix properties regulate stem cell differentiation.* J Biomech, 2010. **43**(1): p. 55-62.

162. Chen, A., et al., *Shrink-film configurable multiscale wrinkles for functional alignment of human embryonic stem cells and their cardiac derivatives.* Advanced Materials, 2011. **23**(48): p. 5785-91.

163. Liu, L., et al., *Chemically-defined scaffolds created with electrospun synthetic nanofibers to maintain mouse embryonic stem cell culture under feeder-free conditions.* Biotechnol Lett, 2012. **34**(10): p. 1951-7.

164. Gerecht, S., et al., *The effect of actin disrupting agents on contact guidance of human embryonic stem cells.* Biomaterials, 2007. **28**(28): p. 4068-77.

165. Nur-E-Kamal, A., et al., *Covalently attached FGF-2 to three-dimensional polyamide nanofibrillar surfaces demonstrates enhanced biological stability and activity.* Molecular and Cellular Biochemistry, 2008. **309**(1-2): p. 157-166.

166. Lee, M.R., et al., *Direct differentiation of human embryonic stem cells into selective neurons on nanoscale ridge/groove pattern arrays.* Biomaterials, 2010. **31**(15): p. 4360-6.

167. Kabiri, M., et al., *Neural differentiation of mouse embryonic stem cells on conductive nanofiber scaffolds.* Biotechnol Lett, 2012. **34**(7): p. 1357-65.

168. Pan, F., et al., *Topographic effect on human induced pluripotent stem cells differentiation towards neuronal lineage.* Biomaterials, 2013. **34**(33): p. 8131-9.

169. Brunner, E.W., et al., *Growth and proliferation of human embryonic stem cells on fully synthetic scaffolds based on carbon nanotubes.* ACS Appl Mater Interfaces, 2014. **6**(4): p. 2598-603.

170. Chao, T.I., et al., *Carbon nanotubes promote neuron differentiation from human embryonic stem cells.* Biochem Biophys Res Commun, 2009. **384**(4): p. 426-30.

171. Pryzhkova, M.V., et al., *Carbon nanotube-based substrates for modulation of human pluripotent stem cell fate.* Biomaterials, 2014. **35**(19): p. 5098-109.

172. Sridharan, I., T. Kim, and R. Wang, *Adapting collagen/CNT matrix in directing hESC differentiation.* Biochem Biophys Res Commun, 2009. **381**(4): p. 508-12.

173. Chen, W., et al., *Nanotopography influences adhesion, spreading, and self-renewal of human embryonic stem cells.* ACS Nano, 2012. **6**(5): p. 4094-103.

174. Ji, L.J., et al., *Changes in Embryonic Stem Cell Colony Morphology and Early Differentiation Markers Driven by Colloidal Crystal Topographical Cues.* European Cells & Materials, 2012. **23**: p. 135-146.

175. Villa-Diaz, L.G., et al., *Synthetic polymer coatings for long-term growth of human embryonic stem cells.* Nat Biotechnol, 2010. **28**(6): p. 581-3.

176. Chen, G.Y., et al., *A graphene-based platform for induced pluripotent stem cells culture and differentiation.* Biomaterials, 2012. **33**(2): p. 418-427.

177. Khademhosseini, A., et al., *Microscale technologies for tissue engineering and biology.* Proc Natl Acad Sci U S A, 2006. **103**(8): p. 2480-7.

178. Pirone, D.M. and C.S. Chen, *Strategies for engineering the adhesive microenvironment.* J Mammary Gland Biol Neoplasia, 2004. **9**(4): p. 405-17.

179. Yang, F., et al., *Electrospinning of nano/micro scale poly(L-lactic acid) aligned fibers and their potential in neural tissue engineering.* Biomaterials, 2005. **26**(15): p. 2603-10.

180. Kenawy, E.R., et al., *Electrospinning of poly(ethylene-co-vinyl alcohol) fibers.* Biomaterials, 2003. **24**(6): p. 907-913.

181. Pham, Q.P., U. Sharma, and A.G. Mikos, *Electrospinning of polymeric nanofibers for tissue engineering applications: a review.* Tissue Engineering, 2006. **12**(5): p. 1197-211.

182. Xu, C.Y., et al., *Electrospun nanofiber fabrication as synthetic extracellular matrix and its potential for vascular tissue engineering.* Tissue Engineering, 2004. **10**(7-8): p. 1160-1168.

183. Elias, K.L., R.L. Price, and T.J. Webster, *Enhanced functions of osteoblasts on nanometer diameter carbon fibers.* Biomaterials, 2002. **23**(15): p. 3279-3287.

184. Zhang, S., *Fabrication of novel biomaterials through molecular self-assembly.* Nat Biotechnol, 2003. **21**(10): p. 1171-8.

185. Menger, F.M., *Supramolecular chemistry and self-assembly.* Proc Natl Acad Sci U S A, 2002. **99**(8): p. 4818-22.

186. Estroff, L.A. and A.D. Hamilton, *Water gelation by small organic molecules.* Chem Rev, 2004. **104**(3): p. 1201-18.

187. Xia, Y.N. and G.M. Whitesides, *Soft lithography.* Angewandte Chemie-International Edition, 1998. **37**(5): p. 551-575.

188. Ostuni, E., et al., *Selective deposition of proteins and cells in arrays of microwells.* Langmuir, 2001. **17**(9): p. 2828-2834.

189. Kane, R.S., et al., *Patterning proteins and cells using soft lithography.* Biomaterials, 1999. **20**(23-24): p. 2363-2376.

190. Ostuni, E., L. Yan, and G.M. Whitesides, *The interaction of proteins and cells with self-assembled monolayers of alkanethiolates on gold and silver.* Colloids and Surfaces B-Biointerfaces, 1999. **15**(1): p. 3-30.

191. Xia, Y.N. and G.M. Whitesides, *Soft lithography.* Annual Review of Materials Science, 1998. **28**: p. 153-184.

192. Suh, K.Y., et al., *Soft lithographic patterning of hyaluronic acid on hydrophilic substrates using molding and printing.* Advanced Materials, 2004. **16**(7): p. 584-+.

193. Khademhosseini, A., et al., *Direct Patterning of protein- and cell-resistant polymeric monolayers and microstructures.* Advanced Materials, 2003. **15**(23): p. 1995-2000.

194. Harris, G.M., T. Shazly, and E. Jabbarzadeh, *Deciphering the combinatorial roles of geometric, mechanical, and adhesion cues in regulation of cell spreading.* PLoS One, 2013. **8**(11): p. e81113.

195. Whitesides, G.M., et al., *Soft lithography in biology and biochemistry.* Annu Rev Biomed Eng, 2001. **3**: p. 335-373.

196. Brangwynne, C., et al., *Symmetry breaking in cultured mammalian cells.* In Vitro Cellular & Developmental Biology-Animal, 2000. **36**(9): p. 563-565.

197. Langer, R. and D.A. Tirrell, *Designing materials for biology and medicine.* Nature, 2004. **428**(6982): p. 487-92.

198. Peppas, N.A., et al., *Physicochemical foundations and structural design of hydrogels in medicine and biology.* Annu Rev Biomed Eng, 2000. **2**: p. 9-29.

199. Drury, J.L. and D.J. Mooney, *Hydrogels for tissue engineering: scaffold design variables and applications.* Biomaterials, 2003. **24**(24): p. 4337-51.

200. Hoffman, A.S., *Hydrogels for biomedical applications.* Adv Drug Deliv Rev, 2002. **54**(1): p. 3-12.

201. Fisher, O.Z., et al., *Bioinspired Materials for Controlling Stem Cell Fate.* Accounts of Chemical Research, 2010. **43**(3): p. 419-428.

202. Hutmacher, D.W., *Scaffold design and fabrication technologies for engineering tissues--state of the art and future perspectives.* J Biomater Sci Polym Ed, 2001. **12**(1): p. 107-24.

203. Hoffman, A.S., *Hydrogels for biomedical applications.* Advanced Drug Delivery Reviews, 2012. **64**: p. 18-23.

204. Zhang, L.J. and T.J. Webster, *Nanotechnology and nanomaterials: Promises for improved tissue regeneration.* Nano Today, 2009. **4**(1): p. 66-80.

205. Li, X.M., Y.B. Fan, and F. Watari, *Current investigations into carbon nanotubes for biomedical application.* Biomedical Materials, 2010. **5**(2).

206. Kam, N.W.S., et al., *Nanotube molecular transporters: Internalization of carbon nanotube-protein conjugates into mammalian cells.* J Am Chem Soc, 2004. **126**(22): p. 6850-6851.

207. Klingeler, R., R.B. Sim, and SpringerLink (Online service), *Carbon nanotubes for biomedical applications*, in *Carbon nanostructures*. 2011, Springer,: Berlin ; Heidelberg ; New York. p. 1 online resource (xix, 278 p.) ill.

208. Li, X.M., et al., *Effect of carbon nanotubes on cellular functions in vitro.* Journal of Biomedical Materials Research Part A, 2009. **91A**(1): p. 132-139.

209. Cheng, Q., K. Rutledge, and E. Jabbarzadeh, *Carbon nanotube-poly(lactide-co-glycolide) composite scaffolds for bone tissue engineering applications.* Ann Biomed Eng, 2013. **41**(5): p. 904-16.

210. Zanello, L.P., et al., *Bone cell proliferation on carbon nanotubes.* Nano Lett, 2006. **6**(3): p. 562-7.

211. Shi, X., et al., *Fabrication of porous ultra-short single-walled carbon nanotube nanocomposite scaffolds for bone tissue engineering.* Biomaterials, 2007. **28**(28): p. 4078-90.

212. Mikael, P.E., et al., *Functionalized carbon nanotube reinforced scaffolds for bone regenerative engineering: fabrication, in vitro and in vivo evaluation.* Biomed Mater, 2014. **9**(3): p. 035001.

213. Hu, H., et al., *Chemically Functionalized Carbon Nanotubes as Substrates for Neuronal Growth.* Nano Lett, 2004. **4**(3): p. 507-511.

214. McKeon-Fischer, K.D., D.H. Flagg, and J.W. Freeman, *Coaxial electrospun poly(epsilon-caprolactone), multiwalled carbon nanotubes, and polyacrylic acid/polyvinyl alcohol scaffold for skeletal muscle tissue engineering.* J Biomed Mater Res A, 2011. **99**(3): p. 493-9.

215. Ni, Y., et al., *Chemically functionalized water soluble single-walled carbon nanotubes modulate neurite outgrowth.* J Nanosci Nanotechnol, 2005. **5**(10): p. 1707-12.

216. Whitesides, G.M., *The origins and the future of microfluidics.* Nature, 2006. **442**(7101): p. 368-73.

217. Lu, H., et al., *Microfluidic shear devices for quantitative analysis of cell adhesion.* Analytical Chemistry, 2004. **76**(18): p. 5257-64.

218. Takayama, S., et al., *Selective chemical treatment of cellular microdomains using multiple laminar streams.* Chem Biol, 2003. **10**(2): p. 123-30.

219. Glasgow, I.K., et al., *Handling individual mammalian embryos using microfluidics.* IEEE Trans Biomed Eng, 2001. **48**(5): p. 570-8.

220. Walters, E.M., et al., *Mammalian embryo culture in a microfluidic device.* Methods Mol Biol, 2004. **254**: p. 375-82.

221. Lucchetta, E.M., et al., *Dynamics of Drosophila embryonic patterning network perturbed in space and time using microfluidics.* Nature, 2005. **434**(7037): p. 1134-8.

222. Yannas, I.V., et al., *Wound Tissue Can Utilize a Polymeric Template to Synthesize a Functional Extension of Skin.* Science, 1982. **215**(4529): p. 174-176.

223. Bell, E., et al., *Living tissue formed in vitro and accepted as skin-equivalent tissue of full thickness.* Science, 1981. **211**(4486): p. 1052-4.

224. Atala, A., et al., *Tissue-engineered autologous bladders for patients needing cystoplasty.* Lancet, 2006. **367**(9518): p. 1241-6.

225. Carrier, P., et al., *Impact of cell source on human cornea reconstructed by tissue engineering.* Invest Ophthalmol Vis Sci, 2009. **50**(6): p. 2645-52.

226. Vrana, N.E., et al., *Development of a reconstructed cornea from collagen-chondroitin sulfate foams and human cell cultures.* Invest Ophthalmol Vis Sci, 2008. **49**(12): p. 5325-31.

227. van Kooten, T.G. and A.F. von Recum, *Cell adhesion to textured silicone surfaces: The influence of time of adhesion and texture on focal contact and fibronectin fibril formation.* Tissue Engineering, 1999. **5**(3): p. 223-240.

228. Jiang, X.Y., et al., *Controlling mammalian cell spreading and cytoskeletal arrangement with conveniently fabricated continuous wavy features on poly(dimethylsiloxane).* Langmuir, 2002. **18**(8): p. 3273-3280.

229. Fidkowski, C., et al., *Endothelialized microvasculature based on a biodegradable elastomer.* Tissue Engineering, 2005. **11**(1-2): p. 302-309.

230. Shin, M., et al., *Endothelialized networks with a vascular geometry in microfabricated poly(dimethyl siloxane).* Biomedical Microdevices, 2004. **6**(4): p. 269-278.

231. Borenstein, J.T., et al., *Microfabrication of three-dimensional engineered scaffolds.* Tissue Engineering, 2007. **13**(8): p. 1837-1844.

232. Cooke, M.N., et al., *Use of stereolithography to manufacture critical-sized 3D biodegradable scaffolds for bone ingrowth.* Journal of Biomedical Materials Research Part B-Applied Biomaterials, 2003. **64B**(2): p. 65-69.

233. Du, Y.A., et al., *Sequential Assembly of Cell-Laden Hydrogel Constructs to Engineer Vascular-Like Microchannels.* Biotechnology and Bioengineering, 2011. **108**(7): p. 1693-1703.

234. Khademhosseini, A. and R. Langer, *Microengineered hydrogels for tissue engineering.* Biomaterials, 2007. **28**(34): p. 5087-5092.

235. Mironov, V., et al., *Organ printing: computer-aided jet-based 3D tissue engineering.* Trends in Biotechnology, 2003. **21**(4): p. 157-161.

236. Yang, H.Y., et al., *Fine ceramic lattices prepared by extrusion freeforming.* Journal of Biomedical Materials Research Part B-Applied Biomaterials, 2006. **79B**(1): p. 116-121.

237. Tan, W. and T.A. Desai, *Layer-by-layer microfluidics for biomimetic three-dimensional structures.* Biomaterials, 2004. **25**(7-8): p. 1355-1364.

238. Raghavan, S., et al., *Geometrically Controlled Endothelial Tubulogenesis in Micropatterned Gels.* Tissue Engineering Part A, 2010. **16**(7): p. 2255-2263.

239. Du, Y.A., et al., *Directed assembly of cell-laden microgels for fabrication of 3D tissue constructs.* Proceedings of the National Academy of Sciences of the United States of America, 2008. **105**(28): p. 9522-9527.

240. Tsang, V.L., et al., *Fabrication of 3D hepatic tissues by additive photopatterning of cellular hydrogels.* Faseb Journal, 2007. **21**(3): p. 790-801.

241. Du, Y.N., et al., *Convection-driven generation of long-range material gradients.* Biomaterials, 2010. **31**(9): p. 2686-2694.

242. Revzin, A., et al., *Fabrication of poly(ethylene glycol) hydrogel microstructures using photolithography.* Langmuir, 2001. **17**(18): p. 5440-5447.

243. Revzin, A., R.G. Tompkins, and M. Toner, *Surface engineering with poly(ethylene glycol) photolithography to create high-density cell arrays on glass.* Langmuir, 2003. **19**(23): p. 9855-9862.

244. Moon, J.J., et al., *Micropatterning of Poly(Ethylene Glycol) Diacrylate Hydrogels with Biomolecules to Regulate and Guide Endothelial Morphogenesis.* Tissue Engineering Part A, 2009. **15**(3): p. 579-585.

245. Burdick, J.A. and K.S. Anseth, *Photoencapsulation of osteoblasts in injectable RGD-modified PEG hydrogels for bone tissue engineering.* Biomaterials, 2002. **23**(22): p. 4315-4323.

246. Dikovsky, D., H. Bianco-Peled, and D. Seliktar, *The effect of structural alterations of PEG-fibrinogen hydrogel scaffolds on 3-D cellular morphology and cellular migration.* Biomaterials, 2006. **27**(8): p. 1496-1506.

247. Raeber, G.P., M.P. Lutolf, and J.A. Hubbell, *Molecularly engineered PEG hydrogels: A novel model system for proteolytically mediated cell migration.* Biophysical Journal, 2005. **89**(2): p. 1374-1388.

248. Brigham, M.D., et al., *Mechanically Robust and Bioadhesive Collagen and Photocrosslinkable Hyaluronic Acid Semi-Interpenetrating Networks.* Tissue Engineering Part A, 2009. **15**(7): p. 1645-1653.

249. Camci-Unal, G., et al., *Surface-modified hyaluronic acid hydrogels to capture endothelial progenitor cells.* Soft Matter, 2010. **6**(20): p. 5120-5126.

250. Gerecht, S., et al., *Hyaluronic acid hydrogen for controlled self-renewal and differentiation of human embryonic stem cells.* Proceedings of the National Academy of Sciences of the United States of America, 2007. **104**(27): p. 11298-11303.

251. Fukuda, J., et al., *Micropatterned cell co-cultures using layer-by-layer deposition of extracellular matrix components.* Biomaterials, 2006. **27**(8): p. 1479-1486.

252. Benton, J.A., et al., *Photocrosslinking of Gelatin Macromers to Synthesize Porous Hydrogels That Promote Valvular Interstitial Cell Function.* Tissue Engineering Part A, 2009. **15**(11): p. 3221-3230.

253. Hutson, C.B., et al., *Synthesis and Characterization of Tunable Poly(Ethylene Glycol): Gelatin Methacrylate Composite Hydrogels.* Tissue Engineering Part A, 2011. **17**(13-14): p. 1713-1723.

254. Arcaute, K., B. Mann, and R. Wicker, *Stereolithography of spatially controlled multi-material bioactive poly(ethylene glycol) scaffolds.* Acta Biomaterialia, 2010. **6**(3): p. 1047-1054.

255. Chan, V., et al., *Three-dimensional photopatterning of hydrogels using stereolithography for long-term cell encapsulation.* Lab on a Chip, 2010. **10**(16): p. 2062-2070.

256. Arcaute, K., B.K. Mann, and R.B. Wicker, *Stereolithography of three-dimensional bioactive poly(ethylene glycol) constructs with encapsulated cells.* Annals of Biomedical Engineering, 2006. **34**(9): p. 1429-41.

257. Borenstein, J.T., et al., *Microfabrication technology for vascularized tissue engineering.* Biomedical Microdevices, 2002. **4**(3): p. 167-175.

258. Madaboosi, N., et al., *Microfluidics meets soft layer-by-layer films: selective cell growth in 3D polymer architectures.* Lab on a Chip, 2012. **12**(8): p. 1434-1436.

259. Tan, W. and T.A. Desai, *Microscale multilayer cocultures for biomimetic blood vessels.* Journal of Biomedical Materials Research Part A, 2005. **72A**(2): p. 146-160.

260. King, K.R., et al., *Biodegradable microfluidics.* Advanced Materials, 2004. **16**(22): p. 2007-+.

261. Choi, N.W., et al., *Microfluidic scaffolds for tissue engineering.* Nature Materials, 2007. **6**(11): p. 908-915.

262. Rivron, N.C., et al., *Tissue deformation spatially modulates VEGF signaling and angiogenesis.* Proceedings of the National Academy of Sciences of the United States of America, 2012. **109**(18): p. 6886-6891.

263. Langer, R. and D.A. Tirrell, *Designing materials for biology and medicine.* Nature, 2004. **428**(6982): p. 487-492.

264. Jadlowiec, J.A., A.B. Celil, and J.O. Hollinger, *Bone tissue engineering: recent advances and promising therapeutic agents.* Expert Opin Biol Ther, 2003. **3**(3): p. 409-23.

265. Murphy, W.L. and D.J. Mooney, *Molecular-scale biomimicry.* Nat Biotechnol, 2002. **20**(1): p. 30-1.

266. Langer, R. and J.P. Vacanti, *Tissue Engineering.* Science, 1993. **260**(5110): p. 920-926.

267. Karageorgiou, V. and D. Kaplan, *Porosity of 3D biomaterial scaffolds and osteogenesis.* Biomaterials, 2005. **26**(27): p. 5474-91.

268. Hollister, S.J., R.D. Maddox, and J.M. Taboas, *Optimal design and fabrication of scaffolds to mimic tissue properties and satisfy biological constraints.* Biomaterials, 2002. **23**(20): p. 4095-103.

269. Hollister, S.J. and W.L. Murphy, *Scaffold Translation: Barriers Between Concept and Clinic.* Tissue Eng Part B Rev.

270. Khan, Y., et al., *Tissue engineering of bone: material and matrix considerations.* J Bone Joint Surg Am, 2008. **90 Suppl 1**: p. 36-42.

271. Mikos, A.G., et al., *Engineering complex tissues.* Tissue Eng, 2006. **12**(12): p. 3307-39.

272. Balasundaram, G. and T.J. Webster, *Nanotechnology and biomaterials for orthopedic medical applications.* Nanomedicine (Lond), 2006. **1**(2): p. 169-76.

273. Athanasiou, K.A., et al., *Orthopaedic applications for PLA-PGA biodegradable polymers.* Arthroscopy, 1998. **14**(7): p. 726-37.

274. Mano, J.F., et al., *Bioinert, biodegradable and injectable polymeric matrix composites for hard tissue replacement: state of the art and recent developments.* Composites Science and Technology, 2004. **64**(6): p. 789-817.

275. Mooney, D.J., et al., *Novel approach to fabricate porous sponges of poly(D,L-lactic-co-glycolic acid) without the use of organic solvents.* Biomaterials, 1996. **17**(14): p. 1417-22.

276. Borden, M., M. Attawia, and C.T. Laurencin, *The sintered microsphere matrix for bone tissue engineering: in vitro osteoconductivity studies.* J Biomed Mater Res, 2002. **61**(3): p. 421-9.

277. Ma, P.X. and J.W. Choi, *Biodegradable polymer scaffolds with well-defined interconnected spherical pore network.* Tissue Engineering, 2001. **7**(1): p. 23-33.

278. Borden, M., et al., *Tissue engineered microsphere-based matrices for bone repair: design and evaluation.* Biomaterials, 2002. **23**(2): p. 551-559.

279. Mu, C.D., et al., *Collagen Cryogel Cross-Linked by Dialdehyde Starch.* Macromolecular Materials and Engineering, 2010. **295**(2): p. 100-107.

280. Wei, G. and P.X. Ma, *Structure and properties of nano-hydroxyapatite/polymer composite scaffolds for bone tissue engineering.* Biomaterials, 2004. **25**(19): p. 4749-57.

281. Fan, H., et al., *Cartilage regeneration using mesenchymal stem cells and a PLGA-gelatin/chondroitin/hyaluronate hybrid scaffold.* Biomaterials, 2006. **27**(26): p. 4573-80.

282. Mo, X.M., et al., *Electrospun P(LLA-CL) nanofiber: a biomimetic extracellular matrix for smooth muscle cell and endothelial cell proliferation.* Biomaterials, 2004. **25**(10): p. 1883-1890.

283. Borden, M., et al., *Structural and human cellular assessment of a novel microsphere-based tissue engineered scaffold for bone repair.* Biomaterials, 2003. **24**(4): p. 597-609.

284. Jukes, J.M., et al., *Endochondral bone tissue engineering using embryonic stem cells.* Proc Natl Acad Sci U S A, 2008. **105**(19): p. 6840-6845.

285. Jiang, T., W.I. Abdel-Fattah, and C.T. Laurencin, *In vitro evaluation of chitosan/poly(lactic acid-glycolic acid) sintered microsphere scaffolds for bone tissue engineering.* Biomaterials, 2006. **27**(28): p. 4894-903.

286. Boskey, A.L., *Matrix proteins and mineralization: an overview.* Connect Tissue Res, 1996. **35**(1-4): p. 357-63.

287. Declercq, H.A., et al., *Calcification as an indicator of osteoinductive capacity of biomaterials in osteoblastic cell cultures.* Biomaterials, 2005. **26**(24): p. 4964-74.

288. Tremoleda, J.L., et al., *Bone tissue formation from human embryonic stem cells in vivo.* Cloning Stem Cells, 2008. **10**(1): p. 119-32.

289. Jukes, J.M., et al., *Potential of embryonic stem cells for in vivo bone regeneration.* Regen Med, 2008. **3**(6): p. 783-5.

290. Trounson, A., *Human embryonic stem cells: mother of all cell and tissue types.* Reprod Biomed Online, 2002. **4 Suppl 1**: p. 58-63.

291. Harris, G.M., et al., *Strategies to direct angiogenesis within scaffolds for bone tissue engineering.* Curr Pharm Des, 2013. **19**(19): p. 3456-65.

292. Fremont, L., *Biological effects of resveratrol.* Life Sci, 2000. **66**(8): p. 663-73.

293. Singh, G. and R.S. Pai, *Optimized PLGA nanoparticle platform for orally dosed trans-resveratrol with enhanced bioavailability potential.* Expert Opin Drug Deliv, 2014. **11**(5): p. 647-59.

294. Jang, M., et al., *Cancer chemopreventive activity of resveratrol, a natural product derived from grapes.* Science, 1997. **275**(5297): p. 218-20.

295. Bradamante, S., L. Barenghi, and A. Villa, *Cardiovascular protective effects of resveratrol.* Cardiovasc Drug Rev, 2004. **22**(3): p. 169-88.

296. Sinha, K., G. Chaudhary, and Y.K. Gupta, *Protective effect of resveratrol against oxidative stress in middle cerebral artery occlusion model of stroke in rats.* Life Sci, 2002. **71**(6): p. 655-65.

297. Wang, Q., et al., *Resveratrol protects against global cerebral ischemic injury in gerbils.* Brain Res, 2002. **958**(2): p. 439-47.

298. Wu, S.L., et al., *Immunosuppression by combined use of cyclosporine and resveratrol in a rat liver transplantation model.* Transplant Proc, 2005. **37**(5): p. 2354-9.

299. Wu, S.L., et al., *Resveratrol prolongs allograft survival after liver transplantation in rats.* World J Gastroenterol, 2005. **11**(30): p. 4745-9.

300. Sun, A.Y., et al., *Botanical Phenolics and Neurodegeneration*, in *Herbal Medicine: Biomolecular and Clinical Aspects*, I.F.F. Benzie and S. Wachtel-Galor, Editors. 2011: Boca Raton (FL).

301. Baur, J.A., et al., *Resveratrol improves health and survival of mice on a high-calorie diet.* Nature, 2006. **444**(7117): p. 337-42.

302. Aggarwal, B.B., et al., *Role of resveratrol in prevention and therapy of cancer: preclinical and clinical studies.* Anticancer Res, 2004. **24**(5A): p. 2783-840.

303. Yan, Y., et al., *Resveratrol-induced cytotoxicity in human Burkitt's lymphoma cells is coupled to the unfolded protein response.* BMC Cancer, 2010. **10**: p. 445.

304. Campagna, M. and C. Rivas, *Antiviral activity of resveratrol.* Biochem Soc Trans, 2010. **38**(Pt 1): p. 50-3.

305. Tsai, S.H., S.Y. Lin-Shiau, and J.K. Lin, *Suppression of nitric oxide synthase and the down-regulation of the activation of NFkappaB in macrophages by resveratrol.* Br J Pharmacol, 1999. **126**(3): p. 673-80.

306. Leiro, J., et al., *Effects of cis-resveratrol on inflammatory murine macrophages: antioxidant activity and down-regulation of inflammatory genes.* J Leukoc Biol, 2004. **75**(6): p. 1156-65.

307. Chung, E.Y., et al., *Resveratrol down-regulates interferon-gamma-inducible inflammatory genes in macrophages: molecular mechanism via decreased STAT-1 activation.* J Nutr Biochem, 2011. **22**(10): p. 902-9.

308. Zhou, H., et al., *Resveratrol augments the canonical Wnt signaling pathway in promoting osteoblastic differentiation of multipotent mesenchymal cells.* Exp Cell Res, 2009. **315**(17): p. 2953-62.

309. Shakibaei, M., et al., *Resveratrol mediated modulation of Sirt-1/Runx2 promotes osteogenic differentiation of mesenchymal stem cells: potential role of Runx2 deacetylation.* PLoS One, 2012. **7**(4): p. e35712.

310. Dosier, C.R., et al., *Resveratrol effect on osteogenic differentiation of rat and human adipose derived stem cells in a 3-D culture environment.* J Mech Behav Biomed Mater, 2012. **11**: p. 112-22.

311. Mizutani, K., et al., *Resveratrol stimulates the proliferation and differentiation of osteoblastic MC3T3-E1 cells.* Biochem Biophys Res Commun, 1998. **253**(3): p. 859-63.

312. Albrektsson, T. and C. Johansson, *Osteoinduction, osteoconduction and osseointegration.* Eur Spine J, 2001. **10 Suppl 2**: p. S96-101.

313. Khan, W.S., et al., *An osteoconductive, osteoinductive, and osteogenic tissue-engineered product for trauma and orthopaedic surgery: how far are we?* Stem Cells Int, 2012. **2012**: p. 236231.

314. Lichte, P., et al., *Scaffolds for bone healing: concepts, materials and evidence.* Injury, 2011. **42**(6): p. 569-73.

315. Jabbarzadeh, E., et al., *VEGF-incorporated biomimetic poly(lactide-co-glycolide) sintered microsphere scaffolds for bone tissue engineering.* J Biomed Mater Res B Appl Biomater, 2012. **100**(8): p. 2187-96.

316. Jiang, T., et al., *Chitosan-poly(lactide-co-glycolide) microsphere-based scaffolds for bone tissue engineering: in vitro degradation and in vivo bone regeneration studies.* Acta Biomater, 2010. **6**(9): p. 3457-70.

317. Rutledge, K., et al., *Enhanced differentiation of human embryonic stem cells on extracellular matrix-containing osteomimetic scaffolds for bone tissue engineering.* Tissue Eng Part C Methods, 2014. **20**(11): p. 865-74.

318. Erdman, C.P., et al., *Effects of resveratrol on enrichment of adipose-derived stem cells and their differentiation to osteoblasts in two-and three-dimensional cultures.* J Tissue Eng Regen Med, 2012. **6 Suppl 3**: p. s34-46.

319. Mobasheri, A. and M. Shakibaei, *Osteogenic effects of resveratrol in vitro: potential for the prevention and treatment of osteoporosis.* Ann N Y Acad Sci, 2013. **1290**: p. 59-66.

320. Boissy, P., et al., *Resveratrol inhibits myeloma cell growth, prevents osteoclast formation, and promotes osteoblast differentiation.* Cancer Res, 2005. **65**(21): p. 9943-52.

321. Costa Cdos, S., et al., *Resveratrol upregulated SIRT1, FOXO1, and adiponectin and downregulated PPARgamma1-3 mRNA expression in human visceral adipocytes.* Obes Surg, 2011. **21**(3): p. 356-61.

322. Tseng, P.C., et al., *Resveratrol promotes osteogenesis of human mesenchymal stem cells by upregulating RUNX2 gene expression via the SIRT1/FOXO3A axis.* Journal of Bone and Mineral Research, 2011. **26**(10): p. 2552-63.

323. Dai, Z., et al., *Resveratrol enhances proliferation and osteoblastic differentiation in human mesenchymal stem cells via ER-dependent ERK1/2 activation.* Phytomedicine, 2007. **14**(12): p. 806-14.

324. *Carbon nanotubes and graphene for photonic applications.* Woodhead publishing series in electronic and optical materials. pages cm.

325. Brown, B.N., et al., *Macrophage polarization: an opportunity for improved outcomes in biomaterials and regenerative medicine.* Biomaterials, 2012. **33**(15): p. 3792-802.

326. Madden, L.R., et al., *Proangiogenic scaffolds as functional templates for cardiac tissue engineering.* Proc Natl Acad Sci U S A, 2010. **107**(34): p. 15211-6.

327. Badylak, S.F., et al., *Macrophage phenotype as a determinant of biologic scaffold remodeling.* Tissue Eng Part A, 2008. **14**(11): p. 1835-42.

328. Brown, B.N., et al., *Macrophage phenotype as a predictor of constructive remodeling following the implantation of biologically derived surgical mesh materials.* Acta Biomaterialia, 2012. **8**(3): p. 978-87.

329. Brown, B.N., et al., *Macrophage phenotype and remodeling outcomes in response to biologic scaffolds with and without a cellular component.* Biomaterials, 2009. **30**(8): p. 1482-91.

330. Gretzer, C., et al., *Monocyte activation on titanium-sputtered polystyrene surfaces in vitro: the effect of culture conditions on interleukin-1 release.* Biomaterials, 1996. **17**(9): p. 851-8.

331. Thomsen, P. and C. Gretzer, *Macrophage interactions with modified material surfaces.* Current Opinion in Solid State & Materials Science, 2001. **5**(2-3): p. 163-176.

332. Omar, O.M., et al., *The stimulation of an osteogenic response by classical monocyte activation.* Biomaterials, 2011. **32**(32): p. 8190-204.

333.   Guihard, P., et al., *Induction of osteogenesis in mesenchymal stem cells by activated monocytes/macrophages depends on oncostatin M signaling.* Stem Cells, 2012. **30**(4): p. 762-72.

334.   Kreutz, M., et al., *1,25-dihydroxyvitamin D3 production and vitamin D3 receptor expression are developmentally regulated during differentiation of human monocytes into macrophages.* Blood, 1993. **82**(4): p. 1300-7.

335.   Champagne, C.M., et al., *Macrophage cell lines produce osteoinductive signals that include bone morphogenetic protein-2.* Bone, 2002. **30**(1): p. 26-31.

336.   Kimble, R.B., S. Bain, and R. Pacifici, *The functional block of TNF but not of IL-6 prevents bone loss in ovariectomized mice.* Journal of Bone and Mineral Research, 1997. **12**(6): p. 935-941.

337.   Cho, T.J., L.C. Gerstenfeld, and T.A. Einhorn, *Differential temporal expression of members of the transforming growth factor beta superfamily during murine fracture healing.* Journal of Bone and Mineral Research, 2002. **17**(3): p. 513-520.

338.   Gerstenfeld, L.C., et al., *Osteogenic growth factors and cytokines and their role in bone repair*, in *Engineering of functional skeletal tissues*. 2007, Springer. p. 17-45.

339.   Deckers, M.M.L., et al., *Expression of vascular endothelial growth factors and their receptors during osteoblast differentiation.* Endocrinology, 2000. **141**(5): p. 1667-1674.

340.   Bouletreau, P.J., et al., *Hypoxia and VEGF up-regulate BMP-2 mRNA and protein expression in microvascular endothelial cells: Implications for fracture healing.* Plastic and Reconstructive Surgery, 2002. **109**(7): p. 2384-2397.

341.   Mayr-Wohlfart, U., et al., *Vascular endothelial growth factor stimulates chemotactic migration of primary human osteoblasts.* Bone, 2002. **30**(3): p. 472-477.

342.   Gaur, T., et al., *Canonical WNT signaling promotes osteogenesis by directly stimulating Runx2 gene expression.* Journal of Biological Chemistry, 2005. **280**(39): p. 33132-40.

343.   Jeon, M.J., et al., *Activation of peroxisome proliferator-activated receptor-gamma inhibits the Runx2-mediated transcription of osteocalcin in osteoblasts.* Journal of Biological Chemistry, 2003. **278**(26): p. 23270-7.

344.   Shockley, K.R., et al., *PPARgamma2 nuclear receptor controls multiple regulatory pathways of osteoblast differentiation from marrow mesenchymal stem cells.* Journal of Cellular Biochemistry, 2009. **106**(2): p. 232-46.

AMBREEN IRSHAD - BSP <ambreenirshad@benthamscience.org>   May 5 ☆   ↰   ▾
to m.ahmed, me ▾

Grant of Permission

Dear Dr. Rutledge:

Thank you for your interest in our copyrighted material, and for requesting permission for its use.

Permission is granted for the following subject to the conditions outlined below:

"Strategies to Direct Angiogenesis within Scaffolds for Bone Tissue Engineering" published in Current Pharmaceutical Design, 2013, Volume 19

To be used in the following manner:

1. Bentham Science Publishers grants you the right to reproduce the material indicated above on a one-time, non-exclusive basis, solely for the purpose described. Permission must be requested separately for any future or additional use.

2. For an article, the copyright notice must be printed on the first page of article or book chapter. For figures, photographs, covers, or tables, the notice may appear with the material, in a footnote, or in the reference list.

Thank you for your patience while your request was being processed. If you wish to contact us further, please use the address below.

Sincerely,

AMBREEN **IRSHAD**

Permissions & Rights Manager
Bentham Science Publishers
Email: ambreenirshad@benthamscience.org
URL: www.benthamscience.com